Prog. Theor. Exp. Phys. **2017**, 033B08 (61 pages)
DOI: 10.1093/ptep/ptx007

BPS boojums in $\mathcal{N} = 2$ supersymmetric gauge theories II

Masato Arai*, Filip Blaschke, and Minoru Eto

Department of Physics, Yamagata University, Kojirakawa-machi 1-4-12, Yamagata 990-8560, Japan
*E-mail: arai@sci.kj.yamagata-u.ac.jp

Received December 2, 2016; Accepted January 8, 2017; Published March 30, 2017

We continue our study of 1/4 Bogomol'nyi–Prasad–Sommerfield (BPS) composite solitons of vortex strings, domain walls, and boojums in $\mathcal{N} = 2$ supersymmetric Abelian gauge theories in four dimensions. In this work, we numerically confirm that a boojum appearing at an endpoint of a string on a thick domain wall behaves as a magnetic monopole with a fractional charge in three dimensions. We introduce a "magnetic" scalar potential whose gradient gives magnetic fields. The height of the magnetic potential has a geometrical meaning that is the shape of the domain wall. We find a semilocal extension of a boojum that has an additional size moduli at an endpoint of a semilocal string on the domain wall. Dyonic solutions are also studied and we numerically confirm that the dyonic domain wall becomes an electric capacitor storing opposite electric charges on its skins. At the same time, the boojum becomes a fractional dyon whose charge density is proportional to $\vec{E} \cdot \vec{B}$. We also study dual configurations with an infinite number of boojums and anti-boojums on parallel lines and analyze the ability of domain walls to store magnetic charge as magnetic capacitors. In understanding these phenomena, the magnetic scalar potential plays an important role. We study the composite solitons from the viewpoints of the Nambu–Goto and Dirac–Born–Infeld actions, and find the semilocal BIon as the counterpart of the semilocal boojum.

Subject Index B06, B10, B35

1. Introduction and summary

Topological solitons, which often appear in physical settings where local or global symmetry is spontaneously broken, are important to various fields in modern physics, such as string theory, field theory, cosmology, nuclear physics, and condensed matter physics. The simplest examples, ordered in increasing number of codimension, are domain walls, vortex strings (Ref. [1]), and 't Hooft-Polyakov magnetic monopoles (Refs. [2,3]). Interestingly, a nontrivial composite of these "elementary" solitons also exists.

Among such configurations, composite solitons that vortex strings attach to domain walls have been studied for a long time. A reason is that such configurations are corresponding objects to the D-branes (Ref. [4]) where F/D strings end in a superstring framework. A pioneering analysis was performed in nonsupersymmetic (SUSY) field theory in Refs. [5,6]. This work was later followed by other studies with SUSY (Refs. [7–12]). In SUSY field theory, it was shown that there exists a Bogomol'nyi–Prasad–Sommerfield (BPS) object with negative energy in a junction point where the vortex string attaches on the wall (Ref. [13]). This is nothing but the binding energy of the vortex string and the domain wall. This configuration with negative energy is called the boojum, a term

Funded by SCOAP[3]

that was originally coined in the context of a ^{3}He superfluid (Refs. [14,15]). An interesting point of such negative binding energy is that there is no corresponding analog in string theory. Further study of the boojum was also performed in $\mathcal{N} = 2$ Abelian gauge theory with two charged matter hypermultiplets (Ref. [16]). In Refs. [13,16] some features of the boojum such as its mass and configuration were investigated. However, until quite recently there were several issues still to be confirmed. For instance, in Ref. [13], although the correct formula for the boojum mass was derived, a certain approximation was used to simplify the calculations. In Ref. [16], it was also discussed that there is an ambiguity in the definition of the boojum mass given in Ref. [13]. Furthermore, no analytic/numerical solutions for the boojums have been obtained and the true shape of the boojum was not known.

In order to clarify these issues, we recently studied the boojum in detail in $\mathcal{N} = 2$ SUSY QED with $N_F \geq 2$ flavors in the presence of the Fayet–Iliopoulos term in the previous work Ref. [17]. The boojum configuration was numerically/analytically obtained by solving the 1/4 BPS equations. Though they are a set of first-order differential equations, they amount to a second-order differential equation called the master equation (see Eq. (2.16)) thanks to the so-called moduli matrix formalism (Refs. [18–20]). Before Ref. [17], it was known that this equation can be solved analytically only when the gauge coupling constant is taken to infinity (Ref. [18]) while the finite case is rather difficult. In principle, a numerical solution can always be obtained if an appropriate boundary condition is given. However, it is not a straightforward task to give it when two or more topological solitons coexist. In Ref. [17], we provided a simple and systematic way to give suitable boundary conditions called the global approximations. We showed that the global approximation is useful not only to solve the master equation numerically but also to figure out the boojum mass exactly without any ambiguity, such as that discussed in Ref. [16]. We also derived several exact solutions for 1/4 BPS equations at the finite-gauge coupling in models with $N_F = 4$ and with $N_F = 6$ flavors. This had not been achieved previously. The only composite soliton known exactly was the 1/4 BPS junction of domain walls (Ref. [21]).

In our previous work Ref. [17], we were oriented to solving the master equation and revealing the real shape of the boojums. In contrast, in this paper, we will focus on physical aspects of the boojums and expand our understanding of composite solitons further by using the developments of our previous work (Ref. [17]). First, we investigate a composite solution that a (semi)local string vortex ends on a wall in a weak-gauge coupling limit. Note that in our analysis it is possible to take any value of the gauge coupling when we solve the master equation. In the weak coupling limit, the domain wall becomes thick and has a fat internal layer where the U(1) gauge symmetry is almost restored. In this situation, we numerically confirm that the boojums can be identified with *magnetic* point-like sources with a fractional charge from the $(3 + 1)$-dimensional viewpoint by taking the thickness of the domain walls into account. This is contrary to the case that the points where vortex-strings terminate on walls are interpreted as *electric* point charges in the low-energy effective theory in the $(2 + 1)$-dimensional world volume of the domain walls (Refs. [10–12]). We show that the two-dimensional distribution of the magnetic flux inside the domain wall can be correctly reproduced by the gradient of a scalar function, which we call the *magnetic* scalar potential. Interestingly, the magnetic scalar potential corresponds to the "position" of the domain wall. Namely, we prove that the shape of the domain wall determines the magnetic force inside the domain walls. Further insights along this direction are brought by the global approximate solutions. We show that the domain wall's position can be approximately – but precisely enough – identified with the solution to the Taubes equation (Ref. [22]).

Second, we study a numerical solution to a configuration of periodically aligned vortex strings attached to the domain wall. The domain wall is bent logarithmically when one vortex string pulls it. In this setup, as mentioned above, the point charges are magnetic charges and the magnetic scalar potential corresponds to the domain wall's position/shape. We consider a configuration where periodically aligned vortex strings end on the domain wall from one side and another infinite series of vortex strings end on the opposite side. As can be easily imagined, such a configuration resembles a *magnetic* capacitor. We compute the magnetic capacitance per unit length and the energy stored there. When we separate the two parallel lines of endpoints far away, a flat but slanting domain wall remains in between with nonzero magnetic flux inside. This is similar to a D-brane with magnetic flux. Putting an additional vortex string ending on the tilted domain wall, the magnetic flux spreading inside the domain wall shows again a one-dimensional structure, which is almost the same as an electric charge placed in an electric capacitor. A similar configuration has already been obtained in the strong-gauge coupling limit (Ref. [19]) and our solution is for the finite-gauge coupling case. This offers a field theoretical D-brane resembling the fundamental string ending on the D-brane with magnetic flux [23,24].

We also study the dyonic extension of the 1/4 BPS solutions. Although the BPS equations were derived in Refs. [25,26], no solutions have been obtained in the literature, except for the strong-gauge coupling limit (Ref. [10]). We first study the 1/2 BPS dyonic domain walls, which are the finite-gauge coupling version of the Q-kinks (Refs. [27,28]). We confirm that positive and negative electric charges are induced on the skin of the domain wall. As a consequence, the dyonic domain wall in the weak-gauge coupling region is an *electric* capacitor. Then, we numerically solve the master equation for the dyonic 1/4 BPS configuration again with the aid of the global approximate solutions. When a vortex string attaches to the dyonic domain wall, both the magnetic and electric fluxes coexist inside the domain wall. We show that almost everywhere except for the vicinity of the junction point, the electric flux $\vec{E}$ and the magnetic flux $\vec{B}$ are perpendicular. Around the junctions points, $\vec{E}$ and $\vec{B}$ become parallel, and, indeed, we show that the boojum charge is proportional to $\vec{E} \cdot \vec{B}$, which is a CP-violating interaction.

As a novel solution, we find a semilocal boojum that appears at the endpoint of the semilocal vortex string (Ref. [29]) on the domain wall in the model with multiple flavors $N_F \geq 3$, with partially degenerate masses for the hypermultiplets. It has an additional zero mode related to the size of the string diameter. We find that the semilocal boojum changes its size in unison with the size of the attached semilocal vortex string.

Finally, we study the 1/4 BPS configuration from the viewpoint of the low-energy effective action, the Nambu–Goto action, and the DBI action, for the domain wall. This kind of study has already been performed, e.g., in Refs. [10–12,30]. In these previous works, as the low-energy effective action, the DBI action (or its linearization) that is obtained by dualizing the internal moduli of the domain wall to the Abelian gauge field was studied. In our paper, we study both the Nambu–Goto action and the DBI action. We first investigate the domain wall and its Q-extension (dyonic extension) in the Nambu–Goto action and find that the energy of these configuration coincides with one in the field-theoretical model. Second, we study the case that a point source of zero size deforms the domain wall to a spike configuration in the Nambu–Goto action. This is precisely the counterpart of the Q-lump string ending on the domain wall in the strong-gauge coupling limit in the original field theory. After that, we study the relation between the Nambu–Goto action and the DBI action. We briefly explain how the Nambu–Goto action is dualized to the DBI action. By using the relations so obtained, we also transform the energy and the BPS equation for the dyonic extension of the spike configuration in terms of the DBI language. We show that the results are the same as in Ref. [10]. By using the DBI action, we also study a point-like source with a finite size that should be a counterpart of the semilocal boojum. We find the semilocal BIon which, contrary to the local BIon, has the tip of its spike smoothed out with the same order as the size of the source.

This paper is organized as follows. Section 2 serves as a summary of our model and all relevant formulas, such as topological charges and 1/4 BPS equations, which we present both in terms of field and also via a moduli matrix method. In that section, we do not repeat the derivation of these quantities, which is done in Ref. [17]. In Sect. 3 we present the notion of a boojum as a fractional magnetic monopole. Section 4 is devoted to studying periodically aligned vortex strings. We investigate the magnetic capacitor there. In Sect. 5, we study the dyonic extension of the 1/4 BPS states. We find that the domain wall plays the role of an electric capacitor and show several numerical solutions. Section 6 is devoted to analysis from the perspective of the Nambu–Goto action, together with the analysis in terms of the DBI action. A brief discussion of future work is given in Sect. 7.

2. The Model

In this section, we write down all relevant formulas such as topological charges, BPS equations, and the master equation for 1/4 BPS solitons, for convenience. A proper derivation of these quantities is skipped and we refer the reader to Ref. [17] for details.

2.1. *Abelian vortex-wall system*

The model we use for our analysis is $\mathcal{N}=2$ supersymmetric U(1) gauge theory in (3+1) dimensions with $2N_F$ complex scalar fields in the charged hypermultiplets. The vector multiplet includes the photon A_μ and a real scalar field σ. The bosonic Lagrangian is given as

$$\mathcal{L} = -\frac{1}{4g^2}(F_{\mu\nu})^2 + \frac{1}{2g^2}(\partial_\mu\sigma)^2 + \left|D_\mu H\right|^2 + \left|D_\mu \hat{H}^\dagger\right|^2 - V, \tag{2.1}$$

$$V = \frac{g^2}{2}\left(v^2 - HH^\dagger + \hat{H}^\dagger\hat{H}\right)^2 + \frac{g^2}{2}\left|H\hat{H}\right|^2 + |\sigma H - HM|^2 + \left|\sigma\hat{H}^\dagger - \hat{H}^\dagger M\right|^2, \tag{2.2}$$

where g is a gauge coupling constant, M is a real diagonal matrix

$$M = \mathrm{diag}(m_1, \ldots, m_{N_F}), \tag{2.3}$$

and v is the Fayet–Iliopoulos D-term. Without loss of generality we can take M to be traceless, namely $\sum_{A=1}^{N_F} m_A = 0$,[1] and align the masses as $m_A > m_{A+1}$. Since $\tilde{H}$ will play no role, we will set $\tilde{H} = 0$ in the rest of this paper.

In the absence of the mass matrix M, the Lagrangian (2.1) is invariant under SU(N_F) flavor transformation of Higgs fields $H \to H\,\mathrm{U}$, $\mathrm{U} \in \mathrm{SU}(N_F)$. The nondegenerate masses in M explicitly break this down to $\mathrm{U}(1)^{N_F-1}$, which we from now on assume to be the case unless stated otherwise.

We consider 1/4 BPS solitons, namely the junctions of vortex strings arranged to be parallel to the x^3-axis and the domain walls perpendicular to the x^3-axis. By completing the energy density (see Ref. [17] for details) we obtain the Bogomol'nyi bound

$$\mathcal{E} \geq \mathcal{T}_{\mathrm{W}} + \mathcal{T}_{\mathrm{S}} + \mathcal{T}_{\mathrm{B}} + \partial_k j_k, \tag{2.4}$$

[1] Any overall factor $M = m\mathbf{1}_{N_F} + \cdots$ can be absorbed into σ by shifting $\sigma \to \sigma - m$.

with

$$\mathcal{T}_{\rm W} = \eta v^2 \partial_3 \sigma, \qquad \mathcal{T}_{\rm S} = -\xi v^2 F_{12}, \qquad \mathcal{T}_{\rm B} = \frac{\eta\,\xi}{g^2}\epsilon_{klm}\partial_k(F_{lm}\sigma) \tag{2.5}$$

and with the nontopological currents defined as

$$j_a = \frac{\xi i}{2}\epsilon_{ab}(HD_bH^\dagger - D_bHH^\dagger) \quad (a = 1, 2), \tag{2.6}$$

$$j_3 = -\eta(\sigma H - HM)H^\dagger. \tag{2.7}$$

The above bound is saturated if the 1/4 BPS equations,

$$D_3H + \eta\big(\sigma H - HM\big) = 0, \tag{2.8}$$

$$\big(D_1 + i\xi D_2\big)H = 0, \tag{2.9}$$

$$\eta\partial_1\sigma = \xi F_{23}, \qquad \eta\partial_2\sigma = \xi F_{31}, \tag{2.10}$$

$$\xi F_{12} - \eta\partial_3\sigma + g^2\big(v^2 - |H|^2\big) = 0, \tag{2.11}$$

are satisfied. Here $\xi = (-1)1$ labels (anti-)vortices and $\eta = (-1)1$ denotes (anti-)walls.

The domain wall and the vortex string energy density, $\mathcal{T}_{\rm W}$ and $\mathcal{T}_{\rm S}$, respectively, are positive definite. $\mathcal{T}_{\rm B}$ is the so-called *boojum* energy density, which is interpreted as the binding energy of a vortex string attached to the domain wall, since it is negative irrespective of the signs of η and ξ (Refs. [13,16]). The total energy of a 1/4 BPS soliton is obtained upon space integration and it consists of three parts,

$$E_{1/4} = T_{\rm W}A + T_{\rm S}L + T_{\rm B}, \tag{2.12}$$

where we have defined the sum of tensions of the domain walls $T_{\rm W} = \int dx^3\ \mathcal{T}_{\rm W}$, and that of the vortex strings $T_{\rm S} = \int dx^1dx^2\ \mathcal{T}_{\rm S}$, respectively. The terms $A = \int dx^1\ dx^2$ and $L = \int dx^3$ stand for the domain wall's area and length of the vortex string. Only the masses of the boojums $T_{\rm B} = \int d^3x\,\mathcal{T}_{\rm B}$ are finite. Summing all the elementary domain walls and vortex strings, we have

$$T_{\rm W} = \sum t_{\rm W} = v^2|\Delta m|, \qquad T_{\rm S} = 2\pi v^2|k|, \tag{2.13}$$

where we have defined $\Delta m = [\sigma]_{x^3=-\infty}^{x^3=+\infty}$ and $k \in \mathbb{Z}$ stands for the number of vortex strings. In Ref. [17] we directly verify the generic formula

$$T_{\rm B} = -\sum \frac{2\pi}{g^2}|m_{A+1} - m_A|, \tag{2.14}$$

where the sum is taken for all the junctions of domain walls and vortex strings in the solution under consideration.

2.2. *The moduli matrix formalism*

The moduli matrix approach (Refs. [18–20]) reduces the set of equations (2.8)–(2.11) into one equation called the master equation. The moduli matrix approach is based on the ansatz

$$H = v\exp(-u/2)\,H_0(z)\exp\big(\eta Mx^3\big), \qquad A_1 + i\xi A_2 = -i\partial_{\bar z}u, \qquad \eta\sigma + iA_3 = \frac{1}{2}\partial_3 u, \tag{2.15}$$

where $H_0(z)$ is the so-called moduli matrix, which is holomorphic in a complex coordinate $z \equiv x^1 + i\xi x^2$. By using the U(1) gauge transformation, we fix $u = u(z, \bar{z}, x^3)$ to be real. Then we have $A_3 = 0$. It is easy to see that this ansatz solves Eqs. (2.8)–(2.10) identically. The last BPS equation (2.11) turns into the master equation

$$\frac{1}{2g^2v^2}\partial_k^2 u = 1 - \Omega_0 \exp(-u), \qquad \Omega_0 = H_0(z)\exp\left(2\eta M x^3\right) H_0^\dagger(\bar{z}). \tag{2.16}$$

Now, all fields can be expressed in terms of u:

$$\sigma = \frac{\eta}{2}\partial_3 u, \qquad F_{12} = -2\xi\,\partial_z\partial_{\bar{z}} u, \qquad F_{23} = \frac{\xi}{2}\partial_3\partial_1 u, \qquad F_{31} = \frac{\xi}{2}\partial_2\partial_3 u. \tag{2.17}$$

The energy densities are also written as

$$\mathcal{T}_{\rm W} = \frac{v^2}{2}\partial_3^2 u, \tag{2.18}$$

$$\mathcal{T}_{\rm S} = 2v^2\partial_z\partial_{\bar{z}} u = \frac{v^2}{2}\left(\partial_1^2 + \partial_2^2\right) u, \tag{2.19}$$

$$\mathcal{T}_{\rm B} = \frac{1}{2g^2}\left\{(\partial_1\partial_3 u)^2 + (\partial_2\partial_3 u)^2 - \left(\partial_1^2 + \partial_2^2\right) u\, \partial_3^2 u\right\}. \tag{2.20}$$

The nontopological current j_k given in Eqs. (2.6) and (2.7) can be rewritten in the following expression by using the BPS equations:

$$j_k = \frac{1}{2}\partial_k (HH^\dagger). \tag{2.21}$$

Thus, we also have

$$\mathcal{T}_4 = \partial_k j_k = \frac{1}{2}\partial^2(HH^\dagger) = -\frac{1}{4g^2}\partial^2\partial^2 u, \tag{2.22}$$

with $\partial^2 \equiv \partial_k^2$. Collecting all the pieces, the total energy density is given by

$$\mathcal{E} = \frac{v^2}{2}\partial_k^2 u + \frac{1}{2g^2}\left\{(\partial_1\partial_3 u)^2 + (\partial_2\partial_3 u)^2 - \left(\partial_1^2 + \partial_2^2\right) u\partial_3^2 u\right\} - \frac{1}{4g^2}(\partial_k^2)^2 u. \tag{2.23}$$

Thus, the scalar function u determines everything.

Finally, for further convenience, we will use the following dimensionless coordinates and mass:

$$\tilde{x}^k = \sqrt{2}gvx^k, \qquad \tilde{M} = \frac{1}{\sqrt{2}gv}M = \mathrm{diag}\left(\frac{\tilde{m}}{2}, -\frac{\tilde{m}}{2}\right). \tag{2.24}$$

The dimensionless fields are similarly defined by

$$\tilde{H} = \frac{H}{v} = \exp(-u/2)\, H_0 \exp\left(\eta\tilde{M}\tilde{x}^3\right), \qquad \tilde{\sigma} = \frac{\sigma}{\sqrt{2}gv} = \frac{\eta}{2}\tilde{\partial}_3 u. \tag{2.25}$$

We will also use the dimensionless magnetic fields

$$\tilde{F}_{12} = \frac{1}{g^2v^2}F_{12} = -\xi\left(\tilde{\partial}_\rho^2 + \frac{1}{\tilde{\rho}}\tilde{\partial}_\rho\right) u, \tag{2.26}$$

$$\tilde{F}_{23} = \frac{1}{g^2v^2}F_{23} = \xi\,\tilde{\partial}_3\tilde{\partial}_\rho u\cos\theta, \tag{2.27}$$

$$\tilde{F}_{31} = \frac{1}{g^2v^2}F_{31} = \xi\,\tilde{\partial}_3\tilde{\partial}_\rho u\sin\theta. \tag{2.28}$$

Then, the dimensionless energy density $\tilde{\mathcal{E}}$ is defined by

$$\mathcal{E} = g^2v^4\tilde{\mathcal{E}} = \tilde{\mathcal{T}}_{\rm W} + \tilde{\mathcal{T}}_{\rm S} + \tilde{\mathcal{T}}_{\rm B} + \tilde{\mathcal{T}}_4, \tag{2.29}$$

where

$$\tilde{\mathcal{T}}_{\rm W} = 2\eta\tilde{\partial}_3\tilde{\sigma} = \tilde{\partial}_3^2 u, \tag{2.30}$$

$$\tilde{\mathcal{T}}_{\rm S} = -\xi\tilde{F}_{12} = \left(\tilde{\partial}_\rho^2 + \frac{1}{\tilde{\rho}}\tilde{\partial}_\rho\right)u, \tag{2.31}$$

$$\tilde{\mathcal{T}}_{\rm B} = 2\eta\xi\,\tilde{\partial}_i\left(\epsilon_{ijk}\tilde{\sigma}\tilde{F}_{jk}\right) = 2\left[\left(\tilde{\partial}_\rho\tilde{\partial}_3 u\right)^2 - \left(\tilde{\partial}_\rho^2 + \frac{1}{\tilde{\rho}}\tilde{\partial}_\rho\right)u\,\tilde{\partial}_3^2 u\right], \tag{2.32}$$

$$\tilde{\mathcal{T}}_4 = -\left(\tilde{\partial}_\rho^2 + \frac{1}{\tilde{\rho}}\tilde{\partial}_\rho + \tilde{\partial}_3^2\right)^2 u. \tag{2.33}$$

The relations to the original values are given as

$$T_{\rm W} = \int dx^3\,\mathcal{T}_{\rm W} = \frac{gv^3}{\sqrt{2}}\int d\tilde{x}^3\,\tilde{\mathcal{T}}_{\rm W} = \frac{gv^3}{\sqrt{2}}\tilde{T}_{\rm W}, \tag{2.34}$$

$$T_{\rm S} = \int d^2x\,\mathcal{T}_{\rm S} = \frac{v^2}{2}\int d^2\tilde{x}\,\tilde{\mathcal{T}}_{\rm S} = \frac{v^2}{2}\tilde{T}_{\rm S}, \tag{2.35}$$

$$T_{\rm B} = \int d^3x\,\mathcal{T}_{\rm B} = \frac{v}{2\sqrt{2}g}\int d^3\tilde{x}\,\tilde{\mathcal{T}}_{\rm B} = \frac{v}{2\sqrt{2}g}\tilde{T}_{\rm B}. \tag{2.36}$$

In what follows, we will not distinguish x^k and $\tilde{x}^k$, unless stated otherwise. An exception is the mass: we will use the notation $\tilde{m}$ in order not to forget that we are using the dimensionless variables.

3. Boojum as a fractional magnetic monopole and monostick

3.1. Weak coupling regime

There are no magnetic sources, namely no magnetic monopoles, in our U(1) gauge theory. Indeed, the Bianchi identity $\epsilon_{ijk}\partial_i F_{jk} = 0$ always holds. The nonzero boojum charge $T_{\rm B}$ seems to yield nonzero magnetic charge, but it is not true. The boojum has $\epsilon_{ijk}\partial_i\hat{F}_{jk} \neq 0$ with $\hat{F}_{ij} = \sigma F_{ij}$ while it has $\epsilon_{ijk}\partial_i F_{jk} = 0$. Of course, $\hat{F}_{ij} = \sigma F_{ij}$ is not a genuine magnetic field. Nevertheless, there is a case that the boojum can be naturally identified as a magnetic source in the weak-gauge coupling region $\tilde{m} \gg 1$. In this region, the domain wall has a fat inner layer of the width $\sim \tilde{m}$, where the U(1) gauge symmetry is almost recovered. When the magnetic flux is injected into the domain wall through the vortex string, the magnetic flux almost freely spreads out inside the domain wall; see Fig. 1. Therefore, for one living inside the domain wall, who is blind to outside world, the boojum is really a magnetic source. It is a point-like source, so one may call it a magnetic monopole. The difference from an ordinary magnetic monopole, be it a Dirac or a 't Hooft-Polyakov monopole, is that the boojum sticks to the boundary of the semicompact world, where it lives.

Note that, here, we are trying to identify the boojum as a magnetic monopole in the semicompact space $d = 2 + 1$ where 2 corresponds to the two-dimensional infinite plane and 1 to the finite

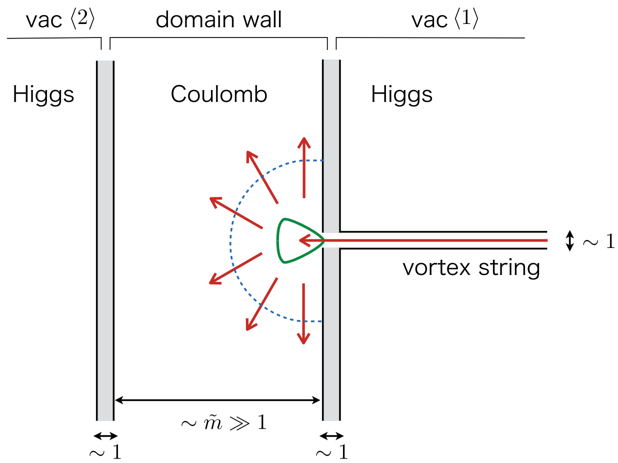

Fig. 1. A sketch of a boojum inside the domain wall in a weak coupling region. The boojum is naturally identified with a magnetic source with a fractional magnetic charge ($2\pi/g$) that sticks to the inner boundary of the domain wall.

segment of width $\sim \tilde{m}$. This is different from the well-known arguments that the endpoint of the vortex string can be identified with an *electric* charge in the $(1+2)$-dimensional (1 is time and 2 is space) effective theory of the domain wall. To this end, one needs to integrate out the normal direction to the domain wall (x^3) and then to dualize the S^1 internal moduli parameter to the dual U(1) gauge field in $(1+2)$-dimensional space-time à la Polyakov. Here, we do not do this and instead we are dealing with the original U(1) gauge field.

In Fig. 2 we see that the magnetic flux inside the fat domain wall ($\tilde{m} \geq 10$) linearly spreads for a while until it encounters the boundary. The characteristic length of this linear spreading is proportional to the width of the inner layer.

An observer inside the domain wall can measure the magnetic charge of the boojum by counting the magnetic flux flowing through a hemisphere enclosing the boojum (blue dotted line in Fig. 1) as

$$\tilde{\Phi}_{\text{boojum}} = \int_{\text{hemisphere}} dS_i \, \frac{1}{2}\epsilon_{ijk}\tilde{F}_{jk} = 4\pi \,. \tag{3.1}$$

Here we have integrated only on the hemisphere, excluding the wall boundary from the surface integral. We have 4π simply due to the flux conservation, $\tilde{\Phi}_{\text{boojum}} = -\tilde{\Phi}_{\text{in}}$. From Gauss's law (the integration is performed only over the hemisphere) we conclude that the magnetic charge of the boojum is

$$\tilde{\mathcal{M}}_{\text{B}} = 4\pi \,. \tag{3.2}$$

Note that this is calculated with dimensionless variables. In terms of the original variables and with respect to the usual notation $A_\mu \to gA_\mu$, the magnetic charge of the boojum in conventional notation is given by

$$\mathcal{M}_{\text{B}} = \frac{2\pi}{g}. \tag{3.3}$$

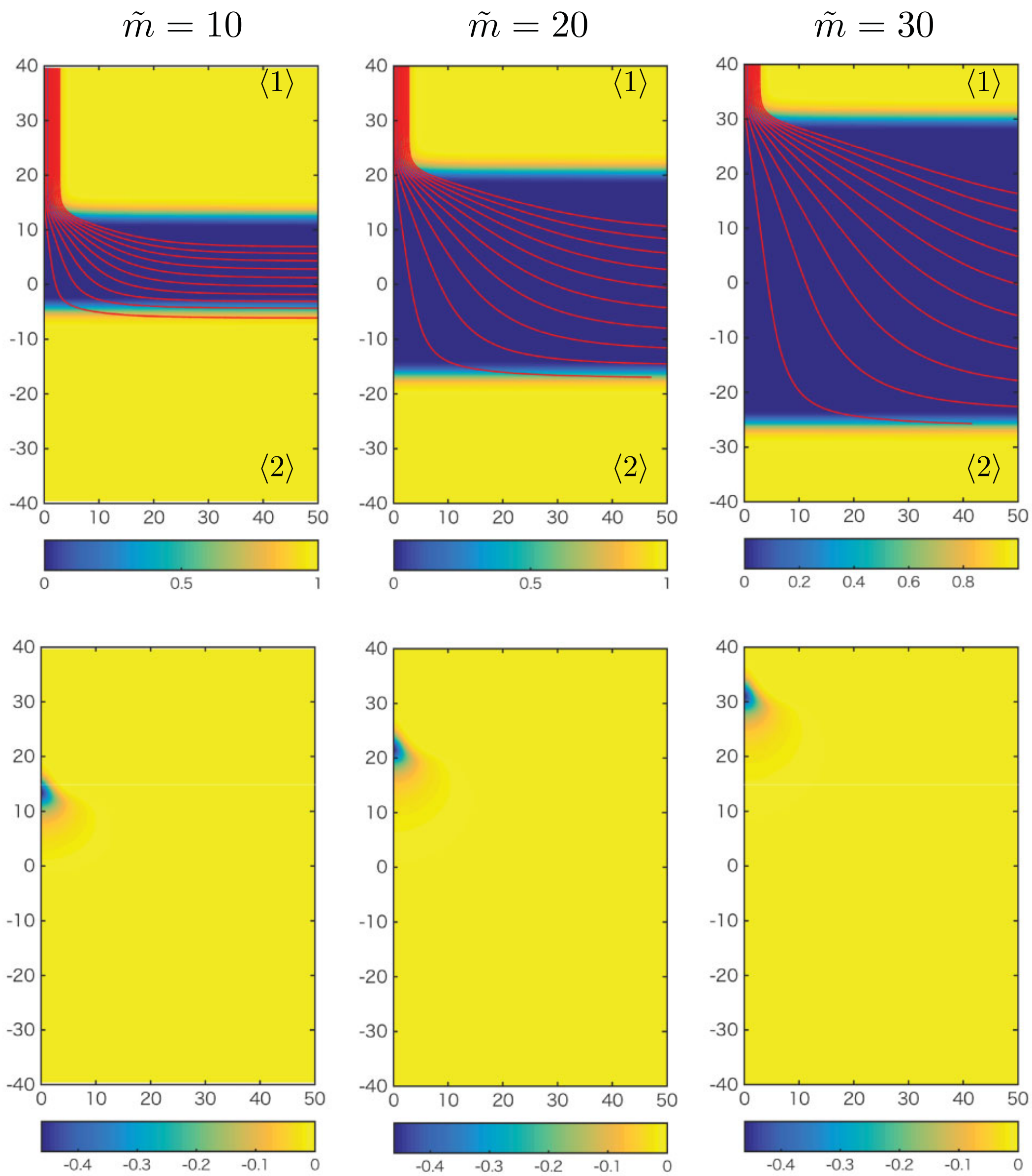

Fig. 2. Fat domain walls with $\tilde{m} = 10, 20, 30$. The first row shows the effective photon mass m_v^2 and the magnetic force lines. The second row shows the boojum charge density.

This is one-half of the magnetic charge $\mathcal{M}_{\mathrm{TP}} = 4\pi/g$ of a 't Hooft–Polyakov-type magnetic monopole. Thus, the boojum can be identified with a fractional magnetic monopole from the point of view of wall-bound observers.

Since we have solved the equation of motion for the finite-gauge coupling constant, we can check this statement numerically. In the Coulomb phase, the magnetic field of the magnetic charge $\tilde{\mathcal{M}}$ stuck on a wall at $x^3 = X$ should obey the normal $(1+3)$-dimensional Coulomb law

$$\tilde{B}_i \equiv \frac{1}{2}\epsilon_{ijk}\tilde{F}_{jk} = \frac{\tilde{\mathcal{M}}}{2\pi r^2}\frac{x^i - \delta^{i3}X}{r}, \quad x^3 < X, \tag{3.4}$$

with $r = \left((x^1)^2 + (x^2)^2 + (x^3 - X)^2\right)^{1/2}$. Note that a factor in the denominator is not $4\pi r^2$ but $2\pi r^2$ (the area of hemisphere surrounding the boojum) appears in the denominator reflecting the fact that

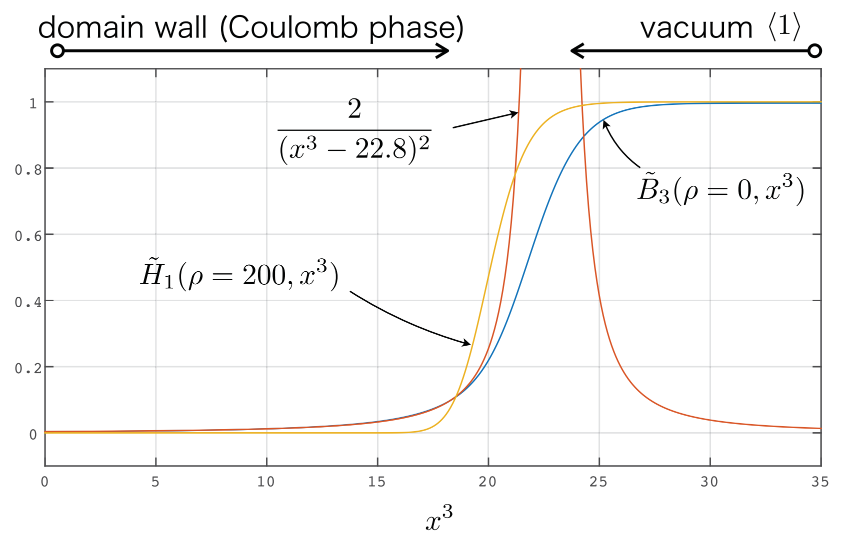

Fig. 3. The magnitude of the magnetic field $\tilde{B}_3$ on the string axis (the x^3-axis) for $\tilde{m} = 20$ is shown by the blue curve. The red curve shows the Coulomb force with an appropriate shift $x^3 \to x^3 - 22.8$. The yellow curve corresponds to $\tilde{H}_1$ on the x^3-axis. The region $\tilde{H}_1 = 0$ is in the Coulomb phase, and $\tilde{B}_3 \to 1$ at the vacuum $\langle 1 \rangle$ corresponds to the magnitude of the magnetic field at the center of the vortex string.

the magnetic flux spread for one side ($x^3 < X$) of the right boundary of the domain wall at $x^3 = X$. Thus the magnitude of the magnetic field from the boojum with $\tilde{\mathcal{M}}_{\mathrm{B}} = 4\pi$ is given by

$$\left|\vec{\tilde{B}}\right| = \frac{2}{(x^1)^2 + (x^2)^2 + (x^3 - X)^2}. \tag{3.5}$$

We show the magnetic flux $\tilde{B}_3(\rho = 0, x^3)$ on the x^3-axis for $\tilde{m} = 20$ in Fig. 3 and find that it asymptotically approaches the Coulomb law as

$$\tilde{B}_3(\rho = 0, x^3) \simeq \frac{-2}{(x^3 - 22.8)^2}, \quad x^3 \lesssim 20. \tag{3.6}$$

Thus, the boojum is identical to the magnetic point particle put at $X = 22.8$ with magnetic charge $\tilde{\mathcal{M}}_{\mathrm{B}} = 4\pi$ if it is observed from sufficiently far away. Since the boundary of the inner layer at the vortex string side is about $x^3 \sim 22$, it is quite natural that the above approximation works well.

Let us now leave the boojum and travel inside the domain wall along the x^1–x^2 plane. When we reach a distance much farther than the domain wall width $\sim 2\tilde{m}$, the magnetic flux expands as if in the two-dimensional plane. Therefore, the magnetic field should behave as $|\tilde{B}| \propto 1/\rho$. Thus, one may expect for $\rho \gg 2\tilde{m}$,

$$\tilde{B}_a = \frac{\tilde{\mathcal{M}}_{\mathrm{B}}}{2\pi\rho}\frac{x^a}{\rho} \quad (a = 1, 2), \tag{3.7}$$

where $2\pi\rho$ in the denominator is the circumference of a circle surrounding the boojum. However, this is too naive. We should not forget that the inner layer is not a two-dimensional plane, but it has thickness $\tilde{d}_{\mathrm{W}} = 2\tilde{m}$. Therefore, the magnetic field lines are parallelly distributed along the x^3-direction and, in effect, the magnetic charge is weakened by $1/2\tilde{m}$. Thus, the correct asymptotic behavior of the magnetic field for $\rho \gg 2\tilde{m}$ should be

$$\tilde{B}_a = \frac{\tilde{\mathcal{M}}_{\mathrm{B}}}{2\pi\tilde{d}_{\mathrm{W}}\rho}\frac{x^a}{\rho}, \qquad B_a = \frac{2\pi g^2 v^2}{m}\frac{x^a}{2\pi\rho^2}. \tag{3.8}$$

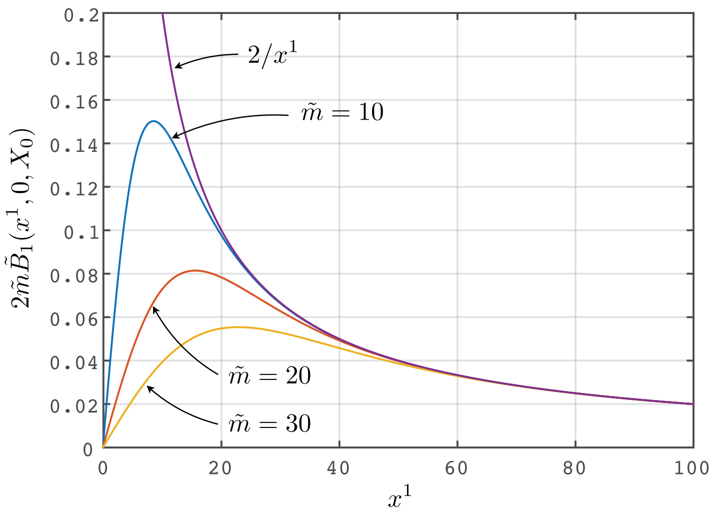

Fig. 4. A numerical verification for formula (3.8). We plot $2\tilde{m}\tilde{B}_1(x^1, 0, X_0)$ for $\tilde{m} = 10, 20, 30$, which is numerically obtained. All functions approach $\tilde{\mathcal{M}}_{\rm B}/(2\pi x^1) = 2/x^1$ for $x^1 > 2\tilde{m}$.

In order to verify this, in Fig. 4 we plot $\tilde{B}_1(x^1, 0, x^3 = X_0)$, where $x^3 = X_0$ is the center of the domain wall for $\tilde{m} = 10, 20, 30$. We read $x^3 = X_0$ at which σ becomes zero, and find $X_0 = 2.07, 2.26, 2.36$ for $\tilde{m} = 10, 20, 30$, respectively. As seen from Fig. 4, the numerical solution perfectly supports the formula (3.8). Thus, when seen from a distance, the boojum is suitable to be called a *magnetic monostick* of height $2\tilde{m}$.

3.2. *Collinear vortex strings from both sides*

Let us next consider collinear vortex strings ending on the domain wall from both sides. Since the tensions of the vortex strings are the same, the domain wall remains flat. For the $N_F = 2$ case with $M = (\tilde{m}/2, -\tilde{m}/2)$, such a configuration is given by the moduli matrix $H_0 = (z, z)$. The collinear vortex strings sit on the x^3-axis and the flat domain wall is at $x^3 = 0$. The corresponding master equation is

$$\left(\partial_3^2 + \partial_\rho^2 + \frac{1}{\rho}\partial_\rho\right) u - 1 + \rho^2 \left(\exp\left(\tilde{m}x^3\right) + \exp\left(-\tilde{m}x^3\right)\right) \exp\left(-u\right) = 0. \tag{3.9}$$

The correct global approximation for the solution of this equations reads (see the discussion below Eq. (5.9) in our previous paper Ref. [17])

$$\mathcal{U} = u_{\rm W}(x^3) + u_{\rm S}(\rho), \tag{3.10}$$

where $u_{\rm W}(x^3)$ is a solution of a single domain wall master equation that is obtained by putting $\partial_\rho = 1$ and $\rho = 1$ in Eq. (3.9), and where $u_{\rm S}(\rho)$ is a solution of the single vortex master equation that is obtained by setting $\partial_3 = 0$ and $x^3 = -\log(2)/\tilde{m}$ in Eq. (3.9).

To help us solve the gradient flow equation

$$\left(\partial_3^2 + \partial_\rho^2 + \frac{1}{\rho}\partial_\rho\right) U - 1 + \rho^2 \left(\exp\left(\tilde{m}x^3\right) + \exp\left(-\tilde{m}x^3\right)\right) \exp\left(-U\right) = \partial_t U, \tag{3.11}$$

we use the above global approximation as the initial condition,

$$U(\rho, x^3, t = 0) = u_{\rm W}(x^3) + u_{\rm S}(\rho). \tag{3.12}$$

We show three typical configurations at weak-gauge coupling with $\tilde{m} = 10, 20, 30$ in Fig. 5. The solution is symmetric under reflection through the x^1–x^2 plane. Since the domain walls have quite wide inner layers of the Coulomb phase, the upper and lower boojums are well isolated; see the panels in the middle column of Fig. 5. Incoming magnetic fluxes from the upper vortex string freely spread inside the domain walls, and then they are swallowed by the lower vortex string. There are no magnetic force lines going to infinity along the domain walls ($\rho = \infty$) due to flux conservation. The expanse of the magnetic flux inside the domain wall is of the same order as the width of the domain wall, as expected in Ref. [13]. We numerically integrate the boojum charge density and get $-\tilde{T}_{\rm B}/8\pi\tilde{m} = 1.95, 1.97, 1.98$ for $\tilde{m} = 10, 20, 30$, respectively. These numbers are in good agreement with the analytical result $-\tilde{T}_{\rm B}/8\pi\tilde{m} = 2$.

For observers sitting near the origin, the upper boojum is the fractional magnetic monopole with magnetic charge $\tilde{\mathcal{M}}_{\rm B} = 4\pi$, whereas the lower boojum is the fractional anti-magnetic monopole with $\tilde{\mathcal{M}}_{\bar{B}} = -4\pi$. The magnetic field observed by them should be a simple superposition,

$$\tilde{B}_i = \frac{\tilde{\mathcal{M}}_{\rm B}}{2\pi r_+^2}\frac{x^i - \delta^{i3}X}{r_+} + \frac{\tilde{\mathcal{M}}_{\bar{B}}}{2\pi r_-^2}\frac{x^i + \delta^{i3}X}{r_-}, \tag{3.13}$$

with $r_\pm = \left((x^1)^2 + (x^2)^2 + (x^3 \mp X)^2\right)^{1/2}$ and $X \geq 0$. In particular, the third element of the x^3-axis for $|x^3| \ll X$ is

$$\begin{aligned}\tilde{B}_3(\rho = 0, x^3) &= \frac{\tilde{\mathcal{M}}_{\rm B}}{2\pi(x^3 - X)^2}\frac{x^3 - X}{|x^3 - X|} + \frac{\tilde{\mathcal{M}}_{\bar{B}}}{2\pi(x^3 + X)^2}\frac{x^3 + X}{|x^3 + X|}\\ &= -\frac{2}{(x^3 - X)^2} - \frac{2}{(x^3 + X)^2}.\end{aligned} \tag{3.14}$$

The parameter X should be tuned to fit the numerically obtained solutions for each $\tilde{m}$. For example, we find $X = 11.2, 21.1, 31.0$ for $\tilde{m} = 10, 20, 30$ respectively; see Fig. 6. The right and the left boundaries of the inner layer are at $x^3 = \pm\tilde{m}$. So the boojums, fractional magnetic monopoles, are really stuck on the boundaries.

3.3. *Semilocal boojums, semilocal magnetic monostick*

So far, we have mostly considered an $N_F = 2$ model that has three kinds of topological objects: the domain wall, the vortex string, and the boojum. In the models with a higher number of flavors, $N_F > 2$, other kinds of topological objects enter the game. Namely, the semilocal vortex strings (Ref. [29]) and the semilocal boojums. They appear when some of the masses are degenerate. The minimal model is $N_F = 3$ with $\tilde{M} = \mathrm{diag}(\tilde{m}/2, \tilde{m}/2, -\tilde{m}/2)$. The model has a non-Abelian flavor symmetry SU(2) × U(1), and two isolated vacua: the first vacuum $\langle 1\rangle$ is determined by $|\tilde{H}_1|^2 + |\tilde{H}_2|^2 = 1$, $\tilde{H}_3 = 0$, and $\tilde{\sigma} = \tilde{m}/2$, while the second vacuum $\langle 2\rangle$ is determined by $\tilde{H}_1 = \tilde{H}_2 = 0$, $\tilde{H}_3 = 1$, and $\tilde{\sigma} = -\tilde{m}/2$. Thus, the vacuum manifold for $\langle 1\rangle$ is $\mathbb{C}P^1$, while that for $\langle 2\rangle$ is a point. The vortex string put in the degenerate vacuum $\langle 1\rangle$ is the so-called semilocal vortex string (Ref. [29]). The semilocal vortex string can change its transverse size with its tension preserved. Namely, it has a size moduli. To prevent confusion, a vortex string in the nondegenerate vacuum $\langle 2\rangle$ is sometimes called a local vortex string. The size-zero limit of the semilocal vortex string corresponds to the local vortex string.

Here we consider the 1/4 BPS configuration of the semilocal vortex string ending on the domain wall. Naturally, the boojum at the junction point changes its size with the semilocal string, therefore

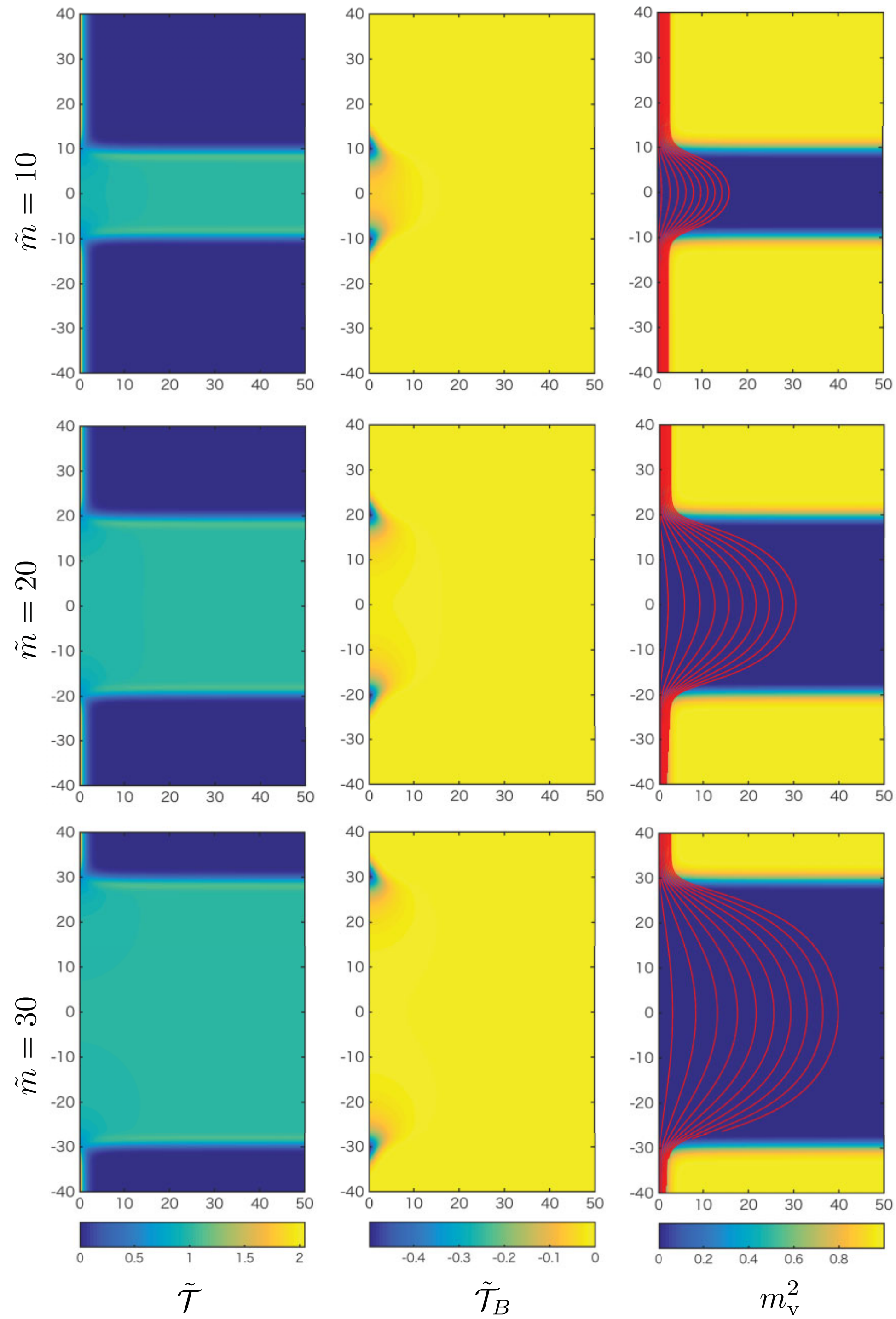

Fig. 5. Collinear vortex strings ending on the thick flat domain wall for the weak coupling region ($\tilde{m} = 10, 20, 30$). The panels in left, middle, and right columns show density plots of the total energy density $\tilde{\mathcal{T}}$, the boojum charge density $\tilde{\mathcal{T}}_\mathrm{B}$, and the photon mass square m_v^2, respectively. The red lines in the right column stand for the magnetic force lines incoming from the upper vortex string and outgoing to the lower one. The horizontal axis is ρ and the vertical one is x^3.

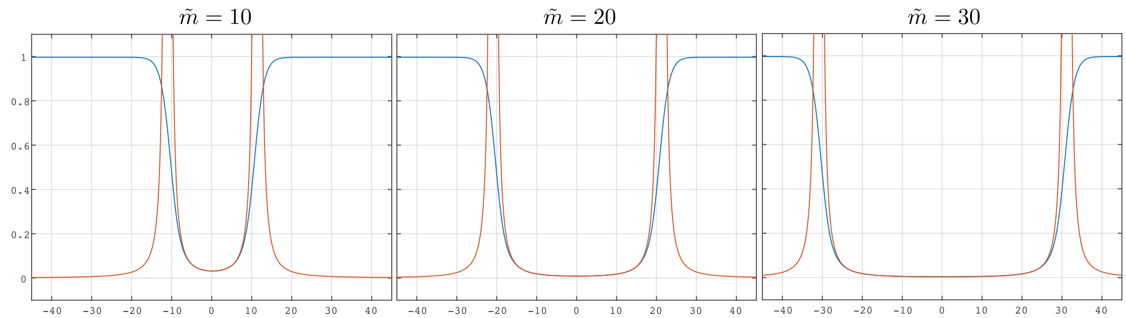

Fig. 6. The blue lines show the magnitude of $\tilde{B}_3$ on the string axis ($\rho = 0$), and are numerically obtained. The red lines correspond to the magnetic fields from the point-like monopole approximations given in Eq. (3.14) with $X = 11.2, 21.1, 31.0$ for $\tilde{m} = 10, 20, 30$. The horizontal axis is x^3.

we may call it a *semilocal boojum*. The simplest configuration is generated by the moduli matrix

$$H_0 = (z, a, 1), \tag{3.15}$$

where a is a complex constant. We can assume that a is a positive real number without loss of generality. This yields an axially symmetric configuration with the master equation

$$\left(\partial_3^2 + \partial_\rho^2 + \frac{1}{\rho}\partial_\rho\right) u - 1 + \left[(\rho^2 + a^2)\exp\left(\tilde{m}x^3\right) + \exp\left(-\tilde{m}x^3\right)\right]\exp(-u) = 0. \tag{3.16}$$

An appropriate initial configuration for the gradient flow equation for Eq. (3.16) is based on the suitable global approximation (see Eq. (5.12) in Ref. [17] for details)

$$U(x^3, \rho, t = 0) = u_{\mathrm{W}}\left(x^3 + \frac{1}{2\tilde{m}}u_{\mathrm{SLS}}\right) + \frac{1}{2}u_{\mathrm{SLS}}, \tag{3.17}$$

We show the numerical solutions with $\tilde{m} = 10$ (in the weak coupling region) and $a = 5, 10, 20$ in Fig. 7. This should be compared with the panels in the left column of Fig. 2, which shows $\tilde{m} = 10$ with $a = 0$ (the local vortex string and local boojum). Increasing the size of the parameter a, the cross-section of the semilocal vortex string grows linearly. At the same time, the semilocal boojum is inflated. Figure 7 clearly shows that the transverse size in the x^1–x^2 plane follows the semilocal vortex string but the vertical size along the x^3-axis is limited by the domain wall size.

Thanks to the moduli matrix formalism and the fact that all physical quantities can be expressed as a function of u, we can immediately conclude that the mass of the semilocal boojum is the same as that of the local boojum, namely

$$\tilde{T}_{\mathrm{SLB}} = -8\pi\tilde{m}, \qquad T_{\mathrm{SLB}} = -\frac{2\pi m}{g^2}. \tag{3.18}$$

This is because the change in the master equation involves only the replacement $\rho \to \left(\rho^2 + a^2\right)^{1/2}$, which does not affect the asymptotic behavior at the boundary where the boojum mass is calculated (compare with the discussion in Ref. [17]). Similarly, due to flux conservation, the magnetic charge of the semilocal boojum is

$$\tilde{\mathcal{M}}_{\mathrm{SLB}} = 4\pi, \qquad \mathcal{M}_{\mathrm{SLB}} = \frac{2\pi}{g}. \tag{3.19}$$

Thus, the quantum numbers of the semilocal boojum are the same as those for the local boojum. Where can we find the effect of the size moduli? It appears in Coulomb's law. When the boojum is

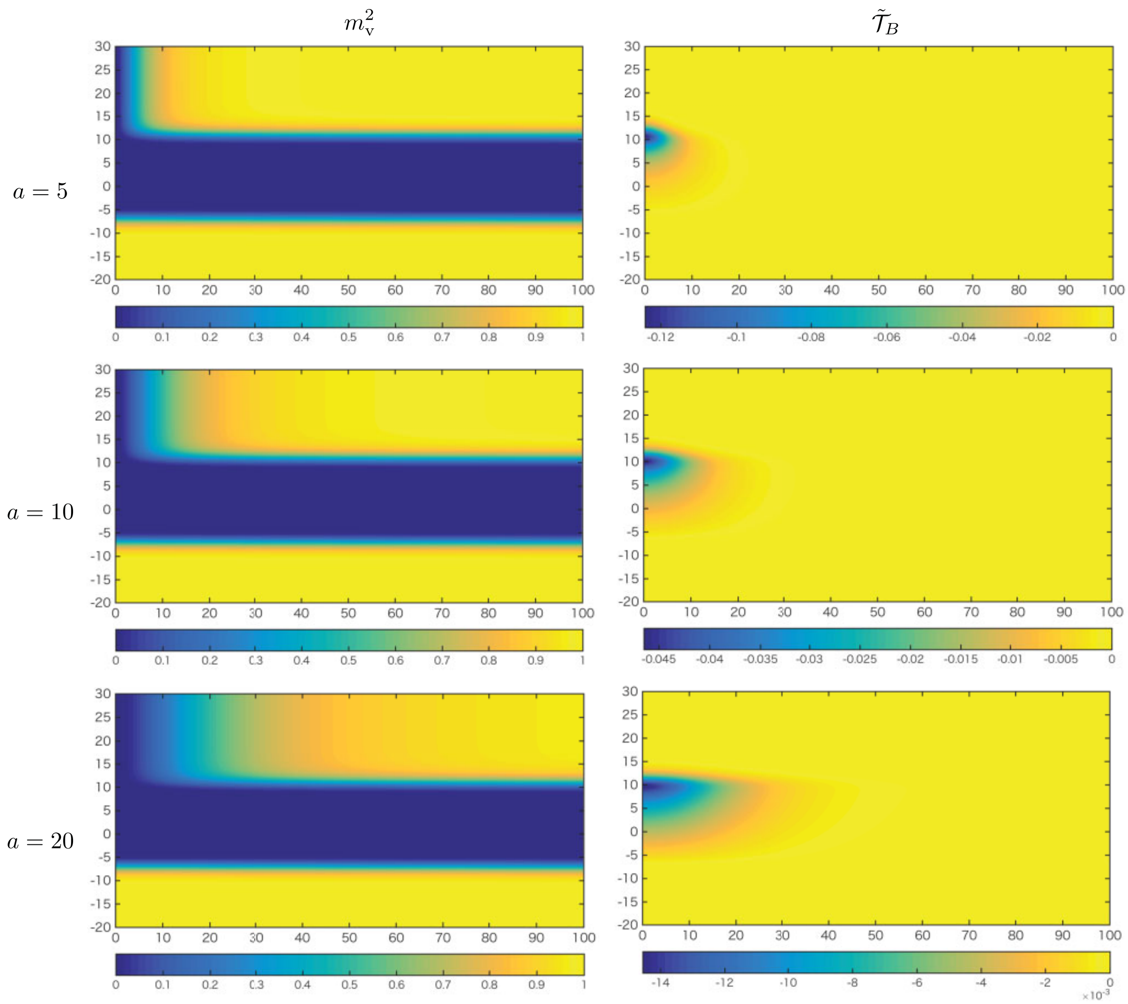

Fig. 7. Semilocal vortex string and semilocal boojum for $\tilde{m} = 10$ and $a = 5, 10, 20$ (top, middle, bottom). The left panels show $m_v^2 = |\tilde{H}_1|^2 + |\tilde{H}_3|^2$ and the boojum charge density is plotted in the right panels.

seen far from the string axis, the magnetic field should spread according to the $(1+2)$-dimensional Coulomb law as in Eq. (3.8) for the local boojum. In the semilocal case, we find the following modified Coulomb law:

$$\tilde{B}_b = \frac{\tilde{\mathcal{M}}_{\rm SLB}}{2\pi \tilde{d}_{\rm W}} \frac{x^b}{\rho^2 + a^2}, \quad B_b = \frac{2\pi g^2 v^2}{m} \frac{x^b}{2\pi(\rho^2 + a^2)}, \quad \text{for} \quad \rho \gg a, \tag{3.20}$$

with $b = 1, 2$ and $\tilde{d}_{\rm W} = 2\tilde{m}$. We compare it with the numerically obtained magnetic field for $\tilde{m} = 10$ and $a = 5$, 20 in Fig. 8, by plotting $\tilde{B}_1(x^1, 0, x^3 = X_0)$ with $X_0 = 2.07$ (and $\tilde{\sigma}(x^3 = X_0) = 0$ as before). We also show the magnetic field with $a = 0$ (the ordinary Coulomb law). As clearly seen in Fig. 8, the modified Coulomb law reproduces the numerical result much better than the normal Coulomb law.

If we extrapolate the magnetic field in Eq. (3.20) to $\rho = 0$, it implies the following $(1+2)$-dimensional Gauss law for the magnetic field:

$$\partial_a \tilde{B}_a = \tilde{f}, \qquad \tilde{f} \simeq \frac{\tilde{\mathcal{M}}_{\rm SLB}}{4\pi \tilde{m}} \frac{2a^2}{\left(\rho^2 + a^2\right)^2}. \tag{3.21}$$

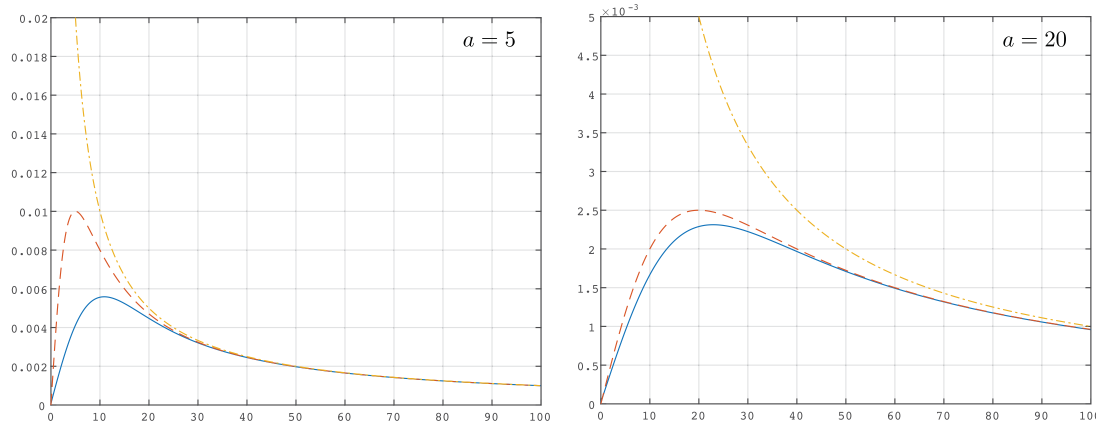

Fig. 8. The modified Coulomb law $\tilde{B}_1(x^1, 0, x^3 = 2.07)$ for $\tilde{m} = 10$ given in Eq. (3.20) is plotted (red dashed line). The blue solid line shows the numerical result and the yellow dot-dashed line is the normal Coulomb law. The left (right) panel corresponds to the case with $a = 5$ ($a = 20$). The horizontal axis is x^1.

Therefore, the semilocal boojum is not point like. Roughly speaking, the magnetic charge is distributed into a cylinder of height $2\tilde{m}$ and radius $\rho = a$. Thus, a semilocal boojum is suitable to be called a *semilocal magnetic monostick*.

Finally, we show collinear semilocal vortex strings with different sizes ending on the domain wall. A minimal model for this is $N_F = 4$ with $\tilde{M} = \mathrm{diag}(\frac{\tilde{m}}{2}, \frac{\tilde{m}}{2}, -\frac{\tilde{m}}{2}, -\frac{\tilde{m}}{2})$. The moduli matrix is $H_0 = (z, a_1, z, a_2)$. A suitable initial function for the gradient flow equation in this case is

$$U(\rho, x^3, t = 0) = u_{\mathrm{W}} \left(x^3 + \frac{u_{\mathrm{SLS}}(a_1) - u_{\mathrm{SLS}}(a_2)}{2\tilde{m}} \right) + \frac{u_{\mathrm{SLS}}(a_1) + u_{\mathrm{SLS}}(a_2)}{2}. \tag{3.22}$$

The domain wall is asymptotically flat, but it can be logarithmically bent around the junction point when the sizes of two strings are very different. Such local bending is visible in the strong-gauge coupling limit $\tilde{m} \ll 1$. In Fig. 9, we show two typical configurations that have two collinear strings, the single local vortex string ($a_2 = 0$) from the $x^3 < 0$ side and the single very fat semilocal vortex string with $a_1 = 30$ from the $x^3 > 0$ side, ending at the domain wall for $\tilde{m} = 1/5$ (strong-gauge coupling) and $\tilde{m} = 20$ (weak-gauge coupling). The domain wall bends steeply near the collinear string axis for $\tilde{m} = 1/5$, but it becomes asymptotically flat at large ρ due to the balance of the tensions of the two vortex strings. On the other hand, the domain wall tension becomes sufficiently large for $\tilde{m} = 20$, so that the local curving structure near the string axis is almost invisible. The well-squeezed magnetic flux tube from the local vortex string is magnified when it goes into the semilocal vortex string as is shown in the right panels of Fig. 9. This is a lens effect for the magnetic force lines.

3.4. *Strong coupling regime*

Let us next consider the strong-gauge coupling limit[2] where the kinetic term of the gauge field disappears in the Lagrangian (2.1), and the Higgs fields are restricted to satisfy $HH^\dagger = v^2$. Because

[2] In this subsection, we will use the original variables x^μ, m, and so on.

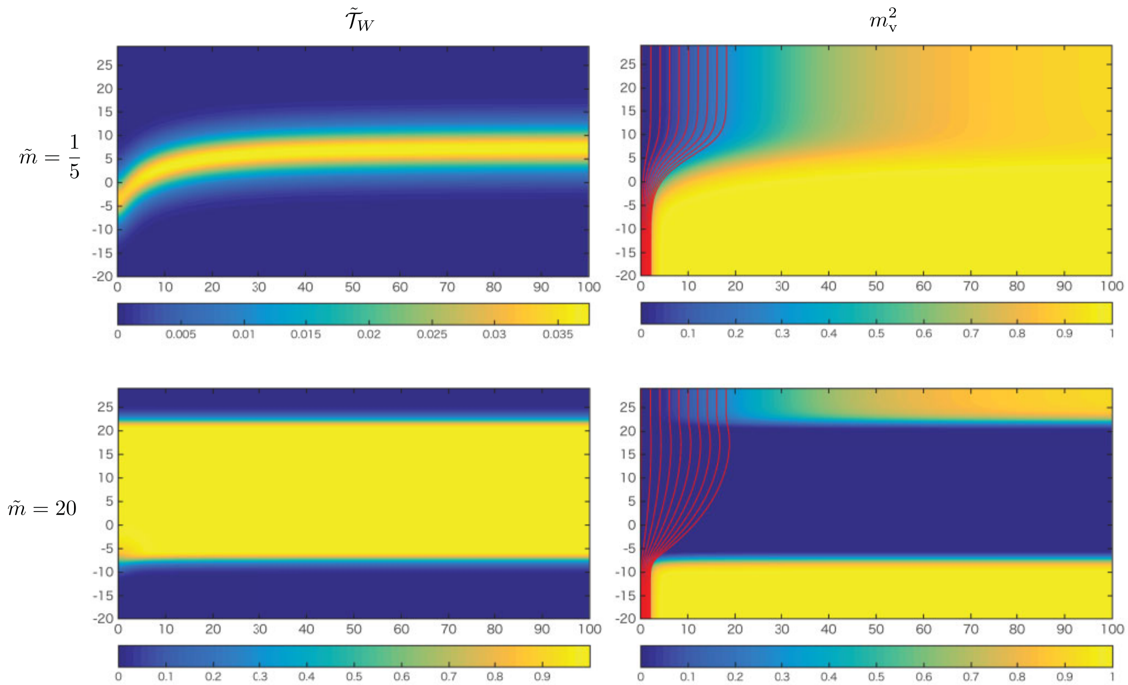

Fig. 9. The collinear semilocal vortex strings with $a_2 = 0$ from blow and $a_1 = 30$ from top end on the asymptotically flat domain wall. The domain wall energy density $\tilde{\mathcal{T}}_{\mathrm{W}}$ and $m_{\mathrm{v}}^2 = |\tilde{H}_1|^2 + |\tilde{H}_3|^2$ are shown in the left and right panels, respectively. The horizontal axis is ρ and the vertical axis is x^3.

of this, the domain wall has no internal structure, namely both inside and outside the domain wall are in the Higgs phase. The gauge fields are infinitely heavy and no longer dynamical. Indeed, their equations of motion give

$$A_\mu = \frac{-i}{2v^2}\left(H\partial_\mu H^\dagger - \partial_\mu H H^\dagger\right). \tag{3.23}$$

As a result, the Abelian-Higgs model with N_F flavor reduces to the massive $\mathbb{C}P^{N_F-1}$ nonlinear sigma model. One can introduce fictitious electromagnetic fields by $F_{\mu\nu} = \partial_\mu A_\nu - \partial_\nu A_\nu$ from the gauge fields given above as

$$F_{\mu\nu} = \frac{-i}{v^2}\left(\partial_\mu H \partial_\nu H^\dagger - \partial_\nu H \partial_\mu H^\dagger\right). \tag{3.24}$$

The BPS equations and the energy formulae obtained in Sect. 2 remain unchanged except for dropping the terms proportional to $1/g^2$. Furthermore, the moduli matrix formalism explained in Sect. 2.2 still works without any changes. One advantage is that the master equation is exactly solvable:

$$u_{g\to\infty} = \log\Omega_0 = \log H_0 \exp\left(2\eta M x^3\right) H_0^\dagger. \tag{3.25}$$

In the following we will set $\eta = \xi = +1$. Let us take the simplest example of a singular lump string (singular at a spatial infinity) ending on the domain wall, which is generated by the moduli matrix $H_0 = (z, 1)$ in the $N_F = 2$ model with $M = (m/2, -m/2)$. The exact solution is given by

$$u_{g\to\infty} = \log\left(\rho^2 \exp\left(m x^3\right) + \exp\left(-m x^3\right)\right). \tag{3.26}$$

The domain wall's position can be read from the condition $\rho^2 \exp\left(mx^3\right) = \exp\left(-mx^3\right)$, namely, it is given by

$$x^3 = -\frac{1}{m}\log\rho. \tag{3.27}$$

The fictitious magnetic flux given in Eq. (3.24) can be easily calculated by making use of formulae (2.17) as

$$B_a = \frac{2mx^a}{\left(\rho^2 \exp\left(mx^3\right) + \exp\left(-mx^3\right)\right)^2}, \qquad B_3 = -\frac{2}{\left(\rho^2 \exp\left(mx^3\right) + \exp\left(-mx^3\right)\right)^2}. \tag{3.28}$$

At the domain wall, the $a = 1, 2$ components become

$$B_a\Big|_{x^3=-(1/m)\log\rho} = \frac{m}{2}\frac{x^a}{\rho^2}. \tag{3.29}$$

Similarly, the configuration with one regular lump string of size a ending on the domain wall given by $H_0 = (z, a, 1)$ in the $N_F = 3$ model with $M = (m/2, m/2, -m/2)$ can be obtained by just replacing $\rho \to \left(\rho^2 + a^2\right)^{1/2}$ in the above results. Therefore, the $a = 1, 2$ components of the magnetic flux at the domain wall are given by

$$B_a\Big|_{x^3=-(1/m)\log\left(\rho^2+a^2\right)^{1/2}} = \frac{m}{2}\frac{x^a}{\rho^2 + a^2}. \tag{3.30}$$

3.5. *The magnetic scalar potential*

As observed in the previous subsections, the boojum, precisely speaking the ending point of the vortex string on the domain wall, can be regarded as the magnetic source inside the domain wall. In order to pursue the identification, let us introduce the *magnetic* scalar potential, whose gradient gives the $a = 1, 2$ components of the magnetic fields:

$$B_a = -\partial_a\varphi(x^b) \quad (a = 1, 2). \tag{3.31}$$

In this subsection, we will use the original variables x^μ, m, and so on, and we will concentrate on $B_{a=1,2}$ only, while ignoring the third component B_3.

3.5.1. *Strong coupling limit*

Let us first consider the strong-gauge coupling limit where the magnetic fields are given as in Eq. (3.29). The magnetic scalar potential for this is given by

$$\varphi = -\frac{q_B}{2\pi}\log\rho, \qquad q_B = m\pi. \tag{3.32}$$

Since $\partial_a^2(\log\rho)/2\pi = \delta^{(2)}(x^a)$, we see that the singular lump string can be thought of as a point magnetic source with charge q_B:

$$\partial_a B_a = -\partial_a^2\varphi = q_B\delta^{(2)}(x^a). \tag{3.33}$$

This identification of the lump string with the point magnetic source is consistent with the fact that the lump string is asymptotically singular far away from the domain wall.

The magnetic charge $q_B = m\pi$ can be understood as follows. The total magnetic flux coming from the lump string is 2π. Furthermore (as explained in Sect. 3.1.1 of Ref. [17]), the width of the domain wall in the strong-gauge coupling is given by $d_\mathrm{W} = 2/m$. Thus, the mean value of the total magnetic flux going through the center of the domain wall corresponds to the magnetic charge

$$\frac{2\pi}{d_\mathrm{W}} = m\pi = q_B. \tag{3.34}$$

Now we come across an interesting coincidence: the domain wall curve given in Eq. (3.27) and the magnetic scalar potential introduced in Eq. (3.32) are related as

$$\varphi = \frac{m^2}{2}x^3 = \frac{mx^3}{d_\mathrm{W}}. \tag{3.35}$$

The factor m^2 is needed for consistency of the mass dimension. If we integrate all the magnetic flux going through the domain wall, we have the total magnetic scalar potential

$$\Phi = d_\mathrm{W}\varphi = mx^3. \tag{3.36}$$

This coincidence tells us that the wall curve function $x^3(\rho)$ gives the magnetic scalar potential.

This is quite similar to another identification of an endpoint of the singular lump string on the domain wall in the massive $\mathbb{C}P^1$ nonlinear sigma model to an *electric* point source of a *dual* electromagnetic field on the $(2+1)$-dimensional domain wall, world volume theory (Ref. [10]), as will be studied in Sect. 6. In this section, however, we do not take the dual viewpoint and we deal with the magnetic field of the original U(1) gauge field.

The endpoint of the finite size lump string on the domain wall can be similarly regarded as a magnetic source and as a source with finite size magnetic density. The magnetic scalar potential leading to Eq. (3.30) is given by

$$\varphi = -\frac{q_B}{4\pi}\log(\rho^2 + a^2). \tag{3.37}$$

As in the case of the singular lump string, the same relation (3.35) between the magnetic scalar potential and the wall curve function holds.

3.5.2. *Weak coupling regime*

Let us next consider the finite-gauge coupling limit in which the vortex string has finite size of order $1/gv$. The boojum also has finite size, so that it should be identified with a magnetic source with finite size distribution in $2+1$ dimensions. In the finite-gauge coupling, the domain wall's position in terms of the original variables is given as (compare with Eq. (3.38) in Ref. [17])

$$x^3(\rho) = -\frac{1}{2m}u_\mathrm{S}(\rho). \tag{3.38}$$

Now we identify this wall curve function with the magnetic scalar potential by Eq. (3.35). Before doing this, let us remember that the width of the domain wall in the weak-gauge coupling region is $d_{\rm W} = m/g^2v^2$. Thus the magnetic scalar potential in the weak-gauge coupling region is given by

$$\varphi = \frac{mx^3}{d_{\rm W}} = -\frac{g^2v^2}{2m}u_{\rm S}. \tag{3.39}$$

Since $u_{\rm S}$ is asymptotically $\log\rho^2$, we read the magnetic charge as

$$q_B = \frac{2\pi g^2v^2}{m} = \frac{2\pi}{d_{\rm W}}. \tag{3.40}$$

This is consistent with the observation in the strong-gauge coupling limit given in Eq. (3.34).

Let us verify whether the magnetic scalar potential correctly reproduces the numerical results explained in Sect. 3. The corresponding magnetic field obtained from the magnetic scalar potential (3.39) is

$$B_a = \frac{q_B}{4\pi}\partial_a u_{\rm S}. \tag{3.41}$$

This asymptotically behaves as

$$B_a \to \frac{q_B}{4\pi}\partial_a \log\rho^2 = \frac{2\pi g^2v^2}{m}\frac{x^a}{2\pi\rho^2} \quad (\rho\to\infty), \tag{3.42}$$

which perfectly agrees with the previous result given in Eq. (3.8).

Distribution of the magnetic charge density can be found as

$$-\partial_a^2\varphi = \frac{q_B}{4\pi}\partial_a^2 u_{\rm S} = -q_B\frac{F_{12}}{2\pi}. \tag{3.43}$$

Thus, we are lead to a quite reasonable magnetic density $F_{12}/2\pi$, which corresponds to the magnetic field made by the vortex string.

The same can be said for the semilocal boojum studied in Sect. 3.3. The domain wall's position can be read from Eq. (3.17), leading to the magnetic scalar potential

$$\varphi = -\frac{q_{\rm SLB}}{4\pi}u_{\rm SLS} \to -\frac{q_{\rm SLB}}{4\pi}\log(\rho^2+a^2) \quad (\rho\to\infty), \tag{3.44}$$

with $q_{\rm SLB} = 2\pi g^2v^2/m$. From this, one can compute the asymptotic magnetic field as

$$B_b = -\partial_b\varphi \to \frac{q_{\rm SLB}}{4\pi}\frac{2x^b}{\rho^2+a^2} = \frac{2\pi g^2v^2}{m}\frac{x^b}{2\pi(\rho^2+a^2)}. \tag{3.45}$$

Again, this perfectly agrees with the previous result given in Eq. (3.20).

We plot the magnetic scalar potentials in Fig. 10 for the strong-gauge coupling limit and the finite-gauge coupling case. In the left panel, the red curve shows the potential made by the point magnetic source at the origin that corresponds to the endpoint of the singular lump string in the strong-gauge coupling limit. When the gauge coupling is finite, the string size becomes finite of order $1/gv$, and the charge distribution gets fat with the same size. Then the magnetic potential shown by the blue curve in the left panel becomes regular at the origin. In the right panel, we show similar potentials for the semilocal configurations with moduli matrix $H_0 = (z, a, 1)$ and mass

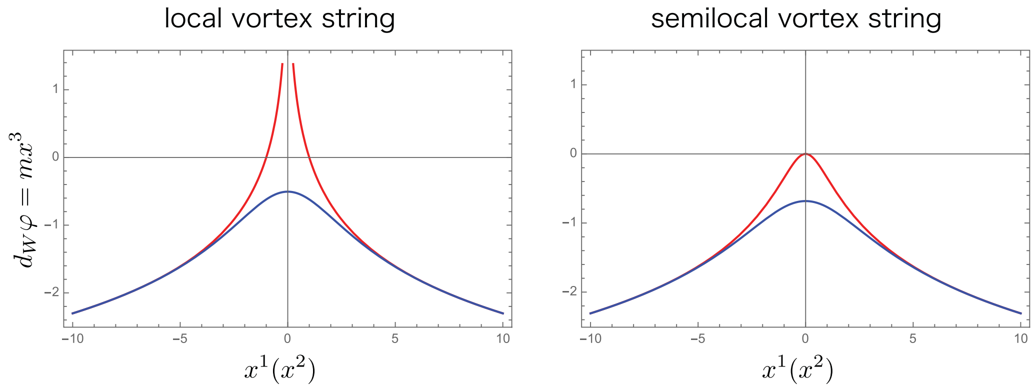

Fig. 10. The magnetic scalar potentials corresponding to a local vortex string (singular lump string) in the left panel and a semilocal vortex string (regular lump string) with size moduli $a = 1$ in the right panel for the strong-gauge coupling limit (red) and finite-gauge coupling (blue). The horizontal axes are in units of $1/\sqrt{2}gv$.

matrix $M = (m/2, m/2, -m/2)$. We set $a = 1$ so that the semilocal strings are nonsingular even in the strong-gauge coupling limit.

The magnetic scalar potential can be explained in a different way at a more technical level as follows. The exact formula for the magnetic field reads

$$B_a = \partial_a \left(\frac{1}{2} \partial_3 u \right), \tag{3.46}$$

where u is a solution to the master equation for the full 1/4 BPS equations. Therefore, we should extract the magnetic scalar potential φ from $\partial_3 u/2$. How can we do it? A hint is in the approximate solution

$$\mathcal{U}(x^k) = u_{\mathrm{W}} \left(x^3 + \frac{1}{2m} u_{\mathrm{S}}(x^a) \right) + u_{\mathrm{S}}(x^a). \tag{3.47}$$

Let us evaluate $\partial_a \partial_3 \mathcal{U}$ on the domain wall's position $x^3 = -u_{\mathrm{S}}/2m$. We find

$$\begin{aligned} \partial_3 \partial_a \mathcal{U}\big|_{x^3=-u_{\mathrm{S}}/2m} &= \partial_3 \left[\left(\frac{\partial_a u_{\mathrm{S}}}{2m} \right) u'_{\mathrm{W}} \left(x^3 + \frac{1}{2m} u_{\mathrm{S}} \right) \right]_{x^3=-u_{\mathrm{S}}/2m} \\ &= \partial_a \left(\frac{u''_{\mathrm{W}}(0)}{2m} u_{\mathrm{S}} \right), \end{aligned} \tag{3.48}$$

where the prime stands for an x^3 derivative. From Eq. (2.17), we have $\sigma = \partial_3 u_{\mathrm{W}}/2$, so that $u''_{\mathrm{W}}(0)/2$ corresponds to $\sigma'(0)$, namely the derivative of σ at the center of the domain wall. Furthermore, σ transits from $-m/2$ to $m/2$ inside the domain wall of thickness d_{W} (Ref. [17]). Thus, we have $u''_{\mathrm{W}}(0)/2 = \sigma'(0) = m/d_{\mathrm{W}}$. Combining all the pieces, we reach the desired result

$$B_a\big|_{x^3=-u_{\mathrm{S}}/2m} = -\partial_a \varphi, \qquad \varphi = -\frac{u_{\mathrm{S}}}{2d_{\mathrm{W}}} = \frac{mx^3}{d_{\mathrm{W}}}. \tag{3.49}$$

In summary, we have found that the solution u_{S} to the master equation for the vortex string gives the magnetic scalar potential for $B_{a=1,2}$.

4. A magnetic capacitor

In this section, we will study the 1/4 BPS solutions that have multiple vortex strings aligned in a line attached to one or both sides of the domain wall in the model with $N_F = 2$ and $M = (\tilde{m}/2, -\tilde{m}/2)$. We have already studied similar configurations in Sect. 4 of our previous paper Ref. [17]. For completeness, let us repeat the corresponding master equation

$$\partial_k^2 u = 1 - \left(|P_{n_1}|^2 \exp\left(\tilde{m}x^3\right) + |P_{n_2}|^2 \exp\left(-\tilde{m}x^3\right)\right) \exp(-u), \tag{4.1}$$

for which an appropriate global approximation is given as

$$\mathcal{U}(x^k) = u_{\mathrm{W}}\left(x^3 + \frac{u_{\mathrm{S}}^{(n_1)} - u_{\mathrm{S}}^{(n_2)}}{2\tilde{m}}\right) + \frac{u_{\mathrm{S}}^{(n_1)} + u_{\mathrm{S}}^{(n_2)}}{2}, \tag{4.2}$$

where $u_{\mathrm{W}}(x^3)$ is the domain wall solution and $u_{\mathrm{S}}^{(n)}(x^1, x^2)$ is the n vortex string solution to the master equation

$$(\partial_1^2 + \partial_2^2) u_{\mathrm{S}}^{(n)} - 1 + |P_n|^2 \exp\left(-u_{\mathrm{S}}^{(n)}\right) = 0. \tag{4.3}$$

4.1. *Linearly aligned vortex strings ending on a domain wall from one side*

First, we align n_1 vortex strings in vacuum $\langle 1\rangle$ on a line, while we set no vortex strings in the opposite vacuum $\langle 2\rangle$. More precisely, we will consider the moduli matrix $H_0 = (P_{n_1}(z),\ P_{n_2}(z))$ with

$$P_{n_1}(z) = \exp(-\tilde{m}X/2) \prod_{k=-(n_1-1)/2}^{(n_1-1)/2} (z - Lk), \quad P_{n_2=0}(z) = \exp(\tilde{m}X/2), \tag{4.4}$$

where L and X are real constants. For this moduli matrix, the n_1 string axes in vacuum $\langle 1\rangle$ are aligned on the x^1-axis with the separation L. The other real parameter X is introduced to shift the configuration along the x^3-direction.

In Fig. 11, we show two examples, for $n_1 = 7$ and $n_1 = 15$. We set $X = 20$ for $n_1 = 7$ and $X = 40$ for $n_1 = 15$, and $L = 3$ for both solutions. Since the vortex strings are degenerate if they are seen very far from the junction points, the asymptotic bending of the domain wall is logarithmic $\sim \log \rho^{2n_1}$. However, the structure near the junction points is not logarithmic. The (b1) panels of Fig. 11 show the domain wall energy density on the cross section at $x^1 = 0$. Increasing the number of aligned vortex strings, the domain wall at the vicinity of junction points becomes locally flat. The area of the flat region increases if we put more and more vortex strings on the line.

The emergence of the flat part can be understood as follows. As before, the domain wall's position can be read from the master equation as

$$x^3(x^1, x^2) = -\frac{1}{2\tilde{m}} u_{\mathrm{S}}^{(n_1)}(x^1, x^2) + X, \tag{4.5}$$

where $u_{\mathrm{S}}^{(n_1)}$ is a solution of the vortex master equation

$$\partial_a^2 u_{\mathrm{S}}^{(n_1)} - 1 + \prod_k |z - kL|^2 \exp\left(-u_{\mathrm{S}}^{(n_1)}\right) = 0. \tag{4.6}$$

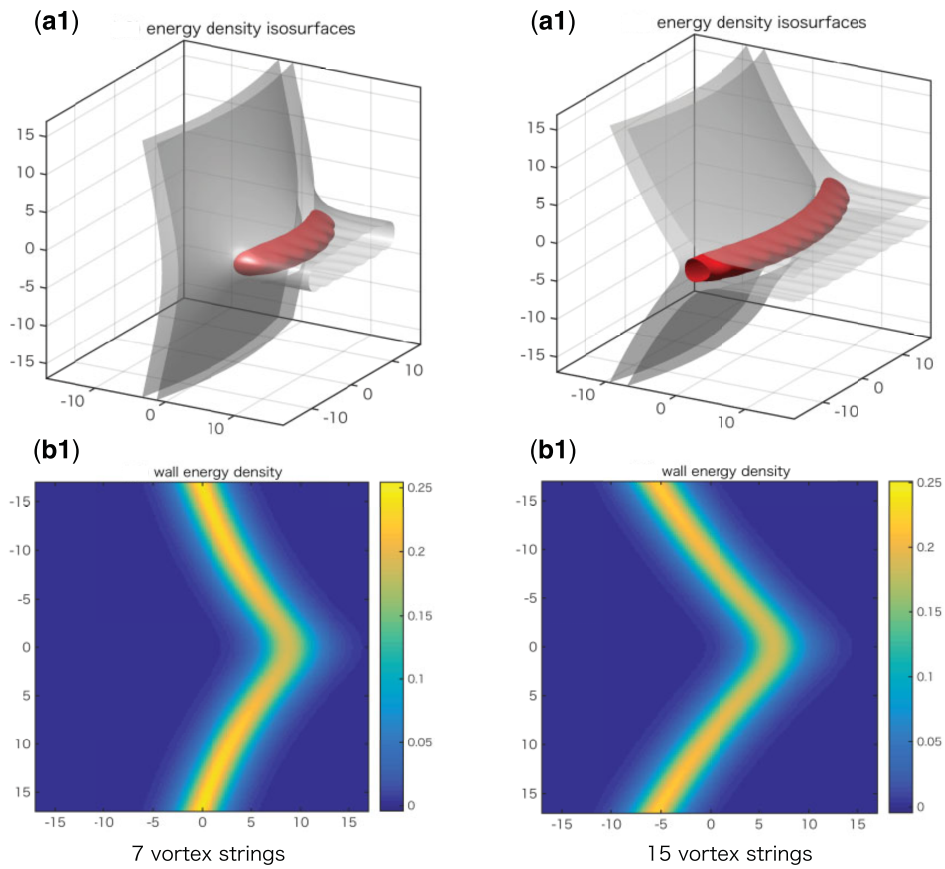

Fig. 11. The $n_1 = 7$ (left) and $n_1 = 15$ (right) vortex strings ending on the domain wall from one side. The separation of neighboring strings is $L = 3$. The gray surfaces in the (a1) panels are energy density isosurfaces and the red ones correspond to boojum charge density isosurfaces. The (b1) panels show the domain wall energy density on the cross section at $x^2 = 0$.

If the separation L is sufficiently larger than 1, the solution $u_{\mathrm{S}}^{(n_1)}$ to the vortex master equation can be well approximated by a simple superposition of $u_{\mathrm{S}}^{(1)}$ as

$$u_{\mathrm{S}}^{(n_1)}(x^1, x^2) \simeq \hat{u}_{\mathrm{S}}^{(n_1)}(x^1, x^2) \equiv \sum_k u_{\mathrm{S}}^{(1);k}(x^1, x^2) \quad (L \gg 1), \tag{4.7}$$

where $u_{\mathrm{S}}^{(1);k}(x^1, x^2)$ is the single vortex string at $z = kL$, namely the solution to the master equation

$$\partial_a^2 u_{\mathrm{S}}^{(1);k} - 1 + |z - kL|^2 \exp\left(-u_{\mathrm{S}}^{(1);k}\right) = 0. \tag{4.8}$$

In the region around $z = kL$, we have $u_{\mathrm{S}}^{(1);k'} \simeq \log|z - k'L|^2$ for $k' \neq k$. Therefore, the approximate solution there becomes

$$\hat{u}_{\mathrm{S}}^{(n_1)}(x^1, x^2) = u_{\mathrm{S}}^{(1);k} + \sum_{k'(\neq k)} \log|z - k'L|^2 \quad (|z - kL| \ll 1). \tag{4.9}$$

Plugging this into Eq. (4.6), one can confirm that the approximation works well.

Thus, the domain wall's position in the $x^1 = 0$ plane is approximated by

$$x^3(0, x^2) \simeq -\frac{1}{2\tilde{m}} \sum_k \hat{u}_{\mathrm{S}}^{(1);k}(0, x^2) + X,$$

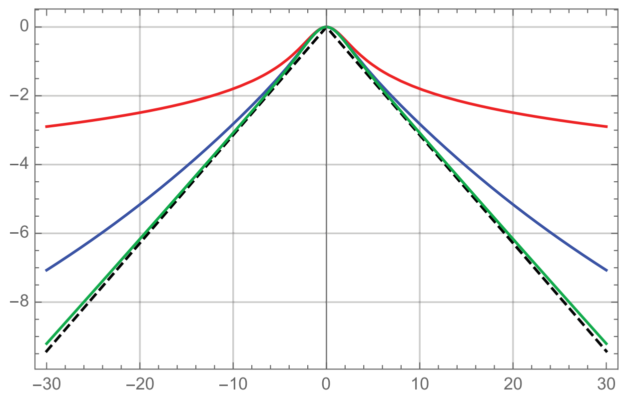

Fig. 12. The approximate solution $-\frac{1}{2}\left(\hat{u}_{\mathrm{S}}^{(n_1)}(x^1=0,x^2)-\hat{u}_{\mathrm{S}}^{(n_1)}(0,0)\right)$ is shown for $n_1=1$ (red), $n_1=7$ (blue), and $n_1=101$ (green). The black dashed line is $-\frac{\pi}{L}|x^2|$, where L is set to be 10.

$$\sim -\frac{1}{2\tilde{m}}\sum_k \log\left((x^2)^2+k^2L^2\right)+X. \tag{4.10}$$

We choose $X=(\sum_k \log kL)/\tilde{m}$, so that the junction point at $z\simeq 0$ is independent of k. In Fig. 12 we show $x^3(0,x^2)$ for $n_1=1,\,7,\,101$ and for $L=10$ and $\tilde{m}=1$. The domain wall becomes linear as n_1 is increased, and it gets close to the following linear function at $n_1\to\infty$ limit:

$$\begin{aligned}
\lim_{n_1\to\infty}\tilde{m}x^3(0,x^2) &= -\frac{1}{2}\sum_{k=-\infty}^{\infty}\log\left((x^2)^2+k^2L^2\right)+\sum_{k=1}^{\infty}\log(kL)\\
&= -\log|x^2|-\sum_{k=1}^{\infty}\log\left(1+\frac{(x^2)^2}{k^2L^2}\right)\\
&= -\log|x^2|-\log\frac{\sinh\frac{\pi|x^2|}{L}}{\frac{\pi|x^2|}{L}}\\
&= -\log\sinh\frac{\pi|x^2|}{L}-\log\frac{L}{2\pi}\\
&\to -\frac{\pi}{L}|x^2|-\log\frac{L}{2\pi}\quad(\pi|x^2|\gg L),
\end{aligned} \tag{4.11}$$

where we have used the relation $\prod_{k=1}^{\infty}\left(1+\frac{\alpha^2}{k^2}\right)=\frac{\sinh\pi\alpha}{\pi\alpha}$.

There is a nice physical observation that explains the appearance of the factor π/L in the asymptotic angle of the flat domain wall. From the viewpoint of the domain wall, the endpoints of vortex strings are interpreted as the magnetic sources in a $(2+1)$-dimensional sense. Consider the magnetic scalar potential defined by

$$\tilde{\varphi}(x^1,x^2)=\frac{\tilde{m}}{\tilde{d}_{\mathrm{W}}}x^3(x^1,x^2)=\frac{-1}{2\tilde{d}_{\mathrm{W}}}u_{\mathrm{S}}^{(n_1)}(x^1,x^2). \tag{4.12}$$

Suppose that we have infinite point-like magnetic sources on a line, say the x^1-axis, with period L. Due to the symmetry of this source arrangement, the magnetic force lines far from the x^1-axis become parallel to the x^2-axis. There is one magnetic source of the magnetic charge $\tilde{q}_B=2\pi/\tilde{d}_{\mathrm{W}}$ (see the

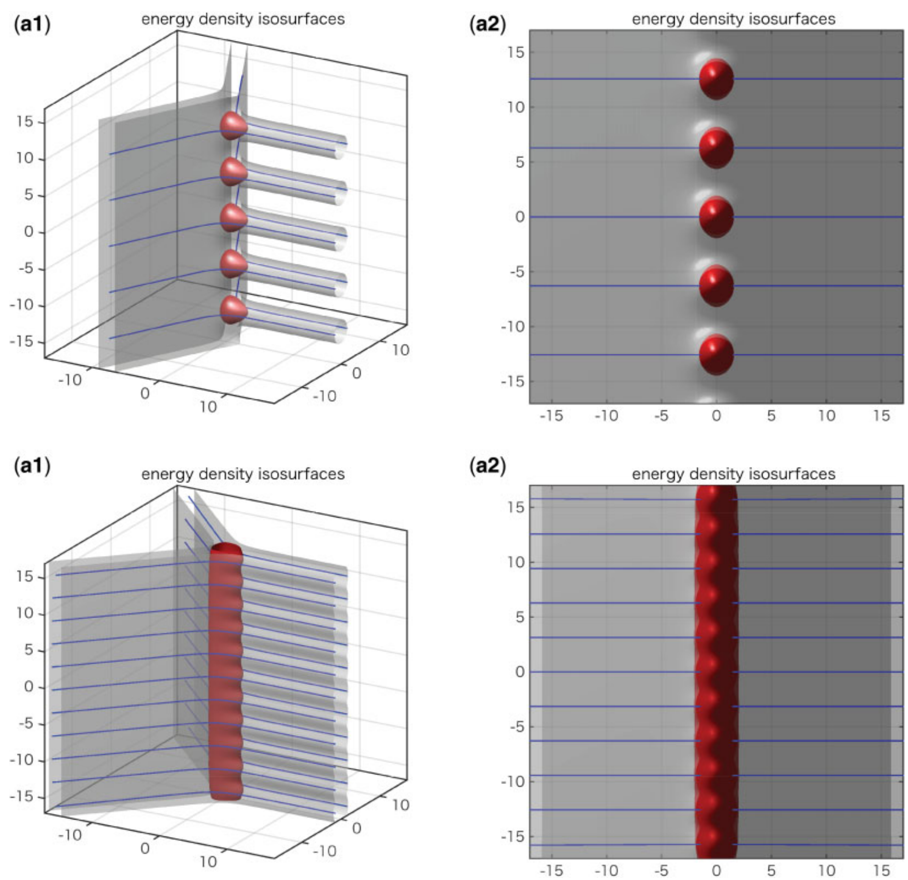

Fig. 13. Periodically aligned vortex strings with period 2π (upper panels) and π (lower panels) are shown. The gray surfaces show the energy density isosurfaces, the red surfaces show the boojum density isosurfaces, and the blue lines show several magnetic force lines.

discussions in Sect. 3.5) at every finite segment $x^1 \in [x_0, x_0 + L]$ for an arbitrary x_0. Therefore, seen far from the sources, the magnetic charge density is $\tilde{q}_B/L$. The magnetic force lines from these sources expand equally to both the $x^2 > 0$ and the $x^2 < 0$ regions. Thus, we should have

$$\tilde{\varphi} \simeq -\frac{\tilde{q}_B}{2L}|x^2| = -\frac{\pi}{\tilde{d}_{\mathrm{W}} L}|x^2|. \tag{4.13}$$

Combining this with Eq. (4.12), we correctly find the asymptotic behavior given in Eq. (4.11).

In order to get vortex strings periodically aligned on a line, it is better to use holomorphic trigonometric functions rather than polynomial functions (Ref. [31]). For example, we choose the moduli matrix

$$H_0 = (\sin i\eta z,\ 1). \tag{4.14}$$

The positions of the vortex strings correspond to the zeros of the first elements, namely $z = (\pi i/\eta)n$ ($n \in \mathbb{Z}$). An advantage of using the trigonometric function is that one does not need to shift the domain wall's position by adjusting the X parameter for the polynomial case in Eq. (4.4). In Fig. 13, we show two examples with sparsely aligned ($\eta = 1/2$: the period is 2π) and densely aligned ($\eta = 1$: the period is π) vortex strings ending on the domain wall from one side. Since the moduli matrix

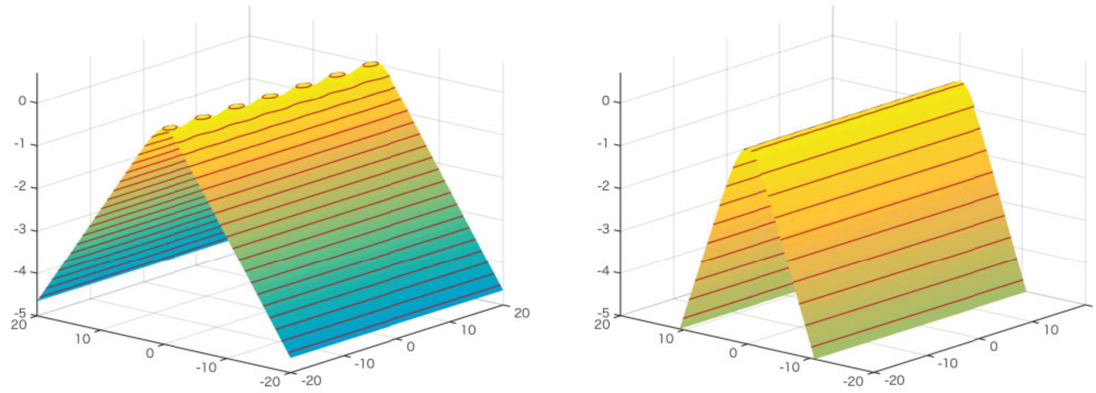

$\eta = 1/2$ $\eta = 1$

Fig. 14. The magnetic scalar potentials for the periodically aligned vortex strings with periods 2π $(\eta = 1/2)$ and π $(\eta = 1)$.

includes an infinite number of vortex strings, the domain wall becomes asymptotically exactly flat with slant angle η. Namely, the domain wall's position is estimated by $\exp\left(-2\tilde{m}x^3\right) \simeq |\sin i\eta z|^2$,

$$
\begin{aligned}
x^3 &= -\frac{1}{2\tilde{m}} \log\left(\cosh^2 \eta x^1 \sin^2 \eta x^2 + \sinh^2 \eta x^1 \cos^2 \eta x^2\right) \\
&\to -\frac{\eta}{\tilde{m}}|x^1| + \frac{1}{\tilde{m}} \log 2 \quad (|x^1| \to \infty).
\end{aligned} \tag{4.15}
$$

The magnetic scalar potentials $\tilde{\varphi} = -u_{\rm S}/2\tilde{d}_{\rm W}$ for $\eta = 1/2$, 1 are shown in Fig. 14 for $\tilde{m} = 1$ ($\tilde{d}_{\rm W} = 2$). As expected, it is clear that the potentials are asymptotically exactly linear in $|x^1|$, reflecting the asymptotic flatness of the domain wall.

4.2. Linearly aligned vortex strings ending on a domain wall from two sides

Let us next consider configurations with periodically aligned infinite vortex strings ending on the domain wall from both sides. The corresponding moduli matrix is given by

$$
H_0 = (\sin i\eta_1(z - Z_1),\ \sin i\eta_2(z - Z_2)), \tag{4.16}
$$

with $Z_{1,2}$ being complex constants. We set $\eta_1 = \eta_2 = \eta$ to be real constants, so that the vortex strings are aligned on the lines $x^1 = \mathrm{Re}(Z_{1,2})$ parallel to the x^2-axis with period π/η. We show two examples of this kind in Figs. 15 and 16 with $\tilde{m} = 1$. In the former figure, we take $Z_1 = -Z_2 = 10, 5, 0$ with $\eta = 1/2$ (the period is 2π). In the latter figure, we shift the vortex strings at the negative x^3 side by $\delta x^2 = \pi$. Namely, we take $Z_1 = -Z_2 + i\pi = 10, 5, 0$. Far from the vortex strings, the domain wall is flat and perpendicular to the x^1–x^2 plane. On the other hand, between the vortex strings, the domain wall is flat but slanting as $x^3 \simeq 2\eta x^1$, which is twice as steep as the domain wall with vortex strings on just one side; see Eq. (4.15). This is, of course, because we have two lines of vortex strings. The shape of the domain wall is determined by superposition. For example, the domain wall's position can be estimated for real positive $Z > 0$ as

$$
\tilde{m}x^3 \simeq -\eta|x_1 - Z| + \eta|x_1 + Z| = \begin{cases} 2\eta Z & \text{for } 2Z < x^1, \\ 2\eta x^1 & \text{for } -2Z < x^1 < 2Z, \\ -2\eta Z & \text{for } x^1 < -2Z. \end{cases} \tag{4.17}
$$

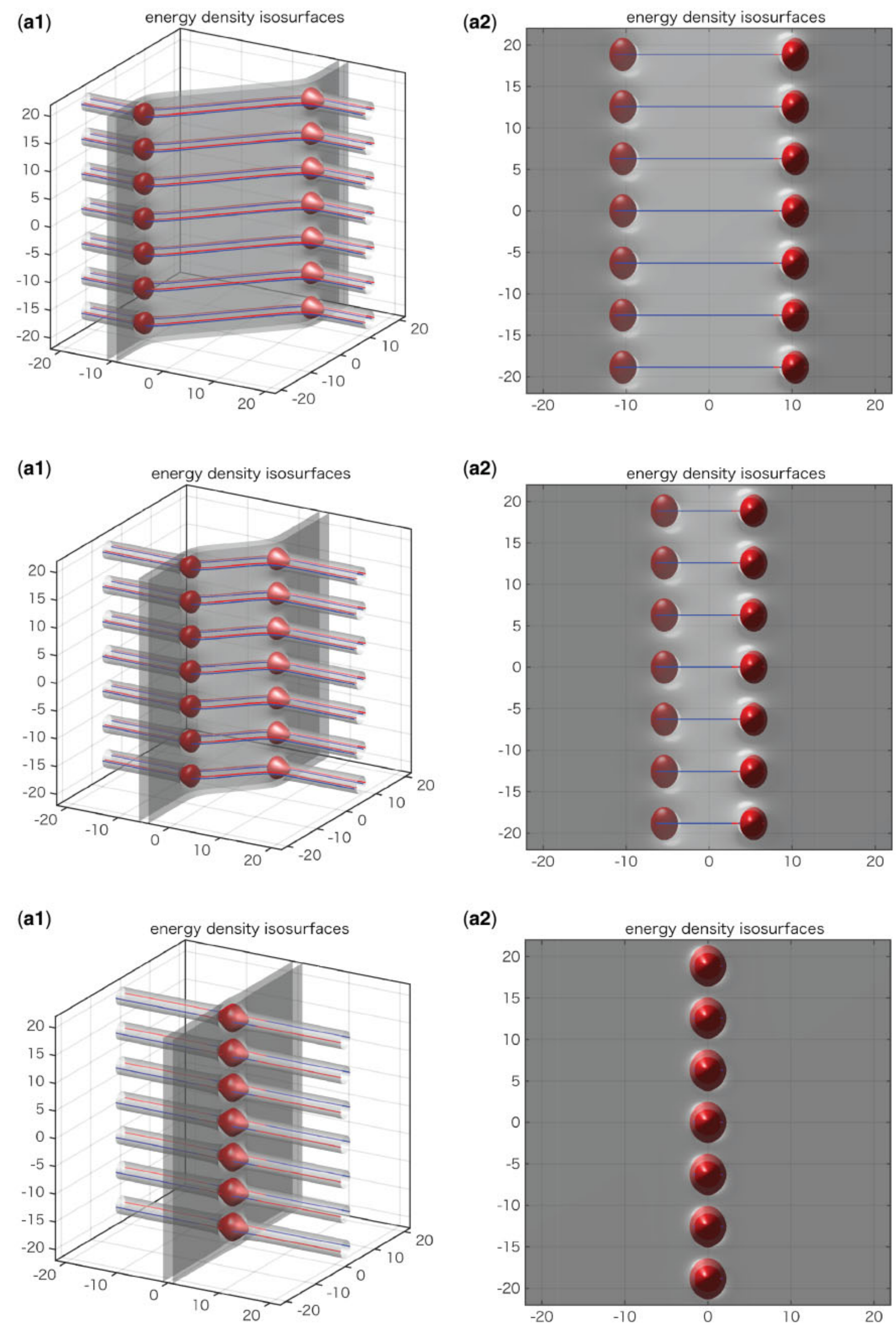

Fig. 15. The plots of the energy density isosurfaces of periodic vortices ending on one wall from two sides. The distances between vortices are $Z = 10$ (top), $Z = 5$ (middle), and $Z = 0$ (bottom).

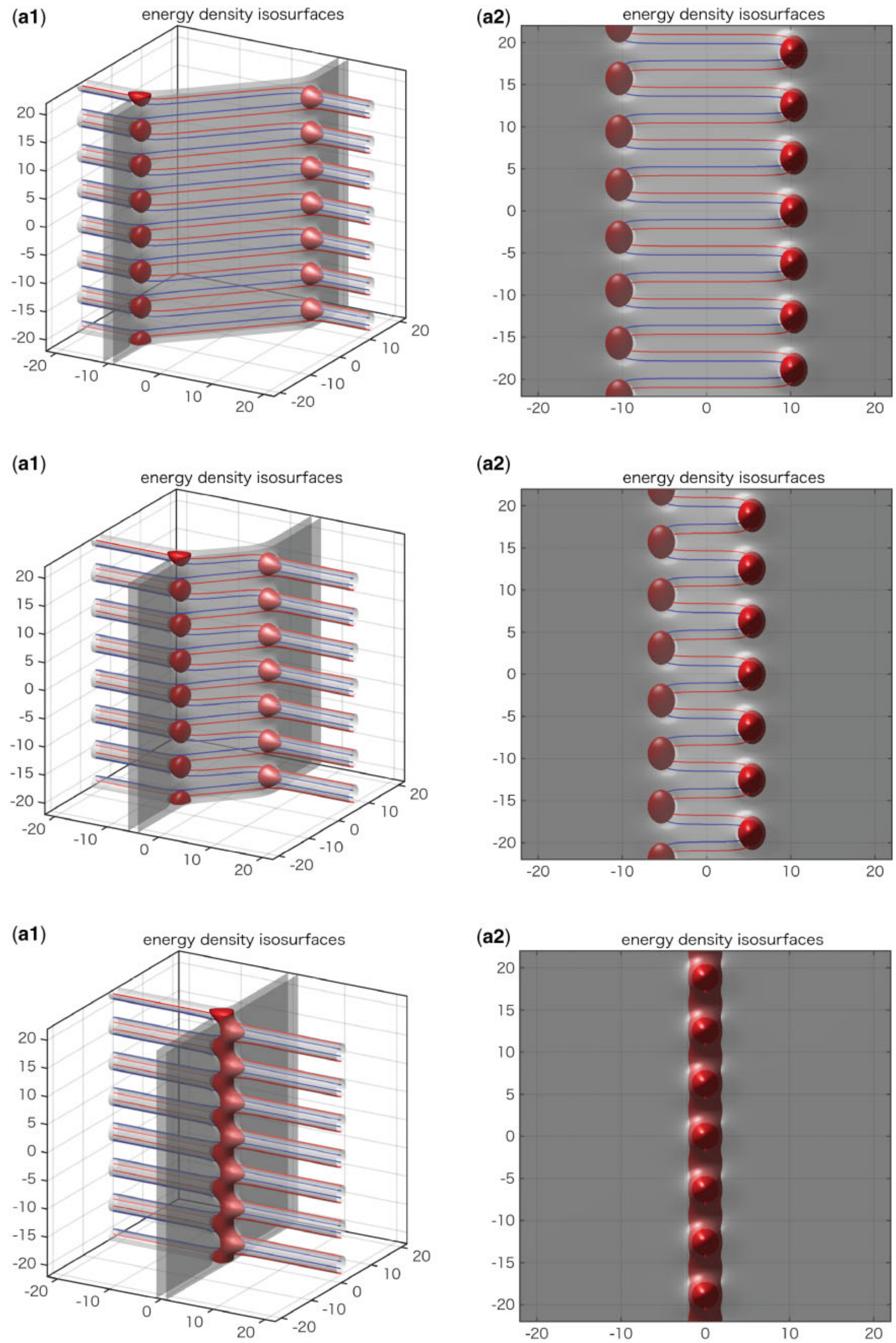

Fig. 16. The plots of the energy density isosurfaces of periodic vortices aligned alternately ending on one wall from two sides. The distances between vortices are $Z = 10$ (top), $Z = 5$ (middle), and $Z = 0$ (bottom).

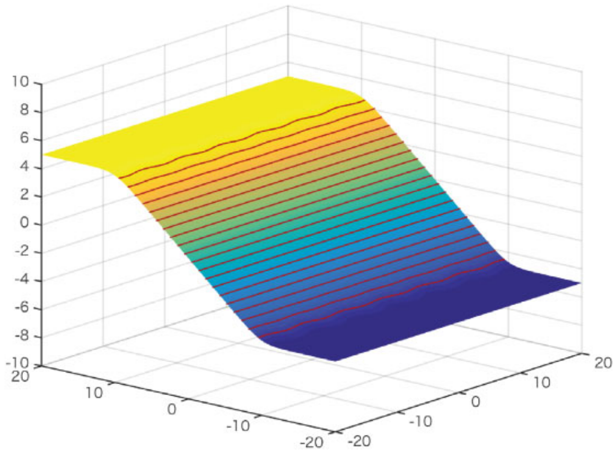

Fig. 17. The magnetic scalar potential (4.18) for the moduli matrix given in Eq. (4.16) with $Z = Z_1 = -Z_2 = 10$, $\eta = 1/2$, and $\tilde{m} = 1$.

Comparing Figs. 15 and 16 we can see that the shift $\delta x^2 = \pi$ in Fig. 16 did not affect the resulting configuration very much. Only the local structure around the endpoints received a small deformation but the asymptotic structure is not changed. Formula (4.17) also remains correct.

Let us interpret the above 1/4 BPS configurations from the viewpoint of $2+1$ dimensions. The corresponding magnetic scalar potential is

$$\begin{aligned}\tilde{\varphi} &= -\frac{1}{2\tilde{d}_{\mathrm{W}}} u_{\mathrm{S}}\big|_{+Z} + \frac{1}{2\tilde{d}_{\mathrm{W}}} u_{\mathrm{S}}\big|_{-Z} \\ &= \frac{\tilde{m}}{\tilde{d}_{\mathrm{W}}}\left(x^3\big|_{+Z} + x^3\big|_{-Z}\right) \\ &\simeq \frac{\eta}{\tilde{d}_{\mathrm{W}}}\left(-|x_1 - Z| + |x_1 + Z|\right). \end{aligned} \tag{4.18}$$

We plot the magnetic scalar potential $\tilde{\varphi}$ in Fig. 17, which reproduces the correct structure of the kinked domain wall.

The last expression in Eq. (4.18) is reminiscent of the electric scalar potential for an electric capacitor. Hence, we may call the configuration with the magnetic scalar potential given in Eq. (4.18) a *magnetic capacitor* in $2+1$ dimensions. Let us define a density of magnetic capacitance $\tilde{c}_M$ by

$$\tilde{c}_M \delta \tilde{V}_B = \frac{\tilde{Q}_B}{\pi/\eta}, \tag{4.19}$$

where $\delta \tilde{V}_B = \tilde{d}_{\mathrm{W}} \tilde{\varphi}\big|_{x^2=Z} - \tilde{d}_{\mathrm{W}} \tilde{\varphi}\big|_{x^2=Z}$ stands for the difference between the magnetic potentials and $\tilde{Q}_B = \tilde{q}_B \tilde{d}_{\mathrm{W}}$ is the magnetic charge per unit length. We have $\delta\tilde{\varphi} = 4\eta Z/\tilde{d}_{\mathrm{W}}$ and $\tilde{q}_B = 2\pi/\tilde{d}_{\mathrm{W}}$; thus we conclude that the domain wall has magnetic capacitance

$$\tilde{c}_M = \frac{1}{2Z}. \tag{4.20}$$

As an ordinary electric capacitance of a flat capacitor, the capacitance is inversely proportional to the distance between the charges.

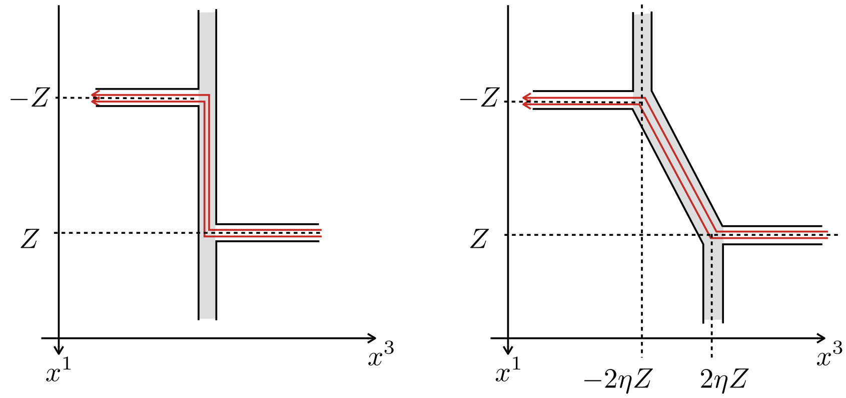

Fig. 18. A schematic picture for the ideal (resp., real) domain wall (gray region) with periodically aligned vortex strings from both sides is shown in the left (resp., right) panel. The red lines represent the incoming and outgoing magnetic fluxes from the vortex strings.

The energy stored in the magnetic capacitor is given by

$$\delta\tilde{\mathcal{E}}_M = \frac{1}{2}\tilde{c}_M \delta\tilde{V}_M^2 = 4\eta^2 Z. \tag{4.21}$$

This can be accounted by the following geometric consideration about the domain wall and the vortex strings. Suppose the domain wall is not bent by the vortex strings. Then the energy for the part between two linearly aligned vortex strings, namely $x^1 \in [-Z, Z]$ is proportional to the distance $2Z$, as depicted in the left panel of Fig. 18. In reality, of course, the domain wall bends linearly as shown in the right panel of Fig. 18. The bent domain wall is longer than the flat one by

$$\delta\tilde{L} = 2Z\left(1+4\eta^2\right)^{1/2} - 2Z \simeq 4\eta^2 Z, \tag{4.22}$$

for $\eta \ll 1$. This coincides with the energy stored in the magnetic capacitor given in Eq. (4.21).

4.3. *Vortex strings ending on a slanting domain wall*

Next, we consider the following moduli matrix, which is slightly different from the one given in Eq. (4.16)

$$\begin{aligned} H_0 &= \left(\frac{\exp\left(-\eta(z-Z)\right) - \exp\left(\eta(z-Z)-2\xi\right)}{2i},\ \frac{\exp\left(-\eta(z+Z)-2\xi\right) - \exp\left(\eta(z+Z)\right)}{2i}\right) \\ &= \exp\left(-\xi\right)\left(\sin i\eta\left(z - Z - \frac{\xi}{\eta}\right),\ \sin i\eta\left(z + Z + \frac{\xi}{\eta}\right)\right). \end{aligned} \tag{4.23}$$

As discussed in the previous subsection, this moduli matrix generates a configuration with linearly aligned vortex strings at $z = i\frac{\pi}{\eta}n \pm \left(Z + \frac{\xi}{\eta}\right)$ with $n \in \mathbb{Z}$. Now, we send all the vortex strings to spatial infinity by taking the limit $\xi \to \infty$. We are left with

$$H_0 = \left(\frac{\exp\left(-\eta(z-Z)\right)}{2i},\ \frac{-\exp\left(\eta(z+Z)\right)}{2i}\right) \simeq (1,\ -\exp\left(2\eta z\right)), \tag{4.24}$$

where we have used the so-called V-transformation that transforms the moduli matrix as $H_0 \to V(z)H_0$ and $u \to 2\log V(z)$ with arbitrary invertible holomorphic function $V(z)$ (Refs. [18–20]). The V-transformation does not change any physics. Since we have just shifted the vortex strings to the spatial infinities, the domain wall shape is given by Eq. (4.17) on replacing Z by $Z + \xi/\eta$. In

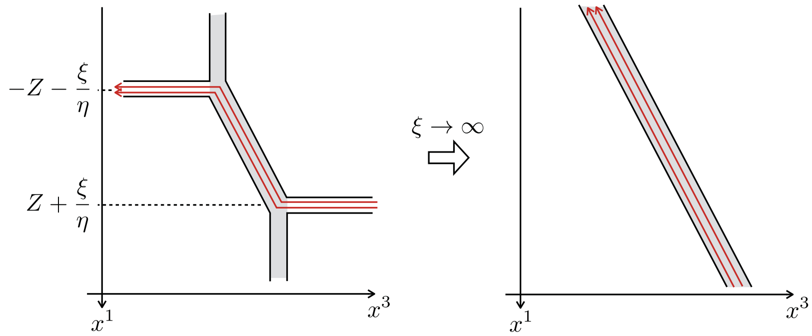

Fig. 19. The slanting domain wall as the limit of sending the vortex strings toward the spatial infinities.

particular, the domain wall between the lines of the vortex strings remains slanted with the same angle; see Fig. 19. This holds even in the limit $\xi \to \infty$. Furthermore, we know of the existence of the vortex strings behind the spatial boundaries $x^1 = \pm\infty$, which provide background magnetic flux $4\pi/(\pi/\eta) = 4\eta$ per unit length. In short, the flat domain wall slants when a background magnetic field is turned on (Ref. [19]). The 1/4 BPS master equation for the moduli matrix (4.24) is given by

$$\partial_k^2 u - 1 + \left(\exp\left(\tilde{m}x^3\right) + \exp\left(4\eta x^1\right)\exp\left(-\tilde{m}x^3\right)\right)\exp\left(-u\right) = 0. \tag{4.25}$$

This can be rewritten as

$$\partial_k^2 u - 1 + \left(\exp\left(\tilde{m}x^3 - 2\eta x^1\right) + \exp\left(-\tilde{m}x^3 + 2\eta x^1\right)\right)\exp\left(-u + 2\eta x^1\right) = 0. \tag{4.26}$$

Introducing new coordinates by

$$\begin{pmatrix} y_3 \\ y_1 \end{pmatrix} = \begin{pmatrix} \cos\alpha & -\sin\alpha \\ \sin\alpha & \cos\alpha \end{pmatrix}\begin{pmatrix} x_3 \\ x_1 \end{pmatrix}, \qquad \tan\alpha = \frac{2\eta}{\tilde{m}}, \tag{4.27}$$

and defining a function by

$$\hat{u} = u - 2\eta x^1, \tag{4.28}$$

we find that $\hat{u}$ is the solution to

$$\left(\frac{\partial^2}{\partial y_3^2} + \frac{\partial^2}{\partial y_2^2}\right)\hat{u} - 1 + \left(\exp\left(\hat{m}y^3\right) + \exp\left(-\hat{m}y^3\right)\right)\exp\left(-\hat{u}\right) = 0, \tag{4.29}$$

where we have defined $\hat{m} \equiv \left(\tilde{m}^2 + 4\eta^2\right)^{1/2}$. Clearly, $\hat{u}$ does not depend on y^1, so we identify that $\hat{u}$ is identical to the domain wall solution written in the rotated coordinate y^3 with mass parameter $\hat{m}$. In the original coordinates, the solution is given by

$$u(x^k) = u_{\mathrm{W}}(x^3 - x^1\tan\alpha) + 2\eta x^1. \tag{4.30}$$

The position of the domain wall is determined by the condition $x^3\cos\alpha - x^1\sin\alpha = 0$, namely it is

$$x^3 = (\tan\alpha)x^1 = \frac{2\eta}{\tilde{m}}x^1. \tag{4.31}$$

This is consistent with the previous result given in Eq. (4.17).

Next, we put a single vortex string in the first vacuum $\langle 1 \rangle$. The corresponding moduli matrix is given by

$$H_0 = (z,\ -\exp(2\eta z)). \tag{4.32}$$

The master equation for this can be expressed as

$$\partial_k^2 u - 1 + \left(\exp\left(\tilde{m}x^3 - 2\eta x^1 + \log|z|\right) + \exp\left(-\tilde{m}x^3 + 2\eta x^1 - \log|z|\right)\right)$$
$$\times \exp\left(-u + 2\eta x^1 + \log|z|\right) = 0. \tag{4.33}$$

An appropriate initial configuration for the gradient flow equation to this is

$$\mathcal{U}(x^k) = u_{\mathrm{W}}\left(x^3 - \frac{2\eta}{\tilde{m}}x^1 + \frac{1}{2\tilde{m}}u_{\mathrm{S}}(x^a)\right) + 2\eta x^1 + \frac{u_{\mathrm{S}}(x^a)}{2}. \tag{4.34}$$

We show a numerical solution for $\tilde{m} = 1$ and $\eta = 1/4$ in Fig. 20 that clearly demonstrates the vortex string parallel to the x^3-axis ending on the slanting and logarithmically bending domain wall. The junction point is accompanied by the boojum, which is also sheared as shown in panel (b3) of Fig. 20. Interestingly, the magnetic force lines supplied by the vortex string do not spread out in the domain wall but flow toward a direction as forming a stringy flux in $2+1$ dimensions; see panels (a1) and (a2) in Fig. 20. This squeezing of the magnetic flux inside the domain wall occurs because the magnetic force lines from the vortex string repel those of the background magnetic flux on the slanting domain wall.

This magnetic scalar potential can be read from Eq. (4.34) as

$$\tilde{\varphi} = -\frac{1}{2\tilde{d}_{\mathrm{W}}}u_{\mathrm{S}} + \frac{2\eta}{\tilde{d}_{\mathrm{W}}}x^1 \tag{4.35}$$

and again correctly captures these features. The first term corresponds to the potential generated by the endpoint of the vortex string and the second one expresses the potential for the background magnetic field. We plot streamlines of the magnetic fields $\tilde{B}_a = -\partial_a\tilde{\varphi}$ for $\eta = 0,\ 1/10,\ 1/4$ in Fig. 21 where we compare two cases: the strong-gauge coupling limit with $u_s = \log\rho^2$ (the first row) and the finite-gauge coupling case (the second row). The flux lines emitted from the positive magnetic source are absorbed into the negative magnetic charges aligned periodically at $x^1 \to -\infty$, so that they are squeezed. This situation is quite similar to the squeezing of the magnetic fluxes by the Higgs mechanism, but it is not the case because no further symmetries are broken in the domain wall.

Finally, we place another vortex string from the other side of the domain wall. The moduli matrix is

$$H_0 = ((z - Z)\exp(\eta z),\ -(z + Z)\exp(-\eta z)). \tag{4.36}$$

The vortex string on the positive (negative) x^3 side is at $z = Z$ ($z = -Z$), and the domain wall is asymptotically flat but slanting as

$$x^3 = -\frac{1}{2\tilde{m}}u_{\mathrm{S}}\big|_{z=+Z} + \frac{1}{2\tilde{m}}u_{\mathrm{S}}\big|_{z=-Z} + \frac{2\eta}{\tilde{m}}x^1 \to \frac{2\eta}{\tilde{m}}x^1 \quad (\rho \to \infty). \tag{4.37}$$

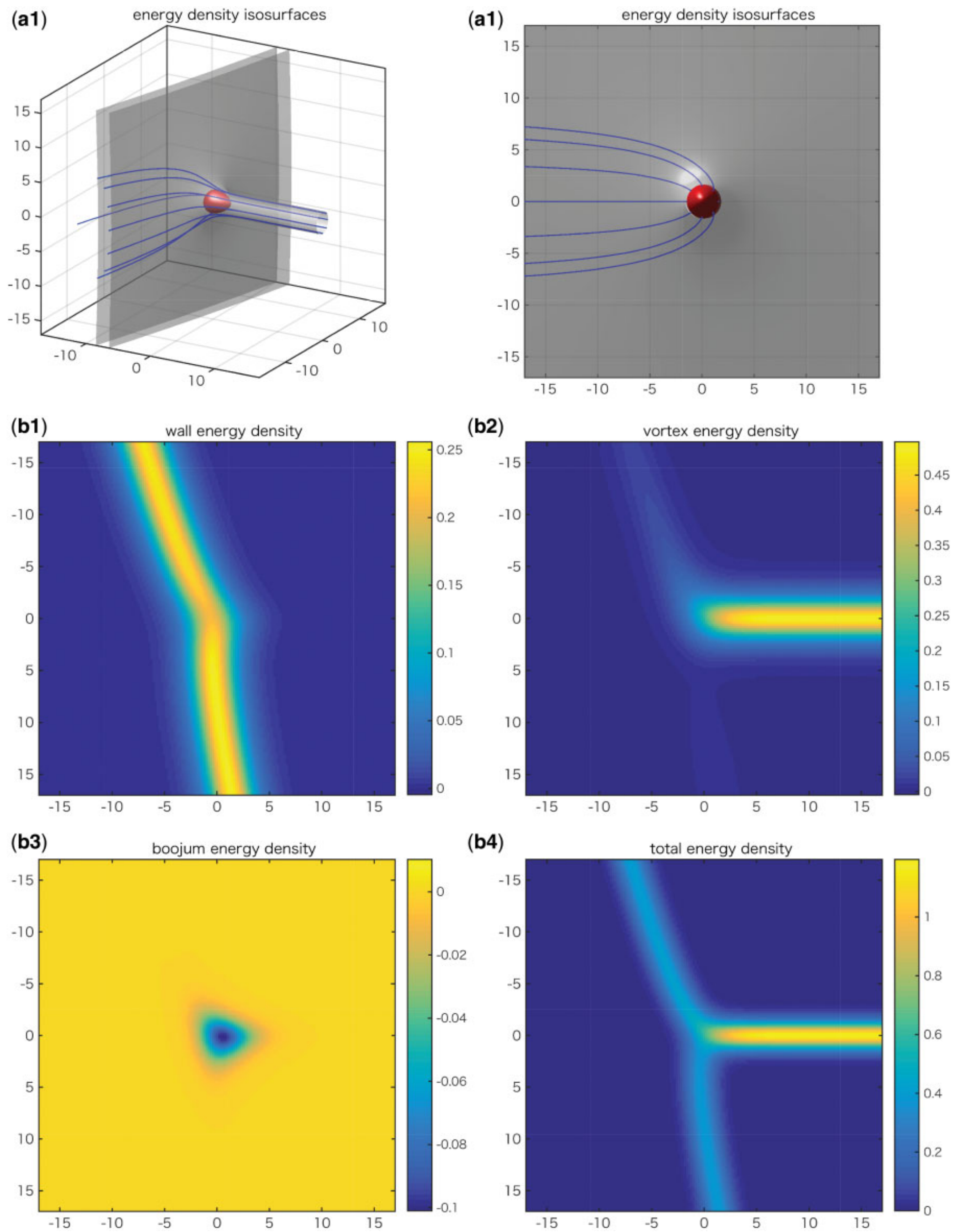

Fig. 20. The plots show the energy density isosurfaces of one vortex ending on one slanting wall (a1, a2), where the blue and the red curves show magnetic fluxes, the wall energy density (b1), the vortex energy density (b2), the boojum energy density (b3), and the total energy density (b4).

We show several numerical solutions in Figs. 22 and 23 for $\tilde{m} = 1$ and $\eta = 1/4$. We set $Z = 6$ in Fig. 22 and $Z = 4, 2, 0$ in Fig. 23. A remarkable difference between nonslanting and slanting configurations can be found in the distribution of the magnetic force lines inside the domain wall. The flux lines are quite similar to those around an ordinary magnetic dipole in the nonslanting domain wall. On the other hand, they are squeezed in the slanting domain wall, so if we arrange the vortex strings in such a way that the line segment connecting two endpoints is exactly parallel to the steepest direction of the slanting domain wall (the injecting vortex string is on the upper side and the ejecting one is on the lower side), the flux lines are as if confined; see Fig. 23.

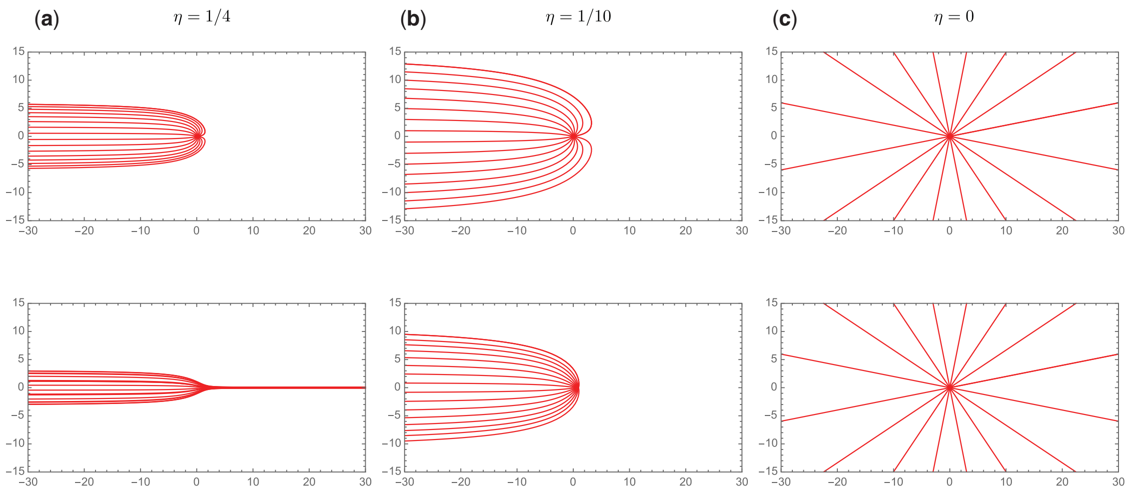

Fig. 21. The streamlines of the magnetic field $\tilde{B}_a = -\partial_a \tilde{\varphi}$. We plot the lines that pass the points on the unit circle surrounding the origin. The figures in the first row are for the point charge with $u_{\rm S} = \log \rho^2$. The figures in the second row are for the finite size source with $u_{\rm S}$ for the finite-gauge coupling.

Now we can naturally generalize the configuration to have any slanting angle and any number of vortex strings from both sides. The magnetic scalar potential is the most useful tool to describe it:

$$\tilde{d}_{\rm W}\tilde{\varphi} = -\sum_{k_1=1}^{n_1} \frac{1}{2} u_{\rm S}\big|_{z=Z_{k_1}} + \sum_{k_2=1}^{n_2} \frac{1}{2} u_{\rm S}\big|_{z=Z_{k_2}} + \tilde{B}_a^{(\rm bg)} x^a, \tag{4.38}$$

where $u_{\rm S}\big|_{z=Z_k}$ stands for the solution for a vortex string at $z = Z_k$, and $\tilde{B}_a^{(\rm bg)}$ is the background magnetic field.

The magnetic flux lines for $(n_1, n_2) = (1, 1)$ are shown in Fig. 24. We put the vortex string at $Z_{n_1=1} = -Z_{n_2=1} = 20 \exp(i\theta)$ with $\theta = 0, \frac{\pi}{4}, \frac{\pi}{2}, \frac{3\pi}{4}, \pi$ for $\tilde{B}_a^{(\rm bg)} = 2\eta\delta_{1a}$ with $\eta = \frac{1}{15}$ and $\tilde{m} = 1$ ($\tilde{d}_{\rm W} = 2$). As shown in panel (a1) of Fig. 24, the magnetic sources are confined only when $\theta = 0$, where the magnetic flux lines from the positive source go into the negative magnetic source. When we rotate the sources, part of the flux lines run toward the boundaries; see panels (a2)–(a5) of Fig. 24. When we turn off the background magnetic field, we have a magnetic dipole regardless of the rotating angle as in panel (b) of Fig. 24.

5. Dyonic extension

5.1. *Basic formulae*

In this section we will study a dyonic extension of the purely magnetic 1/4 BPS equations (2.8)–(2.11) (Refs. [26,32]). A perfect square of the energy density including time dependence is given by

$$\begin{aligned}\mathcal{E} = \frac{1}{2g^2}\Big\{ &\left(\xi F_{12} - \eta\cos\alpha\,\partial_3\sigma - g^2(HH^\dagger - v^2)\right)^2 + (F_{0k} - \sin\alpha\,\partial_k\sigma)^2 + (\partial_0\sigma)^2 \\ &+ (\xi F_{23} - \eta\cos\alpha\,\partial_1\,\sigma)^2 + (\xi F_{31} - \eta\cos\alpha\,\partial_2\sigma)^2\Big\} \\ &+ |(D_1 + i\xi D_2)H|^2 + |D_0 H + i\sin\alpha(\sigma H - HM)|^2\end{aligned}$$

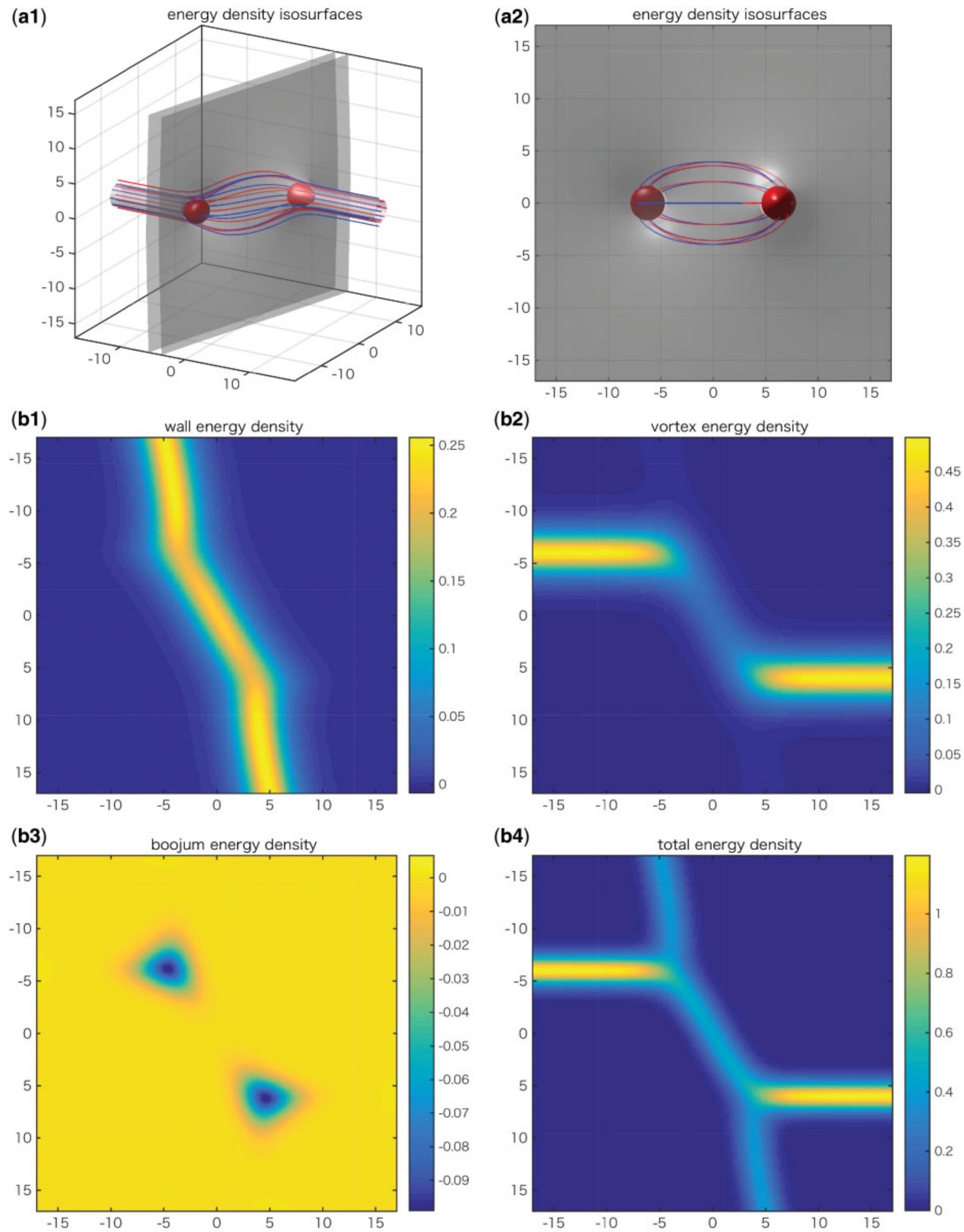

Fig. 22. The plots show the energy density isosurfaces of two vortices ending on one slanting wall (a1, a2), where the blue and the red curves show magnetic fluxes, the wall energy density (b1), the vortex energy density (b2), the boojum energy density (b3), and the total energy density (b4). The distance between two vortices is taken to be $Z = 6$.

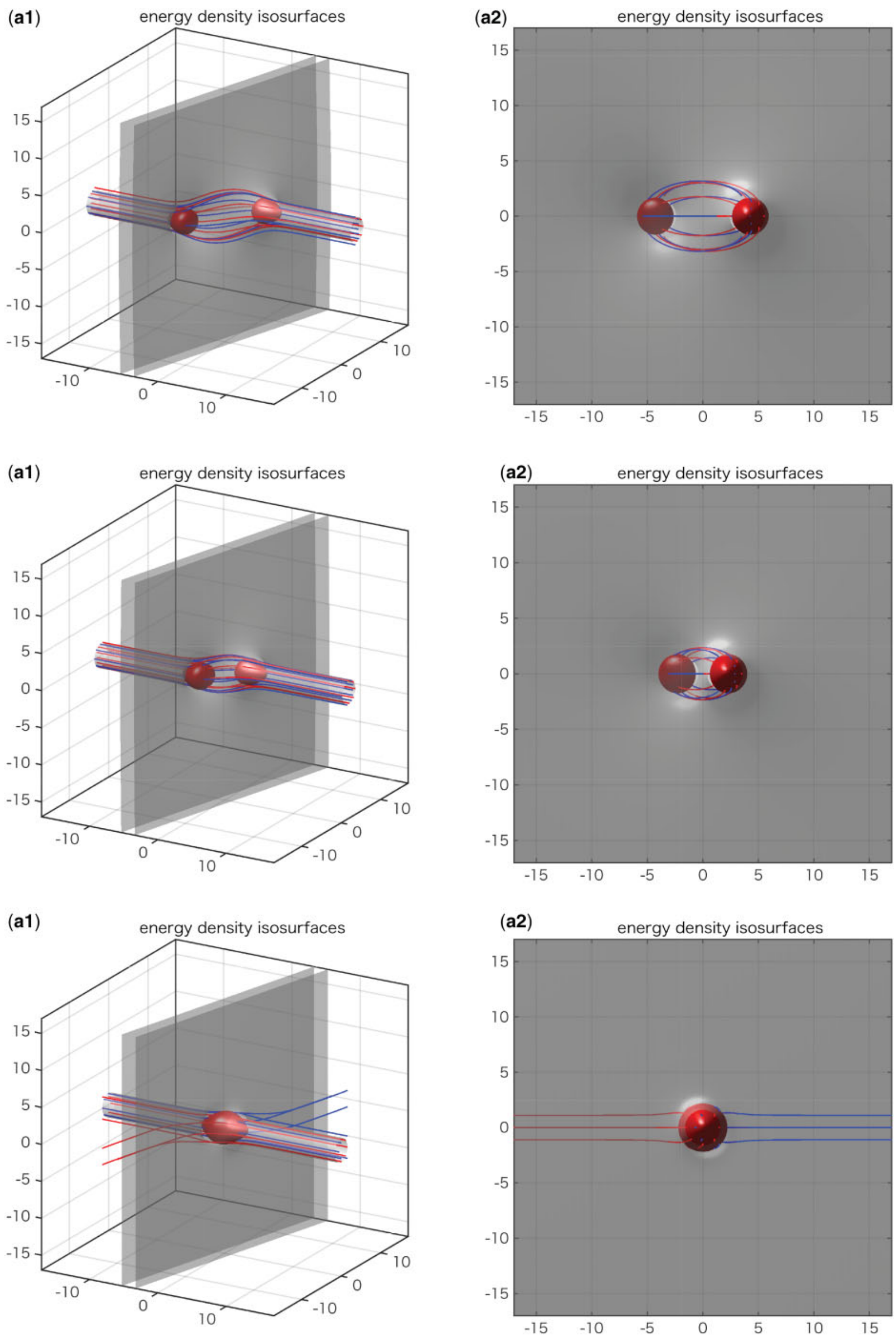

Fig. 23. The plots show the energy density isosurfaces of two vortices ending on one slanting wall from two sides. The distance between two vortices is taken to be $Z = 4, 2, 0$ from top to bottom.

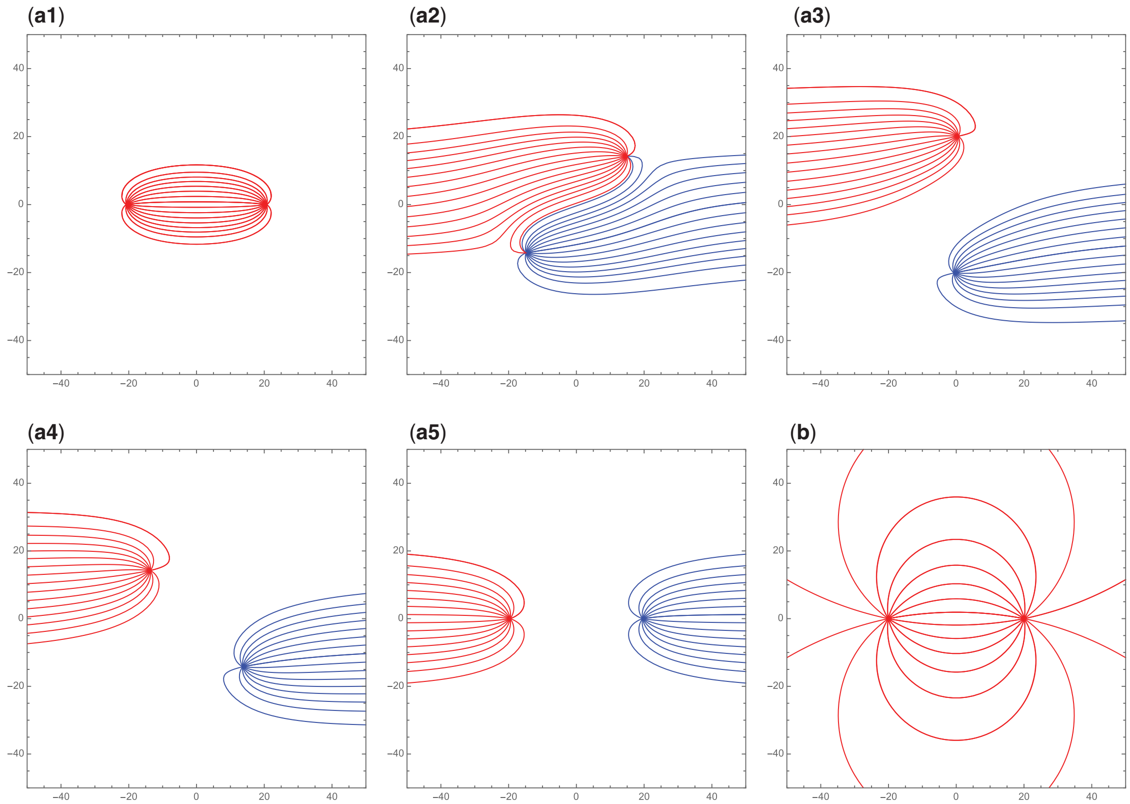

Fig. 24. The streamlines of the magnetic field $\tilde{B}_a = -\partial_a \tilde{\varphi}$. The red lines are fluxes from the positive charge and the blue ones are those going into the negative charge. Panels (a1)–(a5) are with the background magnetic field while panel (b) is without it.

$$
\begin{aligned}
&+ |D_3 H + \eta \cos\alpha (\sigma H - HM)|^2 \\
&+ v^2 \eta \cos\alpha\, \partial_3 \sigma - \xi v^2 F_{12} + \xi \eta \cos\alpha\, \partial_i \left(\frac{\sigma}{g^2} \epsilon_{ijk} F_{jk} \right) \\
&+ i \sin\alpha (HMD_0 H^\dagger - D_0 HMH^\dagger) \\
&+ \partial_k j_k + \sin\alpha\, \partial_k \left(\frac{\sigma}{g^2} F_{0k} \right) \\
&- \sin\alpha \left\{ \frac{1}{g^2} \partial_k F_{0k} + i \left(HD_0 H^\dagger - D_0 HH^\dagger \right) \right\},
\end{aligned} \tag{5.1}
$$

where we restrict α to satisfy $\alpha \in (-\pi/2, \pi/2)$ because $\cos\alpha$ always appears accompanied by $\eta = \pm 1$. The nontopological currents $j_{a=1,2}$ are the same as in Eq. (2.6) while $j_{k=3}$ is given by

$$
j_3 = -\eta \cos\alpha\, (\sigma H - HM)\, H^\dagger. \tag{5.2}
$$

The vanishing of the squared terms leads to the dyonic extension to 1/4 BPS equations:

$$
D_0 H + i \sin\alpha \big(\sigma H - HM\big) = 0, \tag{5.3}
$$

$$
D_3 H + \eta \cos\alpha \big(\sigma H - HM\big) = 0, \tag{5.4}
$$

$$
(D_1 + i\xi D_2) H = 0, \tag{5.5}
$$

$$
\eta \cos\alpha\, \partial_1 \sigma = \xi F_{23}, \qquad \eta \cos\alpha\, \partial_2 \sigma = \xi F_{31}, \tag{5.6}
$$

$$\sin\alpha\,\partial_k\sigma = F_{0k}, \tag{5.7}$$

$$\xi F_{12} - \eta\cos\alpha\,\partial_3\sigma - g^2\left(|H|^2 - v^2\right) = 0, \tag{5.8}$$

$$\partial_0\sigma = 0. \tag{5.9}$$

Also, one has to include Gauss's law,

$$\frac{1}{g^2}\partial_k F_{0k} + i\left(HD_0H^\dagger - D_0HH^\dagger\right) = 0. \tag{5.10}$$

The parameters $\eta^2 = \xi^2 = 1$ label (anti-)vortices $\xi = (-1)1$ and (anti-)walls $\eta = (-1)1$. In the strong-gauge coupling limit, our Abelian-Higgs model reduces to the massive nonlinear sigma model whose target space is $\mathbb{C}P^{N_F-1}$, and the above dyonic extension reduces to the Q-kink lump configuration without the boojums, first studied in Ref. [10].

When the BPS equations (5.3)–(5.9) and Gauss's law are satisfied, the total energy density saturates the Bogomol'nyi bound

$$\mathcal{E} \geq (\mathcal{T}_{\rm W}\cos\alpha + \mathcal{Q}_{\rm W}\sin\alpha) + \mathcal{T}_{\rm S} + (\mathcal{T}_{\rm B}\cos\alpha + \mathcal{Q}_{\rm B}\sin\alpha) + \partial_k j_k, \tag{5.11}$$

where $\mathcal{T}_{\rm W,S,B}$ is defined in Eq. (2.5), and the Noether charge density and the electric boojum charge density are defined by

$$\mathcal{Q}_{\rm W} = i\left(HMD_0H^\dagger - D_0HMH^\dagger\right), \tag{5.12}$$

$$\mathcal{Q}_{\rm B} = \partial_k\left(\frac{\sigma}{g^2}F_{0k}\right). \tag{5.13}$$

The set of BPS equations (5.3)–(5.7) are solved via the moduli matrix formalism

$$H = v\exp\left(-\frac{u}{2}\right)H_0(z)\exp\left(M\left(x^3\eta\cos\alpha + ix^0\sin\alpha\right)\right), \tag{5.14}$$

$$a_1 + i\xi a_2 = -i\partial_{\bar z}u, \tag{5.15}$$

$$\sigma\eta\cos\alpha + ia_3 = \frac{1}{2}\partial_3 u, \tag{5.16}$$

$$\sigma\sin\alpha + a_0 = -\frac{i}{2}\partial_0 u. \tag{5.17}$$

We demand that u is real by fixing the gauge freedom. Thus, Eq. (5.16) gives us

$$a_3 = 0, \qquad \sigma = \frac{\eta}{2\cos\alpha}\partial_3 u. \tag{5.18}$$

From Eq. (5.9), σ is independent of t. Then, Eq. (5.17) gives

$$a_0 = -\sigma\sin\alpha = -\frac{\eta}{2}\tan\alpha\,\partial_3 u. \tag{5.19}$$

Note that this also solves Gauss's law (5.10). Now, we can express the electric and magnetic fields in terms of the single real function u as

$$E_k = \frac{\eta\tan\alpha}{2}\partial_k\partial_3 u, \qquad (B_1, B_2, B_3) = \frac{\xi}{2}\left(\partial_3\partial_1 u,\ \partial_2\partial_3 u,\ -(\partial_1^2 + \partial_2^2)u\right). \tag{5.20}$$

Similarly, the topological charge densities are also expressed as

$$\mathcal{T}_{\rm W} = \eta v^2 \partial_3 \sigma = \frac{v^2}{2\cos\alpha}\partial_3^2 u, \tag{5.21}$$

$$\mathcal{T}_{\rm S} = -\xi v^2 F_{12} = \frac{v^2}{2}\left(\partial_1^2 + \partial_2^2\right) u, \tag{5.22}$$

$$\begin{aligned}\mathcal{T}_{\rm B} &= \frac{\eta\,\xi}{g^2}\epsilon_{klm}\partial_k(F_{lm}\sigma) \\ &= \frac{1}{2g^2\cos\alpha}\left\{(\partial_1\partial_3 u)^2 + (\partial_2\partial_3 u)^2 - \left(\partial_1^2+\partial_2^2\right)u\,\partial_3^2 u\right\}.\end{aligned} \tag{5.23}$$

Finally, we are left with Eq. (5.8), which turns into the master equation

$$\frac{1}{2g^2v^2}\partial_k^2 u = 1 - \Omega_0 \exp(-u), \quad \Omega_0 = H_0 \exp\left(2\eta\cos\alpha\, M x^3\right) H_0^\dagger. \tag{5.24}$$

Comparing this with the master equation (2.16) for the purely magnetic case, the only difference is the replacement of M by $M\cos\alpha$.

The tension of the domain wall is the same as in the purely magnetic case,

$$T_{\rm W} = \int dx^3\ \mathcal{T}_{\rm W} = \eta v^2\left[\sigma\right]_{x^3=-\infty}^{x^3=\infty} = v^2\eta\Delta m = v^2|\Delta m|, \tag{5.25}$$

and similarly for the Noether charge. Combining Eqs. (5.3) and (5.4), we find

$$D_0 H = i\eta\tan\alpha\, D_3 H. \tag{5.26}$$

By using this, we have

$$\mathcal{Q}_{\rm W} = \eta\tan\alpha\,\partial_3\left(HMH^\dagger\right). \tag{5.27}$$

Thus, the Noether charge density upon integration over x^3 gives a constant:

$$Q_{\rm W} = \int dx^3\ \mathcal{Q}_{\rm W} = \eta\tan\alpha\left[HMH^\dagger\right]_{x^3=-\infty}^{x^3=\infty} = v^2\Delta m\eta\tan\alpha. \tag{5.28}$$

Hence, the Noether charge per unit area is proportional to the domain wall tension

$$\frac{Q_{\rm W}}{T_{\rm W}} = \tan\alpha. \tag{5.29}$$

Therefore, the volume integral of $\mathcal{Q}_{\rm W}$ diverges as the domain wall mass, which is proportional to $A = \int dx^1\, dx^2$. Now, part of the BPS mass can be calculated as

$$\int d^3x\ \left(\mathcal{T}_{\rm W}\cos\alpha + \mathcal{Q}_{\rm W}\sin\alpha\right) = \frac{T_{\rm W}}{\cos\alpha}A = \left(T_{\rm W}^2 + Q_{\rm W}^2\right)^{1/2} A. \tag{5.30}$$

The contribution of the vortex string to the total mass is independent of $\cos\alpha$. Therefore, we have $T_{\rm S} = 2\pi v^2|k|$, where k stands for the vortex winding number, and then the mass of the vortex string is given by

$$\int d^3x\ \mathcal{T}_{\rm S} = \int dx^3\ T_{\rm S} = 2\pi v^2|k|L. \tag{5.31}$$

Let us next evaluate $T_{\rm B}$, the boojum mass,

$$T_{\rm B} = \frac{\eta\xi}{g^2}\int d^3x\, \partial_i\,(\sigma B_i). \tag{5.32}$$

This is easy to do for the case of flat domain walls since we have the same number k of straight vortex strings on both sides of the domain walls. The magnetic flux at $x^3 \to \pm\infty$ is given by $\int dx^1\, dx^2\, \xi B_i = -\delta_{i3} 2\pi|k|$. Therefore, we have

$$T_{\rm B} = \frac{\eta}{g^2}\times(-2\pi|k|)\times\left[\sigma\right]_{x^3=-\infty}^{x^3=+\infty} = -\frac{2\pi}{g^2}|\Delta m||k|. \tag{5.33}$$

This is independent of α as $T_{\rm S}$. For configurations including bent domain walls, we should repeat the same computation that we have done in Ref. [17]. But it is clear even for such cases that $T_{\rm B}$ is independent of α. Hence, the formula (5.33) is valid for any configurations. The contribution of the boojum to the total mass is then found as

$$\cos\alpha\; T_{\rm B} = \frac{T_{\rm W}}{\left(T_{\rm W}^2+Q_{\rm W}^2\right)^{1/2}}\; T_{\rm B}. \tag{5.34}$$

Since $T_{\rm B}$ is negative definite, this makes the total mass larger. Next, we evaluate the contribution from $\mathcal{Q}_{\rm B}$ given in Eq. (5.13). Using the BPS equations, it can be written as

$$\mathcal{Q}_{\rm B} = \partial_k\left(\frac{\sigma}{g^2}F_{0k}\right) = \frac{\sin\alpha}{g^2}\partial_k\,(\sigma\,\partial_k\sigma) = \frac{\sin\alpha}{2g^2}\partial_k^2\sigma^2. \tag{5.35}$$

Since the electric field is proportional to the derivative of σ, $E_k \propto \partial_k\sigma$, it is nonzero only inside the domain wall. Therefore, upon integration along x^3, $\mathcal{Q}_{\rm B}$ vanishes. The contribution from the nontopological terms $\partial_k j_k$ also vanishes upon integration. Summing all the contributions, we conclude that the mass of the dyonic 1/4 BPS configuration is given by

$$E_{1/4} = \left(T_{\rm W}^2+Q_{\rm W}^2\right)^{1/2} A + T_{\rm S}L + \frac{T_{\rm W}}{\left(T_{\rm W}^2+Q_{\rm W}^2\right)^{1/2}}\; T_{\rm B}. \tag{5.36}$$

The electric charge density appearing in Gauss's law (5.10) can be written as

$$\mathcal{Q}_E = i\left(D_0HH^\dagger - HD_0H^\dagger\right) = -\eta\tan\alpha\;\partial_3\left(HH^\dagger\right). \tag{5.37}$$

This is very similar to $\mathcal{Q}_{\rm W}$. Since we have $HH^\dagger = v^2$ at any vacua, $\int dx^3\, \mathcal{Q}_E = 0$, so that net electric charge is zero. However, note that the electric charge density is nonzero everywhere.

As a final remark, the relation

$$\begin{aligned}\vec{E}\cdot\vec{B} &= \frac{\eta\xi}{4}\tan\alpha\left\{(\partial_1\partial_3u)^2+(\partial_2\partial_3u)^2-\left(\partial_1^2+\partial_2^2\right)u\;\partial_3^2u\right\}\\ &= \frac{g^2}{2}\xi\eta\sin\alpha\,\mathcal{T}_{\rm B},\end{aligned} \tag{5.38}$$

implies that E_k is perpendicular to B_k far from the boojums, while in their vicinity, it is not.

5.2. *The dyonic domain wall as an electric capacitor*

The Q-extension of the domain wall was first found in nonlinear sigma models in Refs. [27,28], and lots of works have followed them. The Q-extended domain walls in gauge theories are sometimes called the dyonic domain walls (Refs. [26,32,33]). They are characterized by the topological and the

Noether charges, so it is appropriate to call them dyonic solitons. In the previous works Refs. [26,32, 33], the dyonic domain wall was not the main focus. Some qualitative properties, such as derivation of the BPS equations, topological charges, and the BPS mass formula, were given. To the best of our knowledge, very little has been done to solve the BPS equations, especially in the weak-gauge coupling region. Furthermore, while the Noether charge, which gives a finite contribution to the BPS mass, has been studied very well, the electric and/or magnetic charge densities have not been discussed. Therefore, before studying the dyonic 1/4 BPS states, we stop for a while to clarify the dyonic domain wall in the weak-gauge coupling region.

The master equation for the dyonic domain wall in dimensionless coordinates is

$$\partial_3^2 u - 1 + \Omega_0 \exp(-u) = 0, \qquad \Omega_0 = H_0^\dagger \exp\left(2\eta\tilde{M}\cos\alpha\, x^3\right) H_0^\dagger. \tag{5.39}$$

This is formally the same equation as the master equation for the purely magnetic domain wall. If we write $\tilde{M} = \tilde{M}'/\cos\alpha$, the solutions $u(x^3)$ are identical to those that have already been obtained. In order to avoid inessential complications, we will consider $\eta = +1$ and $\tilde{M}' = \mathrm{diag}(\tilde{m}'/2,\ -\tilde{m}'/2)$ with $\tilde{m}' > 0$ in what follows. The tension of the domain wall becomes

$$\tilde{T}_{\mathrm{W}} = \frac{2\tilde{m}'}{\cos\alpha} \qquad \left(T_{\mathrm{W}} = \frac{gv^3}{\sqrt{2}}\tilde{T}_{\mathrm{W}} = \frac{m'v^2}{\cos\alpha}\right), \tag{5.40}$$

because $\tilde{m} = \tilde{m}'/\cos\alpha$.

Since $u = u(x^3)$ and from Eq. (5.20), no magnetic fields are involved. On the other hand, the third component of the electric field does appear:

$$\tilde{E}_3 = 2\tan\alpha\,\partial_3\tilde{\sigma} = \tan\alpha\,\partial_3^2 u. \tag{5.41}$$

Remember, ∂_3 means the derivative in terms of $\tilde{x}^3$ and $\tilde{E}_k = E_k/g^2v^2$. When $N_F = 2$, $\tilde{\sigma}$ is constant outside the domain wall, so no electric fields exist there (see the details in Ref. [17]). On the other hand, a constant electric field E_3 appears inside the domain wall, as $\tilde{\sigma}$ is linear in x^3 there. Since the width of the domain wall is $2\tilde{m}'$ and $\tilde{\sigma}$ changes from $-\tilde{m}'/2\cos\alpha$ to $\tilde{m}'/2\cos\alpha$, we have $\partial_3\tilde{\sigma} \simeq 1/2\cos\alpha$. Therefore, the electric field inside the domain wall for weak coupling is

$$\tilde{E}_k = \frac{\sin\alpha}{\cos^2\alpha}\,\delta_{k3}. \tag{5.42}$$

The induced electric charges that generate this electric field can be found from Eq. (5.37). In terms of the dimensionless coordinates, the electric charge density is rewritten as

$$\tilde{\mathcal{Q}}_E = \frac{\mathcal{Q}_E}{\sqrt{2}gv^3} = -\tan\alpha\,\partial_3\left(\tilde{H}\tilde{H}^\dagger\right) = -\tan\alpha\,\partial_3 m_{\mathrm{v}}^2, \tag{5.43}$$

where $m_{\mathrm{v}}^2 = \tilde{H}\tilde{H}^\dagger$ is 1 in the vacua, while $m_{\mathrm{v}}^2 = 0$ inside the domain wall. Therefore, electric charges are induced on the outer layers; see Fig. 25: there are positive (negative) electric charges on the left outer skin and negative (positive) charges on the right outer skin for $\tan\alpha > 0$ ($\tan\alpha < 0$). Then the electric charge per unit area is given by

$$\tilde{Q}_E = \pm\left[\tilde{H}\tilde{H}^\dagger\tan\alpha\right]_{\mathrm{outside}}^{\mathrm{inside}} = \pm\tan\alpha. \tag{5.44}$$

Since the distance between the two outer layers is $2\tilde{m}'$, the difference in electric potential is

$$\tilde{V} = 2\tilde{m}'\tilde{E}_3 = \frac{2\tilde{m}'}{\cos\alpha}\,\tan\alpha = \frac{2\tilde{m}'}{\cos\alpha}\,|\tilde{Q}_E|. \tag{5.45}$$

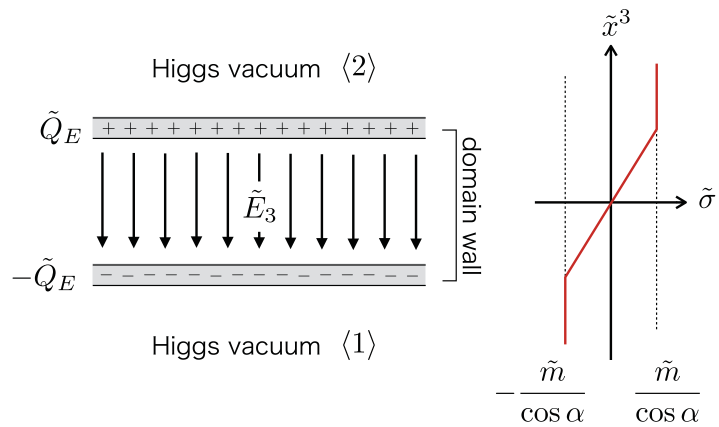

Fig. 25. The dyonic domain wall as an electric capacitor.

Hence, the electric capacitance per unit area is given by

$$\tilde{c} = \frac{\cos\alpha}{2\tilde{m}'} = \frac{1}{\tilde{T}_{\mathrm{W}}}. \tag{5.46}$$

Note that the electric capacitance, in the usual sense, is infinity because the domain wall has infinite area. The energy stored in the capacitor is

$$\frac{1}{2}\tilde{c}\tilde{V}^2 = \frac{1}{2}\tilde{T}_{\mathrm{W}} \tan^2\alpha, \tag{5.47}$$

which is the excess of the domain wall's tension for small α:

$$\left(\tilde{T}_{\mathrm{W}}^2 + \tilde{Q}_{\mathrm{W}}^2\right)^{1/2} - \tilde{T}_{\mathrm{W}} \simeq \frac{1}{2}\frac{\tilde{Q}_{\mathrm{W}}^2}{\tilde{T}_{\mathrm{W}}} = \frac{1}{2}\tilde{T}_{\mathrm{W}}\frac{\tilde{Q}_{\mathrm{W}}^2}{\tilde{T}_{\mathrm{W}}^2} = \frac{1}{2}\tilde{T}_{\mathrm{W}}\tan^2\alpha. \tag{5.48}$$

Note that the dyonic domain wall behaves as the electric capacitor only in the weak-gauge coupling region. This is because $HH^\dagger \simeq v^2$ holds everywhere in the strong-gauge coupling region so that no electric charge can be stored on the outer skins; see Eq. (5.43).

5.3. *1/4 BPS dyonic configurations*

Let us next consider the simplest 1/4 BPS dyonic solution $H_0 = (z, 1)$ in the $N_F = 2$ case. As mentioned below Eq. (5.24), the difference between the master equations for the purely magnetic and the dyonic cases amounts to the replacement of M by $M\cos\alpha$. Therefore, as in the case of dyonic domain walls, all the numerical solutions that we have obtained previously (Ref. [17]) are still valid for the dyonic configurations. Indeed, the master equation (5.24) in terms of the dimensionless parameters given in Eq. (2.24) reduces to

$$\partial_\rho^2 u + \frac{1}{\rho}\partial_\rho u + \partial_3^2 u = 1 - \left(\rho^2 \exp\left(\eta\tilde{m}' x^3\right) + \exp\left(-\eta\tilde{m}' x^3\right)\right)\exp\left(-u\right), \tag{5.49}$$

where we have written $\tilde{m} = \tilde{m}'/\cos\alpha$.

The energy density consists of six parts: the domain wall $\mathcal{T}_{\mathrm{W}}$, vortex string $\mathcal{T}_{\mathrm{S}}$, boojum $\mathcal{T}_{\mathrm{B}}$, $\mathcal{T}_4 = \partial_k j_k$, $\mathcal{Q}_{\mathrm{W}}$, and $\mathcal{Q}_{\mathrm{B}}$. The first four contributions have no changes from the purely magnetic case because of cancelation of $\cos\alpha$:

$$\tilde{\mathcal{T}}_{\mathrm{W};\alpha} = \frac{1}{g^2 v^4}\mathcal{T}_{\mathrm{W}}\cos\alpha = \partial_3^2 u, \tag{5.50}$$

$$\tilde{\mathcal{T}}_{\mathrm{S};\alpha} = \frac{1}{g^2 v^4}\mathcal{T}_{\mathrm{S}} = \left(\partial_1^2 + \partial_2^2\right) u, \tag{5.51}$$

$$\tilde{\mathcal{T}}_{\mathrm{B};\alpha} = \frac{1}{g^2 v^4}\mathcal{T}_{\mathrm{B}} \cos\alpha = 2\left\{(\partial_1\partial_3 u)^2 + (\partial_2\partial_3 u)^2 - \left(\partial_1^2 + \partial_2^2\right)u\, \partial_3^2 u\right\}, \tag{5.52}$$

$$\tilde{\mathcal{T}}_{4;\alpha} = \frac{1}{g^2 v^4}\mathcal{T}_4 = -\partial_k^2 \partial_k^2 u. \tag{5.53}$$

The remaining quantities depend on α as

$$\tilde{\mathcal{Q}}_{\mathrm{W};\alpha} = \frac{1}{g^2 v^4}\mathcal{Q}_{\mathrm{W}} \sin\alpha = \eta\, \partial_3 \left(\tilde{H}\tilde{M}'\tilde{H}^\dagger\right) \tan^2\alpha, \tag{5.54}$$

$$\tilde{\mathcal{Q}}_{\mathrm{B};\alpha} = \frac{1}{g^2 v^4}\mathcal{Q}_{\mathrm{B}} \sin\alpha = \partial_k^2 \left[(\partial_3 u)^2\right] \tan^2\alpha. \tag{5.55}$$

The electric and magnetic fields are given by

$$\tilde{E}_k = \frac{1}{g^2 v^2} E_k = \eta \tan\alpha\, \partial_k \partial_3 u, \tag{5.56}$$

$$(\tilde{B}_1, \tilde{B}_2, \tilde{B}_3) = \frac{1}{g^2 v^2}(B_1, B_2, B_3) = \xi \left(\partial_3\partial_1 u,\ \partial_2\partial_3 u,\ -(\partial_1^2 + \partial_2^2)u\right). \tag{5.57}$$

The electric charge density is

$$\tilde{\mathcal{Q}}_{E;\alpha} = \frac{\mathcal{Q}_E}{\sqrt{2}gv^3} = -\eta \tan\alpha\, \partial_3 \left(\tilde{H}\tilde{H}^\dagger\right). \tag{5.58}$$

Remember that the derivatives are with respect to the rescaled variables $\tilde{x}^k$.

In the following, we will set $\alpha = \pi/4$ and consider the masses $\tilde{m}' = 1/5$, 1, 10 ($\tilde{m} = \sqrt{2}/5$, $\sqrt{2}$, $10\sqrt{2}$), as examples for the strong-, intermediate-, and weak-gauge couplings, respectively.

Let us first look at Fig. 26 in which the dyonic charge densities for $\tilde{m}' = 1/5$ are shown. The distributions are quite different from those in the weak coupling solution. The domain wall steeply bends. Since $HH^\dagger \simeq v^2$ holds everywhere for the strong-gauge coupling, the induced electric charge is tiny ($\partial_3(HH^\dagger) \simeq 0$), so that it is no longer appropriate to regard it as an electric capacitor; see the top-left panel of Fig. 26. Only the region near the junction point is evidently charged positively, whereas the electric charge densities become diluted far away from the junction point. The electric and magnetic force lines are shown in the top-right panel of Fig. 26.

Figure 27 shows the electric charge densities for the intermediate mass $\tilde{m}' = 1$. Since the curvature of the domain wall is now smaller, the separation between the positive and negative electric charges is visible. Mean distance is of the same order as the domain wall width $2\tilde{m}' = 2$. Unlike the strong coupling case, both the positive and negative electric charge densities are not localized near the junction point, but they extend along the domain wall. The positive charges are distributed across the whole domain wall, whereas the negative charges have no support around the junction point. Therefore, the electric force lines bend near the junction point and asymptotically becomes vertical far from the boojum (see the top-right panel of Fig. 27).

Finally, we show the dyonic solution for $\tilde{m}' = 10$ in Fig. 28. As expected, it is clearly similar to an electric capacitor with a large distance $2\tilde{m}' = 20$ between positive and negative charges. The electric force lines are vertical except for the region near the boojum. From Fig. 28 one clearly sees that the electric charge and Noether charge appear on the outer skins of the domain wall in the weak

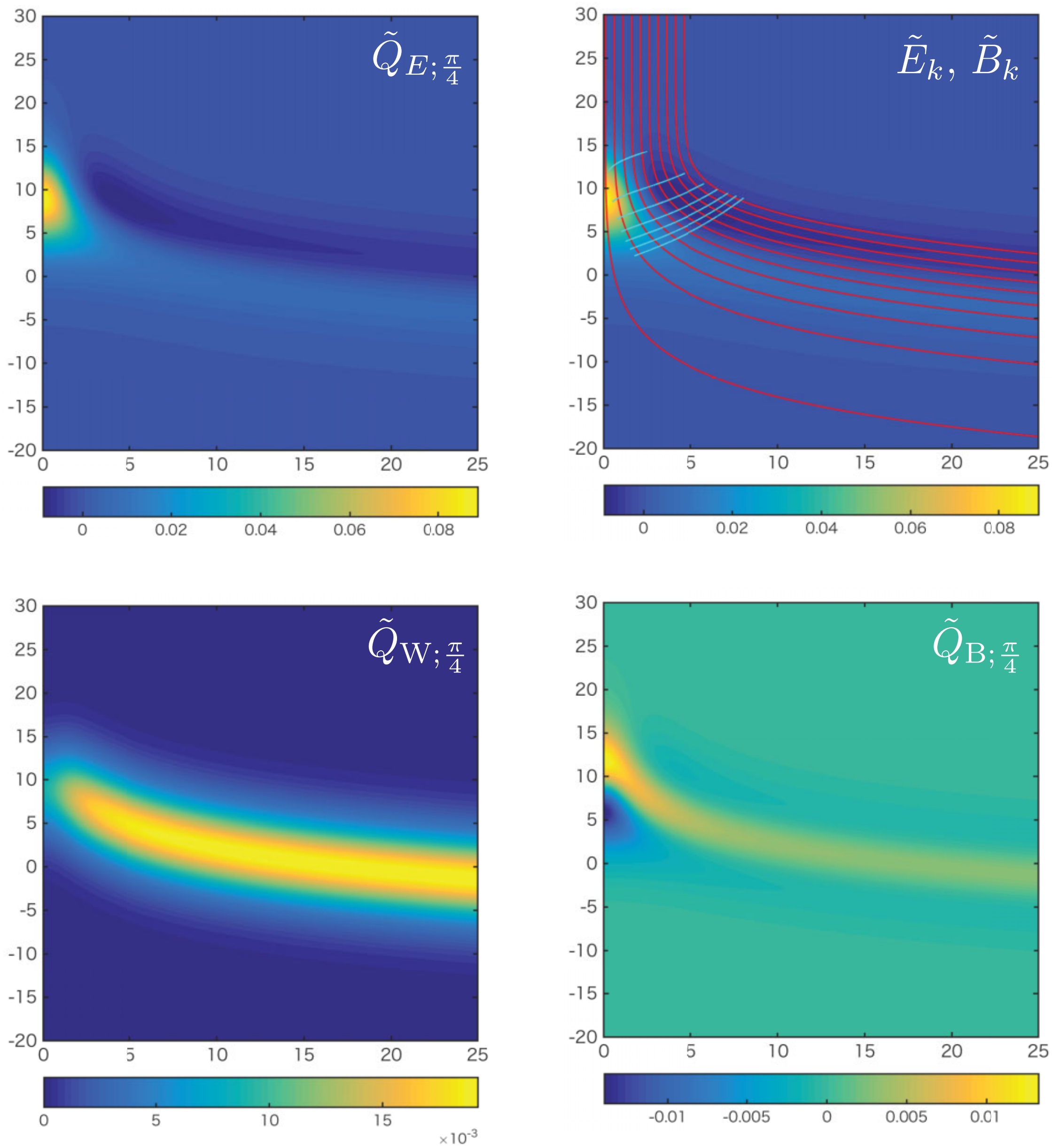

Fig. 26. The dyonic charges $\tilde{Q}_{E,W,B;\alpha=\pi/4}$ are shown for $\tilde{m}' = 1/5$ (strong-gauge coupling region). The topological charge densities are given in in Fig. 5 in Ref. [17]. The red curves show the magnetic force lines and the cyan ones correspond to the electric force lines.

coupling region. The Noether charge densities on the two outer skins have the same sign so that the total Noether charge does not vanish. The charge $\tilde{Q}_B$ is negative on the outer skins but it is positive inside the domain wall, which is consistent with the fact that $\int_{-\infty}^{\infty} dx^3\, \tilde{Q}_B = 0$.

6. Low-energy effective theory and Nambu–Goto/DBI action

In this section, we study 1/2 and 1/4 BPS configurations from the viewpoint of the low-energy effective actions, namely the Nambu–Goto (NG) action and the Dirac–Born–Infeld (DBI) action for the domain wall. As is well known, the low-energy effective theory for a simple domain wall with translational zero modes is the NG action. The low-energy effective action for the domain

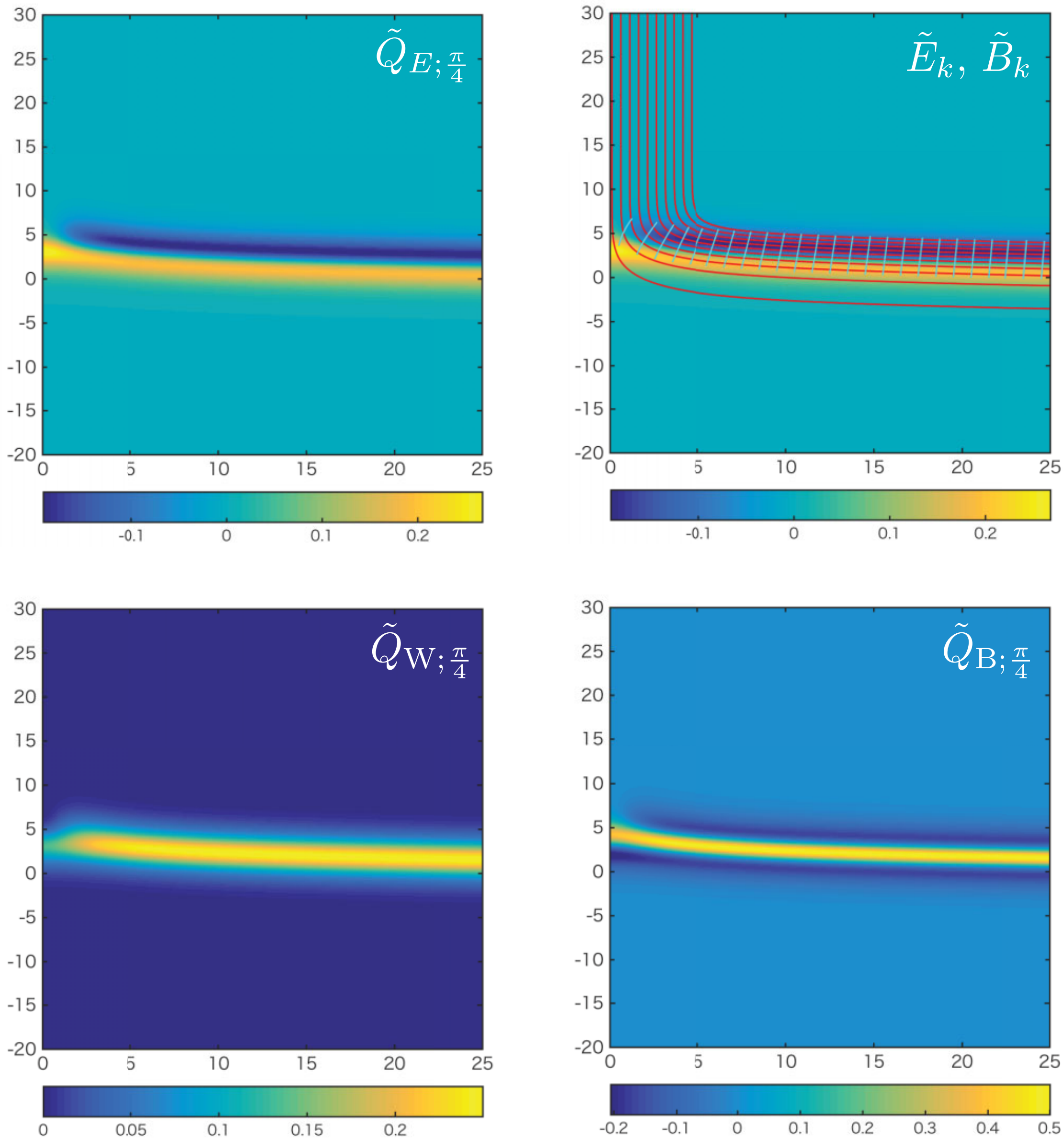

Fig. 27. The dyonic charges $\tilde{Q}_{E,W,B;\alpha=\pi/4}$ are shown for $\tilde{m}' = 1$ (strong-gauge coupling region). The topological charge densities are given in Fig. 6 in Ref. [17]. The red curves show the magnetic force lines and the cyan ones correspond to the electric force lines.

wall with not only translational zero modes but also internal moduli has been found to be the NG type (Refs. [10,34,35]) by regarding the internal space as extra dimensions. It is also known that the DBI action is dual to the NG action. In this section, we show that the domain wall, the vortex string ending on the domain wall, and their dyonic extension are reproduced in the NG action when the gauge coupling constant is taken to infinity. In the strong-gauge coupling limit, the vortex string asymptotically becomes the singular lump string attached to the domain wall. We call this configuration the spike domain wall. The dyonic extension of this configuration has already been studied in the massive nonlinear sigma model on $T^*\mathbb{C}P^1$, and it was shown that the configuration is realized as BIon in the DBI action (Ref. [10]). We review the dyonic extension of the spike domain wall from the viewpoint of the NG action. Finally, we discuss whether the nonsingular

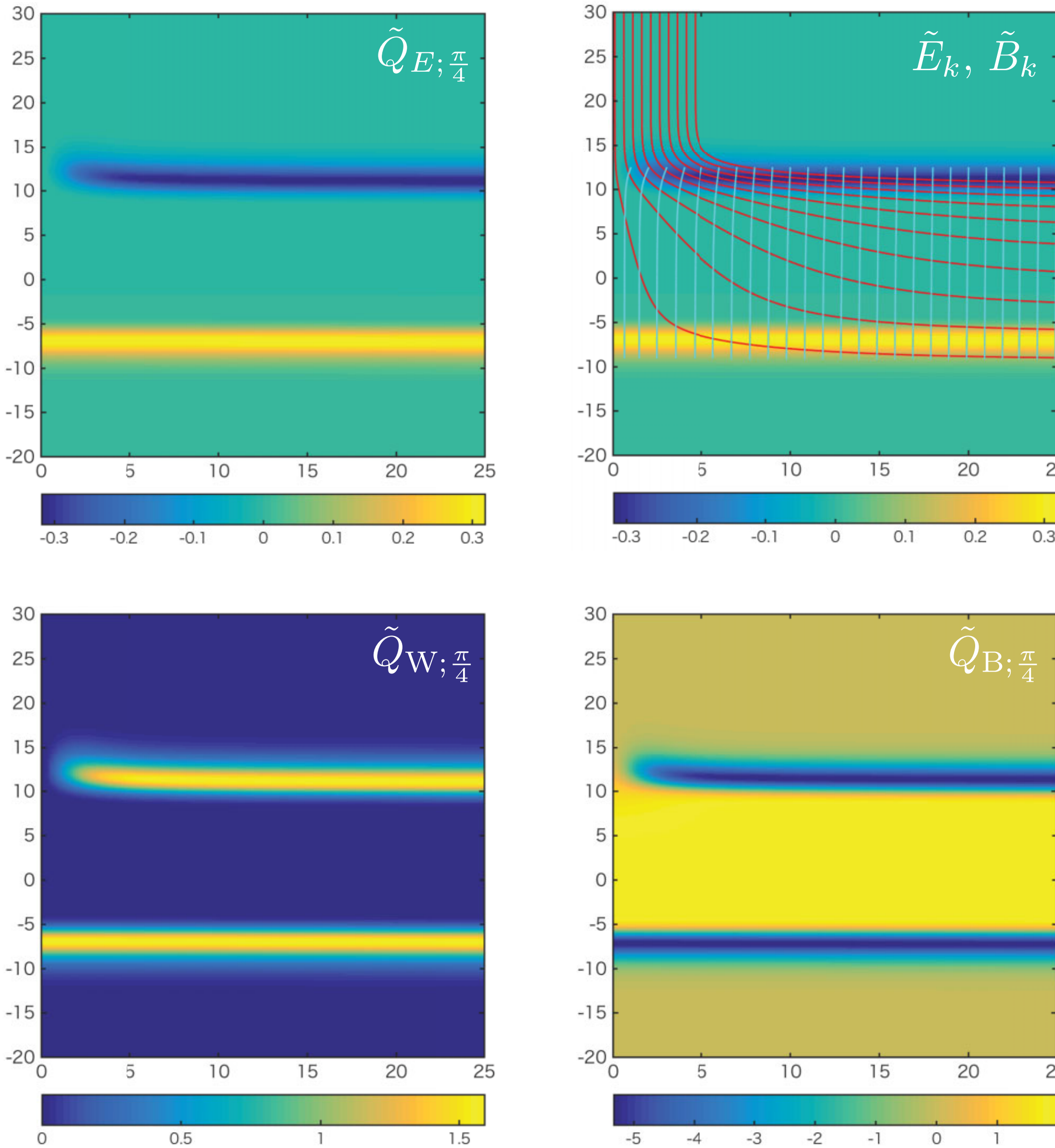

Fig. 28. The dyonic charges $\tilde{Q}_{E,W,B;\alpha=\pi/4}$ are shown for $\tilde{m}' = 10$ (strong-gauge coupling region). The topological charge densities are given in Fig. 7 in Ref. [17]. The red curves show the magnetic force lines and the cyan ones correspond to the electric force lines.

lump string with the size moduli, the semilocal boojums studied in Sect. 3.3, can be realized in the DBI action.

6.1. Nambu–Goto action and the Hamiltonian

We start with the NG action in $(2+1)$ space-time dimensions (Ref. [10]):

$$\mathcal{L}_{\mathrm{NG}} = -\hat{T}_{\mathrm{W}} \left(\det\left(\eta_{\alpha\beta} - \partial_\alpha X \partial_\beta X - \partial_\alpha \phi \partial_\beta \phi\right)\right)^{1/2}, \quad \alpha,\ \beta = 0, 1, 2, \tag{6.1}$$

where X and ϕ are scalar fields, which will be identified with the position and the phase moduli of the domain wall solution and $\hat{T}_{\mathrm{W}}$ is the membrane tension. Here we have used the so-called physical gauge where the induced metric on the world-volume of the brane is flat (i.e., $\eta = \mathrm{diag}(1, -1, -1)$). We can explicitly write this as

$$\mathcal{L}_{\mathrm{NG}} = -\hat{T}_{\mathrm{W}} D_{\mathrm{NG}}^{1/2}, \tag{6.2}$$

where

$$D_{\mathrm{NG}} = 1 - (\partial_\alpha X \partial^\alpha X) - (\partial_\alpha \phi \partial^\alpha \phi) + (\partial_\alpha X \partial^\alpha X)(\partial_\beta \phi \partial^\beta \phi) - (\partial_\alpha X \partial^\alpha \phi)^2. \tag{6.3}$$

The canonical momenta for X and ϕ are given by

$$P_X = \frac{\partial \mathcal{L}}{\partial \dot{X}} = -\hat{T}_{\mathrm{W}} D_{\mathrm{NG}}^{-1/2} \left\{ \dot{X} - \dot{X}(\partial_\alpha \phi \partial^\alpha \phi) + \dot{\phi}(\partial_\alpha X \partial^\alpha \phi) \right\}, \tag{6.4}$$

$$P_\phi = \frac{\partial \mathcal{L}}{\partial \dot{\phi}} = \hat{T}_{\mathrm{W}} D_{\mathrm{NG}}^{-1/2} \left\{ \dot{\phi} - \dot{\phi}(\partial_\alpha X \partial^\alpha X) + \dot{X}(\partial_\alpha X \partial^\alpha \phi) \right\}, \tag{6.5}$$

so that the Hamiltonian is obtained as

$$\begin{aligned} \mathcal{H}_{\mathrm{NG}} &= P_X \dot{X} + P_\phi \dot{\phi} - \mathcal{L}_{\mathrm{NG}} \\ &= \hat{T}_{\mathrm{W}} D_{\mathrm{NG}}^{-1/2} \left\{ 1 + (\partial_i X)^2 + (\partial_i \phi)^2 + (\partial_i X)^2 (\partial_j \phi)^2 - (\partial_i X \partial_i \phi)^2 \right\}, \end{aligned} \tag{6.6}$$

where the indices $i, j = 1, 2$ are summed over.

6.2. *The domain wall, its dyonic extension, and the NG action*

Let us recall the domain wall solution discussed in Sect. 2. The master equation for the flat domain wall is given in Eq. (2.16) when u is restricted to depend on the x^3 coordinate only. In the strong-gauge coupling limit, the master equation can be solved to give

$$u_{g\to\infty} = \log \Omega_0, \tag{6.7}$$

where Ω_0 is given in Eq. (2.16). For simplicity, let us consider the $N_F = 2$ case. In this case, the moduli matrix $H_0(z)$ in Eq. (2.15) is just a constant. We choose

$$H_0(z) = \left(\exp\left(-\frac{m}{2}(X + i\phi) \right), \exp\left(\frac{m}{2}(X + i\phi) \right) \right), \quad M = \mathrm{diag}(m/2, -m/2), \tag{6.8}$$

with $\xi = \eta = 1$. Then Eq. (6.7) gives

$$u_{g\to\infty}(x^3) = \log\left(\exp\left(m(x^3 - X) \right) + \exp\left(-m(x^3 - X) \right) \right). \tag{6.9}$$

This shows that the constant parameter X corresponds to the position moduli. The other constant parameter ϕ is the internal moduli, which is the Nambu–Goldstone mode associated with the spontaneously broken $\mathrm{U}(1)_F$ symmetry. The energy of the domain wall is readily calculated by integrating Eq. (2.18) over all the space directions:

$$E_{\mathrm{wall}} = \int d^3x\, \mathcal{T}_{\mathrm{W}} = T_{\mathrm{W}} A, \tag{6.10}$$

where $T_{\mathrm{W}} = mv^2$ is the domain wall's tension and A is the area of the domain wall.

Now let us study the flat domain wall solution in the NG action. It is just given by considering constants for X and ϕ. The NG Hamiltonian Eq. (6.6) reduces to

$$\mathcal{H}_{\mathrm{NG}} = \hat{T}_{\mathrm{W}}. \tag{6.11}$$

The energy is obtained by integrating along the membrane directions:

$$E_{\rm NG} = \int d^2x\, \mathcal{H}_{\rm NG} = \hat{T}_{\rm W} A. \tag{6.12}$$

The energy equations (6.10) and (6.12) completely coincide if the domain wall tension $T_{\rm W}$ is identified with the membrane tension $\hat{T}_{\rm W}$. Therefore, as expected, the NG action with constant X and ϕ realizes the domain wall in the field-theoretical model.

Next we consider the Q-extension (dyonic extension) of the domain wall. Let us first recall the field theory solution given in Eqs. (5.14)–(5.17). The dyonic extension of the master equation is given in Eq. (5.24). Substituting Eq. (6.8) with X and ϕ being constants into Eq. (5.24), we obtain the solution in the strong-gauge coupling limit as

$$u_{g\to\infty}(x^3) = \log\left(\exp\left(m\cos\alpha\, x^3 - mX\right) + \exp\left(-m\cos\alpha\, x^3 + mX\right)\right). \tag{6.13}$$

The energy of the system is obtained from Eq. (5.30) with Eqs. (5.21) and (5.27):

$$E_{\text{Q-wall}} = \int d^3x \left(\mathcal{T}_{\rm W}\cos\alpha + \mathcal{Q}_{\rm W}\sin\alpha\right) = \left(T_{\rm W}^2 + Q_{\rm W}^2\right)^{1/2} A, \tag{6.14}$$

where we have used Eq. (5.29). The domain wall tension $T_{\rm W}$ and the Noether charge $Q_{\rm W}$ are calculated by Eqs. (5.25) and (5.28): $T_{\rm W} = mv^2$ and $Q_{\rm W} = mv^2\tan\alpha$.

Let us consider the corresponding configuration in the NG action. We take the time-dependent phase

$$X = \text{const.}, \qquad \phi = \frac{\omega}{\hat{m}} t, \tag{6.15}$$

where ω is a constant angular velocity and we have introduced a constant parameter $\hat{m}$ of mass dimension one in order that ϕ has mass dimension -1. In this case, the energy is obtained as

$$E_{\rm NG} = \frac{\hat{T}_{\rm W}}{\left(1 - (\omega/\hat{m})^2\right)^{1/2}} A. \tag{6.16}$$

The conserved momentum P_ϕ for this solution is given by

$$P_\phi = \hat{T}_{\rm W} \frac{\omega/\hat{m}}{\left(1 - (\omega/\hat{m})^2\right)^{1/2}}. \tag{6.17}$$

Then the energy can be written as

$$E_{\rm NG} = \left(\hat{T}_{\rm W}^2 + P_\phi^2\right)^{1/2} A. \tag{6.18}$$

We identify $T_{\rm W} = \hat{T}_{\rm W}$ as before. Furthermore, we should identify $\omega/\hat{m} = \sin\alpha$ from Eq. (5.14), which tells us that the Q-charge Eq. (5.29) in the field theory is understood as

$$P_\phi = \hat{T}_{\rm W}\tan\alpha = Q_{\rm W}. \tag{6.19}$$

Thus, Eq. (6.18) coincides with Eq. (6.14). We conclude that the configuration Eq. (6.15) in the NG action realizes the Q-extension of the domain wall in the field theory.

6.3. *Dyonic extension of the spike domain wall and NG action*

In this subsection, we study the 1/4 BPS dyonic extension of the spike domain wall that the lump vortex attaches on the domain wall. The master equation for this configuration is given in Eq. (5.24) where u depends on all the space coordinates. Considering the $N_F = 2$ case, the moduli matrix and the mass matrix are given by

$$H_0(z) = (z, 1), \qquad M = \mathrm{diag}(m/2, -m/2). \tag{6.20}$$

In the strong-gauge coupling limit the master equation (5.24) is solved as

$$u_{g\to\infty}(z, \bar{z}, x^3) = \log\left(\rho^2 \exp\left(m\cos\alpha\, x^3\right) + \exp\left(-m\cos\alpha\, x^3\right)\right), \tag{6.21}$$

where $|z|^2 = \rho^2$. The total energy of the configuration is

$$E_{1/4} = \int d^3x(\mathcal{T}_{\mathrm{W}}\cos\alpha + \mathcal{Q}_{\mathrm{W}}\sin\alpha + \mathcal{T}_{\mathrm{S}} + \mathcal{T}_{\mathrm{B}}), \tag{6.22}$$

where $\mathcal{T}_{\mathrm{S}}$ and $\mathcal{T}_{\mathrm{B}}$ are defined in Eqs. (5.22) and (5.23), respectively. Taking into account the fact that in the strong-gauge coupling limit Eq. (5.23) is vanishing, the energy is given as

$$E_{1/4} = \left(T_{\mathrm{W}}^2 + Q_{\mathrm{W}}^2\right)^{1/2} A + T_{\mathrm{S}}L. \tag{6.23}$$

Here we have used Eq. (5.29) and T_{S} is the string tension given in Eq. (5.31), $T_{\mathrm{S}} = 2\pi v^2|k|$ where k is the vortex winding number, and L is length of the vortex string.

We consider the corresponding configuration in the NG action. We take the following configuration:

$$X \to X(x^1, x^2), \quad \phi \to \frac{\omega}{\hat{m}}t + \phi(x^1, x^2). \tag{6.24}$$

To simplify notation, let us introduce

$$a_i \equiv \partial_i X, \qquad b_i \equiv \partial_i\phi. \tag{6.25}$$

Then the Hamiltonian (6.6) is expressed as

$$\mathcal{H}_{\mathrm{NG}} = \hat{T}_{\mathrm{W}} \frac{1 + a_i^2 + b_i^2 + (\epsilon_{ij}a_i b_j)^2}{\left(1 + a_i^2 + b_i^2 + (\epsilon_{ij}a_i b_j)^2 - (\omega/\hat{m})^2(1 + a_i^2)\right)^{1/2}}, \tag{6.26}$$

where $\epsilon_{12} = 1$ and we have used $a_i^2 b_j^2 - (a_i b_i)^2 = (\epsilon_{ij}a_i b_j)^2$. Let us further rewrite this in terms of $\tilde{b}_i \equiv b_i/\left(1 - (\omega/\hat{m})^2\right)^{1/2}$:

$$\mathcal{H}_{\mathrm{NG}} = \frac{\hat{T}_{\mathrm{W}}}{\left(1 - (\omega/\hat{m})^2\right)^{1/2}} \left(\mathcal{H}^{1/2} - \frac{(\omega/\hat{m})^2(\tilde{b}_i^2 + (\epsilon_{ij}a_i\tilde{b}_j)^2)}{\mathcal{H}^{1/2}}\right), \tag{6.27}$$

where

$$\mathcal{H} = 1 + (a_i)^2 + (\tilde{b}_i)^2 + (\epsilon_{ij}a_i\tilde{b}_j)^2. \tag{6.28}$$

Now we are ready to minimize the Hamiltonian $\mathcal{H}_{\rm NG}$. To this end, we first minimize $\mathcal{H}$ as

$$\mathcal{H} = (a_i \pm \epsilon_{ij}\tilde{b}_j)^2 + (1 \mp \epsilon_{ij}a_i\tilde{b}_j)^2 \geq (1 \mp \epsilon_{ij}a_i\tilde{b}_j)^2. \tag{6.29}$$

The last inequality is saturated when the equation

$$a_i \pm \epsilon_{ij}\tilde{b}_j = 0 \tag{6.30}$$

is satisfied. The key observation is that when Eq. (6.30) holds, the first term in Eq. (6.27) is minimized while the second term is maximized. Indeed, the numerator in the second term is maximized because $(\epsilon_{ij}a_i\tilde{b}_j)^2$ becomes maximum when a_i is orthogonal to b_i, and at the same time the denominator is minimized. Taking account of the minus sign in front of the second term of Eq. (6.27), it is found that the Hamiltonian is minimized when the BPS equation (6.30) is satisfied. The BPS energy in terms of the original variable X is given by

$$\mathcal{H}_{\rm NG} = \hat{T}_{\rm W}\left\{\frac{1}{\left(1-(\omega/\hat{m})^2\right)^{1/2}} + \left(1-(\omega/\hat{m})^2\right)^{1/2}(\partial_i X)^2\right\}. \tag{6.31}$$

We now consider that a point particle corresponding to the endpoint of the lump string is placed on the membrane. Comparing Eqs. (6.8) and (6.20), one is naturally lead to the following identification:

$$\phi = \pm\frac{1}{\hat{m}}\arctan\frac{x^2}{x^1}. \tag{6.32}$$

Again, we have introduced a certain parameter $\hat{m}$ of mass dimension 1. Combining Eq. (6.30) with Eq. (6.32) gives

$$X(\rho) = -\frac{1}{\left(\hat{m}^2-\omega^2\right)^{1/2}}\log\rho, \tag{6.33}$$

where $\rho = \left((x^1)^2+(x^2)^2\right)^{1/2}$. With the solution (6.33), the Hamiltonian (6.31) turns out to be

$$\mathcal{H}_{\rm NG} = \frac{\hat{T}_{\rm W}}{\left(1-(\omega/\hat{m})^2\right)^{1/2}}\left(1+\frac{1}{\hat{m}^2\rho^2}\right). \tag{6.34}$$

The energy is

$$E_{\rm NG} = \int d^2x\,\mathcal{H}_{\rm NG} = \frac{\hat{T}_{\rm W}}{\left(1-(\omega/\hat{m})^2\right)^{1/2}}A + \frac{2\pi\hat{T}_{\rm W}}{\hat{m}\left(\hat{m}^2-\omega^2\right)^{1/2}}(\log R-\log\delta), \tag{6.35}$$

where we have introduced the ultraviolet cutoff $\rho=\delta$ and the infrared cutoff $\rho=R$. With the use of Eqs. (6.19) and (6.33), the energy is rewritten as

$$E_{\rm NG} = \left(\hat{T}_{\rm W}^2+P_\phi^2\right)^{1/2}A + \frac{2\pi\hat{T}_{\rm W}}{\hat{m}}\hat{L}, \tag{6.36}$$

where $\hat{L} \equiv X(\delta)-X(R)$. Identifying $T_{\rm W}=\hat{T}_{\rm W}$ and $m=\hat{m}$, it is found that $2\pi\hat{T}_{\rm W}/\hat{m}$ ($T_{\rm W}=mv^2$) coincides with the string tension $T_{\rm S}=2\pi v^2$ in the field theory. Relating $\hat{L}$ to the length of the vortex string, the energy (6.36) coincides with Eq. (6.23) in the field-theoretical model.

6.4. Relation between solutions of NG action and DBI action

In this subsection, we show that the dyonic extension of the spike domain wall (6.20) in the field theory is also realized in the DBI action (Ref. [10]). Rather than minimizing the Hamiltonian of the DBI action we derive the BPS equations in the DBI action by transforming Eq. (6.30).

First we derive the $(2+1)$-dimensional DBI action from the NG action (6.1) by dualization:

$$\mathcal{L}_{\rm DBI} = \mathcal{L}_{\rm NG} + \frac{\kappa}{2}\hat{T}_{\rm W}\varepsilon_{\alpha\beta\gamma}\hat{F}^{\alpha\beta}\partial^{\gamma}\phi, \tag{6.37}$$

where the last term is called the BF term consisting of $\hat{F}_{\alpha\beta} = \partial_\alpha\hat{A}_\beta - \partial_\beta\hat{A}_\alpha$, being an Abelian field strength, and κ an arbitrary constant of mass dimension -2. Notice that the term we added is a total divergence with no effect on dynamics. Let us eliminate ϕ by using its equation of motion. Variation of the above Lagrangian with respect to $\partial_\alpha\phi$ leads to the condition

$$\kappa\hat{F}^*_\alpha = \frac{-1}{(D_{\rm NG})^{1/2}}\Big[\big\{1-(\partial_\beta X\partial^\beta X)\big\}\,\partial_\alpha\phi + \big(\partial_\beta X\partial^\beta\phi\big)\partial_\alpha X\Big], \tag{6.38}$$

where $\hat{F}^*_\alpha = \frac{1}{2}\varepsilon_{\alpha\beta\gamma}\hat{F}^{\beta\gamma}$ ($\epsilon_{123}=1$). Contracting the above with $\partial^\alpha\phi$ we obtain

$$\kappa(\hat{F}^*_\alpha\partial^\alpha\phi) = (D_{\rm NG})^{1/2} - \frac{1-(\partial_\alpha X\partial^\alpha X)}{(D_{\rm NG})^{1/2}}. \tag{6.39}$$

Substituting this into Eq. (6.37), we have

$$\mathcal{L}_{\rm DBI} = -\hat{T}_{\rm W}\frac{1-(\partial_\alpha X\partial^\alpha X)}{(D_{\rm NG})^{1/2}}. \tag{6.40}$$

In order to eliminate ϕ in $D_{\rm NG}$, we consider contractions of Eq. (6.38) with $\partial^\alpha X$ and $\hat{F}^{*\alpha}$ as

$$\kappa(\hat{F}^*_\alpha\partial^\alpha\phi) = \frac{-1}{(D_{\rm NG})^{1/2}}(\partial_\alpha\phi\partial^\alpha X), \tag{6.41}$$

$$\begin{aligned}&\kappa(\partial_\alpha\phi\partial^\alpha\phi)(1-(\partial_\beta X\partial^\beta X))^2\\ &\quad= \frac{-1}{(D_{\rm NG})^{1/2}}\Big\{(1-(\partial_\alpha X\partial^\alpha X))(\partial_\beta\phi\hat{F}^{\beta*}) + (\partial_\alpha X\partial^\alpha\phi)(\partial_\beta X\hat{F}^{\beta*})\Big\}.\end{aligned} \tag{6.42}$$

Equations (6.39)–(6.42) can be combined to solve for $D_{\rm NG}$:

$$D_{\rm NG} = \frac{\big(1-(\partial_\alpha X\partial^\alpha X)\big)^2}{1-(\partial_\beta X\partial^\beta X)+\kappa^2(\hat{F}^*_\beta\hat{F}^{\beta*})-\kappa^2\big(\partial_\beta X\hat{F}^{\beta*}\big)^2}. \tag{6.43}$$

With this expression at hand we use Eq. (6.39) to obtain the DBI action

$$\begin{aligned}\mathcal{L}_{\rm DBI} &= -\hat{T}_{\rm W}\Big(1-(\partial_\alpha X\partial^\alpha X)+\kappa^2(\hat{F}^*_\alpha\hat{F}^{\alpha*})-\kappa^2\big(\partial_\alpha X\hat{F}^{\alpha*}\big)^2\Big)^{1/2}\\ &= -\hat{T}_{\rm W}\Big(\det\big(\eta_{\alpha\beta}-\partial_\alpha X\partial_\beta X+\kappa\hat{F}_{\alpha\beta}\big)\Big)^{1/2},\end{aligned} \tag{6.44}$$

where the validity of the last equality can be checked by direct evaluation of the determinant.

Next, we derive the Hamiltonian. In the following, we set $\dot{X} = 0$ since we are not interested in the configuration where X depends on time. First we shall write the Lagrangian (6.44) in terms of the electric and magnetic fields defined by $\hat{F}_{0i} = \hat{E}_i$ $(i = 1, 2)$ and $\hat{F}_{12} = \hat{B}$:

$$\mathcal{L}_{\rm DBI} = -\hat{T}_{\rm W}\sqrt{D_{\rm DBI}}, \tag{6.45}$$

where

$$D_{\rm DBI} = 1 + (\partial_i X)^2 - \kappa^2 \hat{E}_i^2 + \kappa^2 \hat{B}^2 - \kappa^2 \left(\epsilon_{ij}\hat{E}_i \partial_j X\right)^2. \tag{6.46}$$

Here the indices i, j are summed over. In the following we rescale:

$$\kappa \hat{E}_i \to \hat{E}_i, \qquad \kappa \hat{B}_i \to \hat{B}_i. \tag{6.47}$$

A canonical momentum is obtained by differentiating Eq. (6.45) with respect to $\hat{E}_i$:

$$\Pi_i = \frac{\partial \mathcal{L}_{\rm DBI}}{\partial \hat{E}_i} = -\hat{T}_{\rm W} D_{\rm DBI}^{-1/2}(\hat{E}_i - \epsilon_{ij}\partial_j A), \tag{6.48}$$

where

$$A = \epsilon_{ij}\partial_i X \hat{E}_j. \tag{6.49}$$

The Hamiltonian of the DBI action is then obtained as

$$\begin{aligned}\mathcal{H}_{\rm DBI} &= \Pi_i \hat{E}_i - \mathcal{L}_{\rm DBI} \\ &= \hat{T}_{\rm W} D_{\rm DBI}^{-1/2}(1 + (\partial_i X)^2 + \hat{B}^2).\end{aligned} \tag{6.50}$$

The remaining task for the derivation of the Hamiltonian is to write $D_{\rm DBI}$ in terms of X, Π_i, and $\hat{B}$. To this end, we calculate Π_i^2 and $\epsilon_{ij}\partial_i X \Pi_j$:

$$\Pi_i^2 = \hat{T}_{\rm W}^2 D_{\rm DBI}^{-1}\left\{\hat{E}_i^2 + A^2 + (1 + (\partial_i X)^2)A^2\right\}, \tag{6.51}$$

$$\epsilon_{ij}\partial_i X \Pi_j = \hat{T}_{\rm W} D_{\rm DBI}^{-1/2}(1 + (\partial_i X)^2)A. \tag{6.52}$$

From Eq. (6.52) we have

$$A = \frac{D_{\rm DBI}^{1/2}}{\hat{T}_{\rm W}(1 + (\partial_i X)^2)}(\epsilon_{kl}\partial_k \Pi_l). \tag{6.53}$$

From Eq. (6.46) we find

$$\hat{E}_i^2 + A^2 = 1 + (\partial_i X)^2 + \hat{B}^2 - D_{\rm DBI}. \tag{6.54}$$

Substituting Eqs. (6.53) and (6.54) into Eq. (6.51), we reach

$$\Pi_i^2 = \hat{T}_{\rm W}^2 D_{\rm DBI}^{-1}\left\{1 + (\partial_i X)^2 + \hat{B}^2 - D_{\rm DBI} + \frac{D_{\rm DBI}(\epsilon_{ij}\partial_i X \Pi_j)^2}{1 + (\partial_k X)^2}\right\}. \tag{6.55}$$

Solving this equation with respect to D_{DBI}, we have

$$D_{\mathrm{DBI}} = \frac{\hat{T}_{\mathrm{W}}^2(1+(\partial_i X)^2+\hat{B}^2)(1+(\partial_i X)^2)}{\hat{T}_{\mathrm{W}}^2(1+(\partial_i X)^2)+\Pi_i^2+(\partial_i X\Pi_i)^2}. \tag{6.56}$$

We substitute Eq. (6.56) into the Hamiltonian (6.50) and obtain the final expression for the Hamiltonian:

$$\mathcal{H}_{\mathrm{DBI}} = \left(\frac{\left\{\hat{T}_{\mathrm{W}}^2(1+(\partial_i X)^2)+\Pi_i^2+(\partial_i X\Pi_i)^2\right\}\left\{1+(\partial_j X)^2+\hat{B}^2\right\}}{1+(\partial_k X)^2}\right)^{1/2}. \tag{6.57}$$

Note that this is different from the DBI Hamiltonian obtained in Ref. [10].

Let us next rewrite the BPS equation (6.30) in terms of the DBI variables. To this end, we first show how $\hat{B}$ and $\hat{E}_i$ are written in terms of the fields X and ϕ in the NG action. For $X \to X(x^1,x^2)$ and $\phi \to (\omega/\hat{m})t+\phi(x^1,x^2)$ as is given in Eq. (6.24), from Eq. (6.38) we have

$$\hat{B} = -\frac{(\omega/\hat{m})}{(D_{\mathrm{NG}})^{1/2}}(1+(\partial_i X)^2), \tag{6.58}$$

$$\hat{E}_i = \frac{1}{(D_{\mathrm{NG}})^{1/2}}\left\{(1+(\partial_k X)^2)\epsilon_{ij}\partial_j\phi-(\partial_k X\partial_k\phi)(\epsilon_{ij}\partial_j X)\right\}, \tag{6.59}$$

from which we find

$$\hat{B}^2 = \frac{(\omega/\hat{m})^2}{D_{\mathrm{NG}}}(1+(\partial_i X)^2)^2, \tag{6.60}$$

$$\hat{E}_i^2 = \frac{1}{D_{\mathrm{NG}}}\left\{(1+(\partial_i X)^2)^2(\partial_j\phi)^2-(\partial_i X\partial_i\phi)^2(\partial_j X)^2-2(\partial_i X\partial_i\phi)^2\right\}. \tag{6.61}$$

Combining Eq. (6.49) with Eq. (6.61) we obtain

$$A^2 = (\partial_i X)^2\hat{E}_j^2-(\partial_i X\hat{E}_i)^2 = \frac{(\partial_i X\partial_i\phi)^2}{D_{\mathrm{NG}}}. \tag{6.62}$$

Substituting Eqs. (6.60)–(6.62) into D_{DBI} given in Eq. (6.46), it can be shown that

$$D_{\mathrm{DBI}} = \frac{(1+(\partial_i X)^2)^2}{D_{\mathrm{NG}}}. \tag{6.63}$$

Now we are ready to rewrite the BPS equation (6.30) in terms of the DBI language. From Eq. (6.30) we have

$$\partial_i\phi\partial_i X = 0, \tag{6.64}$$

and

$$\begin{aligned} D_{\mathrm{NG}} &= \left(1+(\partial_i X)^2\right)\left(1-(\omega/\hat{m})^2+(\partial_j\phi)^2\right) \\ &= (1-(\omega/\hat{m})^2)\left(1+(\partial_i X)^2\right)^2. \end{aligned} \tag{6.65}$$

Substituting this into Eq. (6.63), we have

$$D_{\mathrm{DBI}} = \frac{1}{1-(\omega/\hat{m})^2}. \tag{6.66}$$

Furthermore, Eq. (6.59) gives us the relation

$$\hat{E}_i = \sqrt{D_{\mathrm{DBI}}}\,\epsilon_{ij}\partial_j\phi. \tag{6.67}$$

Since $A = 0$, Eq. (6.48) is simplified as

$$\Pi_i = \hat{T}_{\mathrm{W}}\frac{\hat{E}_i}{\sqrt{D_{\mathrm{DBI}}}}. \tag{6.68}$$

Combining Eqs. (6.67) and (6.68) tells us that

$$\epsilon_{ij}\partial_j\phi = \hat{T}_{\mathrm{W}}^{-1}\Pi_i. \tag{6.69}$$

Substituting Eq. (6.30) into Eq. (6.58), we find

$$\hat{B} = -\frac{\omega}{\hat{m}}\left(\frac{1+(\partial_i X)^2}{1-\omega^2+(\partial_i\phi)^2}\right)^{1/2} = -\frac{\omega}{\left(\hat{m}^2-\omega^2\right)^{1/2}}. \tag{6.70}$$

Using Eqs. (6.69) and (6.70), the BPS equation (6.30) in the NG action is rewritten as

$$\partial_i X = \pm\left(1+\hat{B}^2\right)^{1/2}\ \hat{T}_{\mathrm{W}}^{-1}\Pi_i. \tag{6.71}$$

This is the BPS equation for the dyonic extension of the spike domain wall in terms of the DBI variables. Note that we eventually arrive at the same BPS equation given in Ref. [10], although our Hamiltonian (6.57) is different from one in Ref. [10].

In order to check that this equation leads to the desired result, we substitute Eq. (6.71) into the Hamiltonian (6.57). It yields

$$\mathcal{H}_{\mathrm{DBI}} = \hat{T}_{\mathrm{W}}\left(1+\hat{B}^2\right)^{1/2}\left(1+\hat{T}_{\mathrm{W}}^{-1}\Pi_i^2\right). \tag{6.72}$$

We shall consider the following configuration:

$$\Pi_i = \frac{\hat{T}_{\mathrm{W}}}{\hat{m}}\frac{x_i}{\rho^2}. \tag{6.73}$$

This configuration represents a unit electric charge placed on the membrane. This fact is understood from the relation (6.68), which gives

$$\hat{E}_i = \hat{T}_{\mathrm{W}}^{-1}\Pi_i = \frac{1}{\hat{m}}\frac{x_i}{\rho^2}. \tag{6.74}$$

Thus, the factor $1/\hat{m}$ is interpreted as an electric charge. A solution of the BPS equation (6.71), which is called a BIon, is in this case

$$X = -\frac{1}{\hat{m}}\left(1+\hat{B}^2\right)^{1/2}\log\rho. \tag{6.75}$$

Substituting Eq. (6.73) into Eq. (6.72) and integrating over the membrane directions, we find the energy of the configuration to be

$$E_{\mathrm{DBI}} = \hat{T}_{\mathrm{W}}\left(1+\hat{B}^2\right)^{1/2}A + \frac{2\pi\hat{T}_{\mathrm{W}}}{\hat{m}}\left(1+\hat{B}^2\right)^{1/2}(\log R - \log\delta), \tag{6.76}$$

where we have introduced the infrared and ultraviolet cutoff $\rho = R$ and $\rho = \delta$, respectively. The energy is rewritten as

$$E_{\rm DBI} = \hat{T}_{\rm W}\left(1+\hat{B}^2\right)^{1/2} A + \frac{2\pi \hat{T}_{\rm W}}{\hat{m}}\hat{L}, \tag{6.77}$$

where $\hat{L} = X(\delta) - X(R)$. Taking Eq. (6.70) with the choice $\omega/\hat{m} = \sin\alpha$, $\hat{T}_{\rm W} = T_{\rm W}$, and $\hat{m} = m$ into account, it is found that this expression is the same as Eq. (6.36) obtained in the NG action. Therefore it is concluded that the BPS equation (6.71) in the DBI action reproduces the dyonic extension of the spike domain wall Eq. (6.20) in the field theory.

Before closing this subsection, let us make a comment on the relation between the magnetic scalar potential φ introduced by Eq. (3.31) in Sect. 3.5 and X given in Eq. (6.75). The scalar potential for the magnetic field $B_i(x^1, x^2)$ in the original gauge theory is represented by φ. We have found the relation $\varphi = mx^3(x^1, x^2)/d_{\rm W}$ and $x^3(x^1, x^2) = -u_{\rm S}(x^1, x^2)/2m$. In the strong-gauge coupling limit, we have $u_{\rm S} = \log\rho^2$, so that $x^3(x^1, x^2) = -(\log\rho)/m$, which precisely coincides with Eq. (6.75) in the case that $\hat{B} = 0$. On the other hand, from Eqs. (6.74) and (6.75), X is the scalar potential for the dual electric field $\hat{E}_i(x^1, x^2)$. Thus, the magnetic field B_i in the original gauge theory and the dual electric field $\hat{E}_i$ in the effective theory are generated by the same static potential.

6.5. The semilocal BIon: Round spike configuration and DBI action

In this subsection, we discuss the semilocal BIon—the round spike domain wall configuration, where the spike's tip is smoothed out by introducing a lump size moduli. This configuration should be a DBI counterpart to the semilocal boojum that we studied for the finite-gauge coupling in Sect. 3.3. Our purpose in this subsection is to investigate whether the semilocal boojum in the strong-gauge coupling limit in the field theory is realized in the DBI action.

As the simplest example of the semilocal vortex, let us consider the $N_F = 3$ case with vanishing Q-charge. The moduli matrix of the configuration is

$$H_0(z) = (z, a, 1), \qquad M = {\rm diag}(m/2, m/2, -m/2). \tag{6.78}$$

where $a \in \mathbb{R}$ is a size moduli. Supposing that the u depends on all the space directions, the master equation (2.16) is solved as

$$u_{g\to\infty} = \log\left\{(\rho^2 + a^2)\exp\left(mx^3\right) + \exp\left(-mx^3\right)\right\}. \tag{6.79}$$

The domain wall position is read from the condition $(\rho^2 + a^2)\exp\left(mx^3\right) = \exp\left(-mx^3\right)$, which gives

$$x^3(\rho) = -\frac{1}{2m}\log(\rho^2 + a^2). \tag{6.80}$$

In the strong-gauge coupling limit, since the boojum energy density in Eq. (2.20) is vanishing, the total energy (2.12) is just the sum of the domain wall tension and the vortex string tension:

$$E_{1/4} = \int d^3x\, (\mathcal{T}_{\rm W} + \mathcal{T}_{\rm S}), \tag{6.81}$$

where $\mathcal{T}_{\rm W}$ and $\mathcal{T}_{\rm S}$ are given in Eqs. (2.18) and (2.19). We perform the integral along only x^3-direction:

$$E_{1/4} = T_{\rm W}A + \int d^2x\, \mathcal{E}_{\rm S}(x^2, x^2), \tag{6.82}$$

where $\mathcal{E}_{\rm S}$ is given by

$$\mathcal{E}_{\rm S}(x_1, x_2) = \frac{v^2}{m}\left[\frac{\rho^2}{(\rho^2+a^2)^2} + \frac{a^2}{(\rho^2+a^2)^2}\log\left\{1+(\rho^2+a^2)\exp(2m\Lambda)\right\}\right]. \tag{6.83}$$

Here we have introduced the infrared cutoff $x_3 = \Lambda$. In the following, we focus on the contribution of the energy from the vortex string in Eq. (6.83). We separate it into two parts as

$$E_{\rm S} = \int d^2x\, \mathcal{E}_{\rm S}(x_1, x_2) = E_{\rm S1} + E_{\rm S2}, \tag{6.84}$$

where

$$E_{\rm S1} = \frac{v^2}{m}\int d^2x\, \frac{\rho^2}{(\rho^2+a^2)^2}, \tag{6.85}$$

$$E_{\rm S2} = \frac{v^2}{m}\int d^2x\, \frac{a^2}{(\rho^2+a^2)^2}\log\left\{1+(\rho^2+a^2)\exp(2m\Lambda)\right\}. \tag{6.86}$$

Integration over ρ from a UV cutoff $\rho = \delta$ ($\delta \ll a$) to an IR cutoff $\rho = R$ ($R \gg a$) (see Fig. 29), we find

$$E_{\rm S1} = \frac{\pi v^2}{m}\left\{\log(R^2+a^2) - \left(\frac{a^2}{\delta^2+a^2} + \log(\delta^2+a^2)\right)\right\}, \tag{6.87}$$

$$E_{\rm S2} \simeq \frac{\pi v^2 a^2}{m}\left\{\frac{1+\log(\delta^2+a^2)}{\delta^2+a^2} - 2m\Lambda\left(\frac{1}{R^2+a^2} - \frac{1}{\delta^2+a^2}\right)\right\}, \tag{6.88}$$

where we have assumed that the cutoff Λ is sufficiently large and that the second term in the logarithm in Eq. (6.86) is dominant. Taking account of Eq. (6.80) and assuming $a > \delta$, Eqs. (6.87) and (6.88) are rewritten as

$$E_{\rm S1} \simeq -2\pi v^2\left(x^3(R) - x^3(\delta) + \frac{1}{2m}\right) + \mathcal{O}\left(\frac{\delta^2}{a^2}\right), \tag{6.89}$$

$$E_{\rm S2} \simeq -2\pi v^2(x^3(\delta) - \Lambda) + \mathcal{O}\left(\frac{\delta^2}{a^2}\right). \tag{6.90}$$

These results tell us that $E_{\rm S1}$ is the vortex string energy between $x^3(R)$ and $x^3(\delta)$ while $E_{\rm S2}$ is the one between $x^3(\delta)$ and Λ. We show each contribution schematically in Fig. 29. As can be seen from Fig. 29, $E_{\rm S2}$ corresponds to the energy contributed by the lump string that is perpendicular to the domain wall. On the other hand, $E_{\rm S1}$ is the contribution from the part of the lump string ($\rho > a$) whose angle from the x^1–x^2 plane is in the range $[0, \pi/2)$. Thus, we expect that only $E_{\rm S1}$ is reproduced within the DBI theory.

For $a > 1$ the curve (6.80) does not cross the ρ-axis (the upper panel in Fig. 29). As a is decreased, the curve crosses the ρ-axis and $x^3(\delta)$ goes to the right along the x^3-axis and the contribution of $E_{\rm S1}$ is dominant (the lower panel in Fig. 29) in $E_{\rm S}$. As a decreases further, the expressions (6.89) and (6.90) are no longer valid. In such a case, it is convenient to go back to the original expressions (6.87) and (6.88). There we can safely take a to be zero and find that $E_{\rm S2}$ is vanishing while $E_{\rm S1}$ becomes

$$E_{\rm S1} = \frac{2\pi v^2}{m}(\log R - \log\delta). \tag{6.91}$$

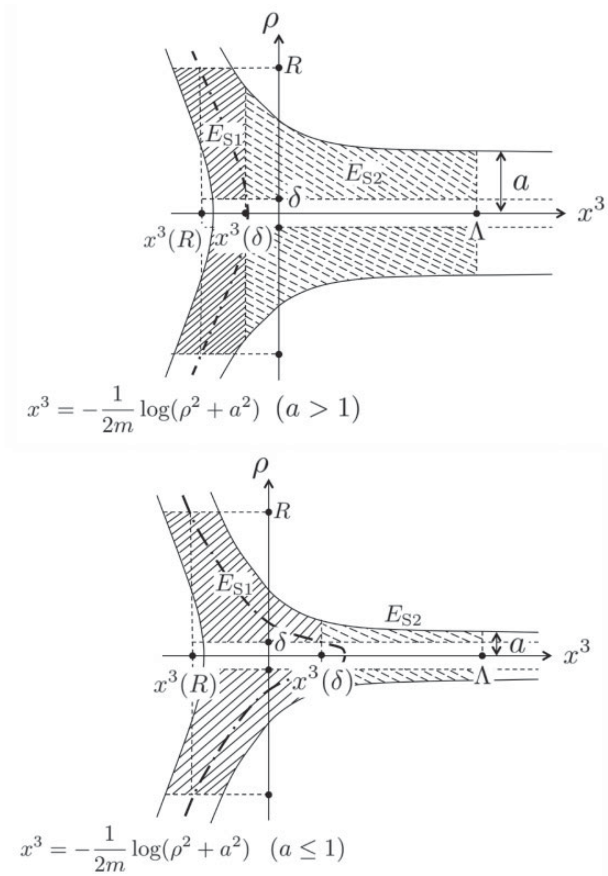

Fig. 29. Schematic picture of the semilocal vortex ending on the domain wall for $a > 1$ (upper) and $a \leq 1$ (lower). The dashed-dotted curve shows the position of the domain wall described by $x^3 = -1/(2m)\log(\rho^2 + a^2)$. The solid-line shaded part of the configuration contributes to the vortex string energy E_{S1} while the dashed-line shaded part contributes to E_{S2}.

Using Eq. (6.80) with $a = 0$, this expression is rewritten as

$$E_{S1} = T_S L, \tag{6.92}$$

where $L = x^3(\delta) - x^3(R)$ is the string length. Therefore, E_{S1} at $a = 0$ is nothing but the lump string energy of zero size. Note that the lump string with $a = 0$ becomes singular at $x^3 \to \infty$. Thus, the $a = 0$ lump string attached to the domain wall is regular except for $\rho = 0$, namely the angle to the x^1–x^2 plane is always in the range $[0, \pi/2)$, except for the junction point. Therefore, the lump string of zero size E_{S1} should be reproduced in the DBI theory for the whole region on the domain wall except for $\rho = 0$.

Now let us consider the corresponding configuration in the DBI action. The Hamiltonian and the BPS equation in the DBI action are Eqs. (6.72) and (6.71) with $\hat{B} = 0$:

$$\mathcal{H}_{\rm DBI} = \hat{T}_{\rm W}\left(1 + \hat{T}_{\rm W}^{-1}\Pi_i^2\right), \tag{6.93}$$

$$\partial_i X = \pm\hat{T}_{\rm W}^{-1}\Pi_i. \tag{6.94}$$

The energy of the configuration is

$$E_{\rm DBI} = \hat{T}_{\rm W} A + \hat{T}_{\rm W}^{-1}\int d^2x\ \Pi_i^2. \tag{6.95}$$

We expect that the second term of Eq. (6.95) coincides with $E_{\rm S1}$ given in Eq. (6.87). In order to check this under the identification $T_{\rm W} = \hat{T}_{\rm W}$, the following relation should hold:

$$\frac{v^2}{m}\frac{\rho^2}{(\rho^2+a^2)^2} = \hat{T}_{\rm W}^{-1}\Pi_i^2 \quad (\hat{T}_{\rm W} = mv^2). \tag{6.96}$$

This is solved by

$$\hat{T}_{\rm W}^{-1}\Pi_i = \frac{1}{m}\frac{x_i}{\rho^2+a^2}. \tag{6.97}$$

Combining this with Eq. (6.94), we find

$$X = -\frac{1}{2m}\log(\rho^2+a^2). \tag{6.98}$$

This is precisely equal to Eq. (6.80)! Thus, we find the semilocal BIon that is the desired counterpart of the semilocal boojum in the original gauge theory. Note that $E_{\rm S1}$ in Eq. (6.89) with $\delta = 0$ does not depend on a, since we can absorb it into the IR cutoff by taking $R = (1+\tilde{R})a$, where $\tilde{R} > 0$ is a new cutoff. In this sense, we can interpret a as a moduli parameter of the semilocal BIon.

While $E_{\rm S1}$ is correctly reproduced in the DBI action, $E_{\rm S2}$ is missing. As explained above, $E_{\rm S2}$ corresponds to the part of the lump string perpendicular to the domain wall. To reproduce this correctly, we should take additional zero modes into account. So far, we have considered only the zero modes localized on the domain wall. However, there are nonnormalizable zero modes in the bulk because a part of the flavor symmetry remains unbroken in the model with the partially degenerate masses (Eq. (6.78)). We expect that $E_{\rm S2}$ will be correctly reproduced once we include coupling between the localized zero modes and nonnormalizable zero modes. It would be interesting to figure out the interaction, but it is beyond the scope of this paper, so we leave it as future work.

The last comment is on the dual electric charge. The electric field Eq. (6.74) for the semilocal BIon is given by

$$\hat{E}_i = \frac{1}{\kappa\hat{m}}\frac{x_i}{\rho^2+a^2}, \tag{6.99}$$

where we recover the dimensional parameter κ. Interestingly, the behavior of $\hat{E}_i$ is similar to the magnetic field in the domain wall discussed in Sect. 3.3. There it was found that the observer in the domain wall sees that the magnetic field of the magnetic point source obeys the modified Coulomb law in a region far from the magnetic source. Similarly, in the DBI theory the observer in the domain wall sees that the electric field obeys the modified Coulomb law in a region far from the electric point source placed in the domain wall. Recalling the discussion in Sect. 3.5, we see that the electric charge placed on the membrane is

$$q_E = \frac{2}{\hat{m}\kappa}. \tag{6.100}$$

7. Outlook

In this paper, using our previous results (Ref. [17]), we have furthered the understanding of 1/4 BPS composite solitons in the Abelian-Higgs theory.

We obtained the solution for the vortex strings attached to the tilted domain walls on which constant background magnetic field is turned on. This is similar to D1-branes suspended between tilted D3-branes. The D1-branes can be seen as magnetic monopoles in noncommutative space-time (Refs. [23,24]). As a natural analogy, the vortex strings suspended between tilted domain walls in the gauge theory should be seen as electrically charged particles in a low-energy effective theory that is a noncommutative theory. If this is the case, the similarity between the solitons in field theories and D-branes in string theories, which is repeated in the literature, is further reinforced.

Further studies of composite solitons, especially in a non-Abelian setting, may be useful for ironing out the phenomenology of dynamically realized brane-world scenarios. In string theory, it is known that intersecting D-branes can generate Standard Model gauge group, chiral fermions, and family replication (see Ref. [36] and references therein). Similar results were obtained within the field theory as well. Indeed, domain walls and magnetic vortices have long since been used to localize scalar and fermionic fields (Refs. [37,38]). The localization of gauge fields is achieved either by the Dvali–Shifman mechanism (Ref. [39]), where the confining phase in the bulk is assumed, or dynamically using a field-dependent gauge coupling constant via the Ohta–Sakai mechanism (Ref. [40]). Using the former, the Standard Model gauge group has been constructed at the junction of perpendicular domain walls in Ref. [41], while the latter was used to localize a large gauge group on coincident domain walls (Refs. [42,43]). In the future, using the method developed here, we would like to construct a realistic brane-world scenario on intersecting solitons at a finite-gauge coupling constant and to clarify the role of negative binding energy on low-energy effective theory.

We have shown that the spike domain wall configuration in the field theory can be reproduced in the NG action and the DBI action. We have also observed that the DBI action correctly realizes the semilocal boojum as the semilocal BIon. On the other hand, as is addressed in Sect. 6.5, the DBI action cannot reproduce the semilocal lump string itself (E_{S2}), that is perpendicular to the domain wall. A possible reason for this situation is that perhaps not all the massless modes are taken into account in the low-energy effective theory. The semilocal boojum is constructed by introducing partially degenerate masses such as Eq. (6.78). If there is a mass splitting in the first two components, there are three discrete vacua and an extra domain wall appears. Associated with this, extra massless modes localize around the extra domain wall. The extra domain wall becomes increasingly broader as the mass splitting disappears. Correspondingly, the extra massless modes spread into the whole half-space and they become nonnormalizable. We expect that these nonnormalizable modes will be necessary for reproducing E_{S2} in the low-energy effective theory. Normally, it is not easy to deal with nonnormalizable modes. We may achieve it by considering a small mass splitting that introduces the broad extra domain wall. Further, we may consider a low-energy effective action for the two parallel domain walls and investigate the limit when we turn on the mass degeneracy. We leave this problem for future work.

Acknowledgements

This work is supported by Grant-in-Aid for Scientific Research No. 25400280 (M.A.) and by the Ministry of Education, Culture, Sports, Science, and Technology (MEXT) of Japan. The work of M.E. is supported in part by JSPS Grant-in-Aid for Scientific Research (KAKENHI Grant No. 26800119) and the MEXT-Supported Program for the Strategic Research Foundation at Private Universities "Topological Science" (Grant No. S1511006). F.B. is an international research fellow of the Japan Society for the Promotion of Science. This work was supported by Grant-in-Aid for JSPS Fellows, Grant No. 26004750.

Funding

Open Access funding: SCOAP3.

References

[1] H. B. Nielsen and P. Olesen, Nucl. Phys. B **61**, 45 (1973).
[2] G. 't Hooft, Nucl. Phys. B **79**, 276 (1974).
[3] A. M. Polyakov, JETP Lett. **20**, 194 (1974). [Pis'ma Zh. Eksp. Teor. Fiz. **20**, 430 (1974)].
[4] J. Polchinski, S. Chaudhuri, and C. V. Johnson, arXiv:hep-th/9602052 [Search INSPIRE].
[5] S. M. Carroll and M. Trodden, Phys. Rev. D **57**, 5189 (1998) [arXiv:hep-th/9711099] [Search INSPIRE].
[6] M. Bowick, A. De Felice, and M. Trodden, J. High Energy Phys. **10**, 067 (2003) [arXiv:hep-th/0306224] [Search INSPIRE].
[7] E. Witten, Nucl. Phys. B **507**, 658 (1997) [arXiv:hep-th/9706109] [Search INSPIRE].
[8] I. I. Kogan, A. Kovner, and M. A. Shifman, Phys. Rev. D **57**, 5195 (1998) [arXiv:hep-th/9712046] [Search INSPIRE].
[9] A. Campos, K. Holland, and U. J. Wiese, Phys. Rev. Lett. **81**, 2420 (1998), [arXiv:hep-th/9805086] [Search INSPIRE].
[10] J. P. Gauntlett, R. Portugues, D. Tong, and P. K. Townsend, Phys. Rev. D **63**, 085002 (2001) [arXiv:hep-th/0008221] [Search INSPIRE].
[11] M. Shifman and A. Yung, Phys. Rev. D **67**, 125007 (2003) [arXiv:hep-th/0212293] [Search INSPIRE].
[12] M. Shifman and A. Yung, Phys. Rev. D **70**, 025013 (2004) [arXiv:hep-th/0312257] [Search INSPIRE].
[13] N. Sakai and D. Tong, J. High Energy Phys. **03**, 19 (2005) [arXiv:hep-th/0501207] [Search INSPIRE].
[14] N. D. Mermin, *Quantum Fluids and Solids* (Plenum, New York, 1977).
[15] G. E. Volovik, JETP Lett. **51**, 449 (1990).
[16] R. Auzzi, M. Shifman, and A. Yung, Phys. Rev. D **72**, 025002 (2005) [arXiv:hep-th/0504148] [Search INSPIRE].
[17] M. Arai, F. Blaschke, and M. Eto, BPS boojums in N=2 supersymmetric gauge theories I [arXiv:hep-th/603.00447]
[18] Y. Isozumi, M. Nitta, K. Ohashi, and N. Sakai, Phys. Rev. Lett. **93**, 161601 (2004) [arXiv:hep-th/0404198] [Search INSPIRE].
[19] Y. Isozumi, M. Nitta, K. Ohashi, and N. Sakai, Phys. Rev. D **71**, 065018 (2005) [arXiv:hep-th/0405129] [Search INSPIRE].
[20] M. Eto, Y. Isozumi, M. Nitta, K. Ohashi, and N. Sakai, J. Phys. A **39**, 315 (2006) [arXiv:hep-th/0602170] [Search INSPIRE].
[21] K. Kakimoto and N. Sakai, Phys. Rev. D **68**, 065005 (2003) [arXiv:hep-th/0306077] [Search INSPIRE].
[22] C. H. Taubes, Commun. Math. Phys. **72**, 277 (1980).
[23] K. Hashimoto, J. High Energy Phys. **07**, 016 (1999) [arXiv:hep-th/9905162] [Search INSPIRE].
[24] A. Hashimoto and K. Hashimoto, J. High Energy Phys. **11**, 005 (1999) [arXiv:hep-th/9909202] [Search INSPIRE].
[25] M. Eto, Y. Isozumi, M. Nitta, and K. Ohashi, Nucl. Phys. B **752**, 140 (2006) [arXiv:hep-th/0506257] [Search INSPIRE].
[26] K.-M. Lee and H.-U. Yee, Phys. Rev. D **72**, 065023 (2005) [arXiv:hep-th/0506256] [Search INSPIRE].
[27] E. R. C. Abraham and P. K. Townsend, Phys. Lett. B **291**, 85 (1992).
[28] E. R. C. Abraham and P. K. Townsend, Phys. Lett. B **295**, 225 (1992).
[29] T. Vachaspati and A. Achucarro, Phys. Rev. D **44**, 3067 (1991).
[30] D. Tong, J. High Energy Phys. **02**, 30 (2006) [arXiv:hep-th/0512192] [Search INSPIRE].
[31] M. Eto, Y. Isozumi, M. Nitta, K. Ohashi, and N. Sakai, Phys. Rev. D **72**, 025011 (2005) [arXiv:hep-th/0412048] [Search INSPIRE].
[32] M. Eto, Y. Isozumi, M. Nitta, and K. Ohashi, Nucl. Phys. B **752**, 140 (2006) [arXiv:hep-th/0506257] [Search INSPIRE].
[33] D. Tong, Theoretical Advanced Study Institute in Elementary Particle Physics: Many Dimensions of String Theory (TASI 2005), Boulder, Colorado, June 5–July 1 (2005) [arXiv:hep-th/0509216] [Search INSPIRE].
[34] M. Eto, J. High Energy Phys. **06**, 160 (2015) [arXiv:hep-th/1504.00753] [Search INSPIRE].
[35] M. Eto and K. Hashimoto, [arXiv:hep-th/1508.00433] [Search INSPIRE].

[36] R. Blumenhagen, M. Cvetič, P. Langacker, and G. Shiu, Annu. Rev. Nucl. Part. Sci. **55**, 71 (2005) [arXiv:hep-th/0502005] [Search INSPIRE].
[37] K. Akama, arXiv:hep-th/0001113 [Search INSPIRE].
[38] V. A. Rubakov and M. E. Shaposhnikov, Phys. Lett. B **125**, 136 (1983).
[39] G. Dvali and M. Shifman, Phys. Lett. B **396**, 64 (1997) [arXiv:hep-th/9612128] [Search INSPIRE].
[40] K. Ohta and N. Sakai, Prog. Theor. Phys. **124**, 71 (2010) [arXiv:hep-th/1004.4078] [Search INSPIRE].
[41] B. D. Callen and R. R. Volkas, Phys. Rev. D **89**, 056004 (2014) [arXiv:hep-th/1310.4097] [Search INSPIRE].
[42] M. Arai, F. Blaschke, M. Eto, and N. Sakai, Prog. Theor. Exp. Phys. **2013**, 013B05 (2013) [arXiv:hep-th/1208.6219] [Search INSPIRE].
[43] M. Arai, F. Blaschke, M. Eto, and N. Sakai, Prog. Theor. Exp. Phys. **2013**, 093B01 (2013) [arXiv:hep-th/1303.5212] [Search INSPIRE].